

Spring 2010

# Accurate and stable numerical methods for solving micro heat transfer models in an N-carrier system in spherical coordinates

Di Zhao

Follow this and additional works at: <https://digitalcommons.latech.edu/dissertations>

 Part of the [Applied Mathematics Commons](#), and the [Computer Sciences Commons](#)

---

## **NOTE TO USERS**

**This reproduction is the best copy available.**

**UMI<sup>®</sup>**



**ACCURATE AND STABLE NUMERICAL METHODS  
FOR SOLVING MICRO HEAT TRANSFER  
MODELS IN AN *N*-CARRIER SYSTEM  
IN SPHERICAL COORDINATES**

by

Di Zhao, B.A., M.E.

A Dissertation Presented in Partial Fulfillment  
of the Requirement for the Degree  
Doctor of Philosophy

COLLEGE OF ENGINEERING AND SCIENCE  
LOUISIANA TECH UNIVERSITY

May 2010

UMI Number: 3411209

All rights reserved

**INFORMATION TO ALL USERS**

The quality of this reproduction is dependent upon the quality of the copy submitted.

In the unlikely event that the author did not send a complete manuscript and there are missing pages, these will be noted. Also, if material had to be removed, a note will indicate the deletion.



UMI 3411209

Copyright 2010 by ProQuest LLC.

All rights reserved. This edition of the work is protected against unauthorized copying under Title 17, United States Code.



ProQuest LLC  
789 East Eisenhower Parkway  
P.O. Box 1346  
Ann Arbor, MI 48106-1346

LOUISIANA TECH UNIVERSITY

THE GRADUATE SCHOOL

April 1, 2010

Date

We hereby recommend that the dissertation prepared under our supervision  
by Di Zhao

entitled ACCURATE AND STABLE NUMERICAL METHODS FOR SOLVING  
MICRO HEAT TRANSFER MODELS IN AN N-CARRIER SYSTEM  
IN SPHERICAL COORDINATES

be accepted in partial fulfillment of the requirements for the Degree of  
Doctor of Philosophy

Wei Sheng Dai  
Supervisor of Dissertation Research  
Wei Sheng Dai  
Head of Department

Computational Analysis and Modeling  
Department

Recommendation concurred in:

[Signature]

Kear Coulters

Kate A. Gwan

Hou Songji

Advisory Committee

Approved:  
[Signature]  
Director of Graduate Studies

Approved:  
[Signature]  
Dean of the Graduate School

[Signature]  
Dean of the College

## ABSTRACT

Energy exchange between electrons and phonons in metal provides the best example in describing non-equilibrium heating during the ultrafast transient. In times comparable to the thermalization and relaxation time of electrons and phonons, which are in the range of a few to several tens of picoseconds, heat continuously flows from hot electrons to cold phonons through mutual collisions. Consequently, electron temperature continuously decreases whereas phonon temperature continuously increases until thermal equilibrium is reached. Tien developed the well-known parabolic two-step model for describing the non-equilibrium heating in the electron-phonon system in 1992, and Tzou developed the parabolic model for the non-equilibrium heating in an  $N$ -carrier system in one-dimensional (1D) Cartesian coordinates in 2009.

In the early 1990s, it was discovered that biological tissue, along with a number of other common materials, exhibits a relatively long thermal relaxation (or lag) time before equilibrium heating. Because a biological cell may contain proteins, water, and dissolved minerals, the non-equilibrium heating may also exist in the biological cell when exposed to ultrafast heating.

This dissertation considers the generalized micro heat transfer models in an  $N$ -carrier system with the Neumann boundary condition in 1D and three-dimensional (3D) spherical coordinates, which can be applied to describe the non-equilibrium in biological cells. The generalized models in 1D and 3D spherical coordinates are shown to be well-posed.

An improved unconditionally stable Crank-Nicholson (CN) scheme is presented for solving the generalized model in 1D spherical coordinates, where a second-order accurate finite difference scheme for the Neumann boundary condition is developed so that the overall truncation error of the 1D improved CN scheme is second-order. Two improved unconditionally stable CN schemes are then presented for solving the generalized model in 3D spherical coordinates. In particular, two second-order accurate finite difference schemes for the Neumann boundary condition are developed so that overall truncation errors of 3D improved CN schemes are second-order with respect to the spatial variable  $r$ . The stability of the 1D improved CN scheme and two 3D improved CN schemes is proved.

The convergence rates of the solution of the 1D improved CN scheme are calculated by a numerical example. Results show that the convergence rates of the 1D improved CN scheme are about 2 with respect to both spatial and temporal variables respectively, while the convergence rates of the CN scheme with the convective scheme for the Neumann boundary condition are about 1 and about 2 with respect to the spatial and temporal variables, respectively.

The convergence rates of the numerical solution of two 3D improved CN schemes are calculated by two examples. Results show that the convergence rate of both 3D improved CN schemes are about 2 with respect to the spatial variable  $r$ , while the convergence rate of the 3D CN scheme is about 1 with respect to the spatial variable  $r$ .

## APPROVAL FOR SCHOLARLY DISSEMINATION

The author grants to the Prescott Memorial Library of Louisiana Tech University the right to reproduce, by appropriate methods, upon request, any or all portions of this Dissertation. It is understood that "proper request" consists of the agreement, on the part of the requesting party, that said reproduction is for his personal use and that subsequent reproduction will not occur without written approval of the author of this Dissertation. Further, any portions of the Dissertation used in books, papers, and other works must be appropriately referenced to this Dissertation.

Finally, the author of this Dissertation reserves the right to publish freely, in the literature, at any time, any or all portions of this Dissertation.

Author



Date

April 1, 2010

## TABLE OF CONTENTS

ABSTRACT .....	iii
LIST OF TABLES .....	viii
LIST OF FIGURES .....	ix
NOMENCLATURE .....	xii
ACKNOWLEDGEMENTS .....	xiv
CHAPTER ONE INTRODUCTION .....	1
1.1 General Overview .....	1
1.2 Research Objectives .....	2
1.3 Organization of the Dissertation .....	3
CHAPTER TWO BACKGROUND AND PREVIOUS WORK .....	5
2.1 Macro Heat Transfer .....	5
2.2 Micro Heat Transfer .....	6
2.2.1 Parabolic Model in a <i>Two</i> -carrier System in Cartesian Coordinates .....	7
2.2.2 Parabolic Model in a <i>Two</i> -carrier System in Spherical Coordinates .....	8
2.3 Previous Work .....	8
2.3.1 Parabolic Model in an <i>N</i> -carrier System in Cartesian Coordinates .....	9
2.3.2 Hyperbolic Model in an <i>N</i> -carrier System in Cartesian Coordinates .....	11
2.4 Conclusion .....	12
CHAPTER THREE MATHEMATICAL MODEL .....	13
3.1 Governing Equation .....	13
3.1.1 1D Case .....	13
3.1.2 3D Case .....	14
3.2 Well-posedness .....	16
3.2.1 1D Case .....	16
3.2.2 3D Case .....	20
CHAPTER FOUR NUMERICAL METHOD .....	25
4.1 Finite Difference Schemes .....	25

4.1.1 1D Improved CN Scheme.....	25
4.1.2 3D First Improved CN Scheme .....	32
4.1.3 3D Second Improved CN Scheme .....	36
4.2 Stability .....	39
4.2.1 Stability of 1D Improved CN Scheme.....	39
4.2.2 Stability of 3D First Improved CN Scheme.....	43
4.2.3 Stability of 3D Second Improved CN Scheme .....	47
4.3 General Algorithms.....	52
4.3.1 1D Case.....	52
4.3.2 3D Case.....	53
CHAPTER FIVE NUMERICAL EXAMPLES.....	55
5.1 1D Improved CN Scheme Case .....	55
5.1.1 Example Description.....	55
5.1.2 Results and Analysis .....	56
5.2 3D First Improved CN Scheme Case.....	67
5.2.1 Example Description.....	67
5.2.2 Results and Analysis .....	68
5.3 3D Second Improved CN Scheme Case .....	78
5.3.1 Example Description.....	78
5.3.2 Results and Analysis .....	79
CHAPTER SIX CONCLUSION .....	89
APPENDIX SOURCE CODE .....	91
REFERENCES .....	107
VITA .....	113

## LIST OF TABLES

Table 5.1	Comparison of $l_2$ -norm errors and convergence rates with respect to $r$ of the 1D improved CN scheme and the 1D CN scheme with $0 \leq t \leq 1.0$ , $\Delta t = 10^{-5}$ .....	57
Table 5.2	Comparison of $l_2$ -norm errors and convergence rates with respect to $t$ of the 1D the improved CN scheme and the 1D CN scheme.....	58
Table 5.3	Comparison of $l_2$ -norm errors and convergence rates between the 3D first improved CN scheme and the 3D CN scheme with $0 \leq t \leq 0.2$ , $\Delta t = 10^{-4}$ .....	69
Table 5.4	Comparison of $l_2$ -norm errors and convergence rates between the 3D second improved CN scheme and the 3D CN scheme with $0 \leq t \leq 0.2$ , $\Delta t = 10^{-4}$ .....	80

## LIST OF FIGURES

Figure 2.1	Energy exchanges in an $N$ -carrier system .....	10
Figure 4.1	Mesh and locations of grid points in the 1D improved CN scheme in spherical coordinates.....	27
Figure 4.2	Mesh and locations of grid points in the 3D second improved CN scheme in spherical coordinates.....	37
Figure 5.1	Comparison of $l_2$ -norm errors between the 1D improved CN scheme and the 1D CN scheme along the time $t$ .....	60
Figure 5.2	Distribution of the temperature $T_1$ from the 1D improved CN scheme along the radial distance $r$ at different time (a) $t = 0.1$ (b) $t = 0.2$ and (c) $t = 1.0$ with $\Delta r = 2 \times 10^{-3}$ , $10^{-3}$ and $5 \times 10^{-4}$ .....	61
Figure 5.3	Distribution of the temperature $T_2$ from the 1D improved CN scheme along the radial distance $r$ at different time (a) $t = 0.1$ (b) $t = 0.2$ and (c) $t = 1.0$ with $\Delta r = 2 \times 10^{-3}$ , $10^{-3}$ and $5 \times 10^{-4}$ .....	62
Figure 5.4	Distribution of the temperature $T_3$ from the 1D improved CN scheme along the radial distance $r$ at different time (a) $t = 0.1$ (b) $t = 0.2$ and (c) $t = 1.0$ with $\Delta r = 2 \times 10^{-3}$ , $10^{-3}$ and $5 \times 10^{-4}$ .....	63
Figure 5.5	Distribution of the temperature $T_1$ from the 1D CN scheme along the radial distance $r$ at different time (a) $t = 0.1$ (b) $t = 0.2$ and (c) $t = 1.0$ with $\Delta r = 2 \times 10^{-5}$ , $10^{-5}$ and $5 \times 10^{-6}$ .....	64
Figure 5.6	Distribution of the temperature $T_2$ from the 1D CN scheme along the radial distance $r$ at different time (a) $t = 0.1$ (b) $t = 0.2$ and (c) $t = 1.0$ with $\Delta r = 2 \times 10^{-5}$ , $10^{-5}$ and $5 \times 10^{-6}$ .....	65
Figure 5.7	Distribution of the temperature $T_3$ from the 1D CN scheme along the radial distance $r$ at different time (a) $t = 0.1$ (b) $t = 0.2$ and (c) $t = 1.0$ with $\Delta r = 2 \times 10^{-5}$ , $10^{-5}$ and $5 \times 10^{-6}$ .....	66

Figure 5.8	Comparison of $l_2$ -norm errors between the 3D first improved CN scheme and the 3D CN scheme.....	71
Figure 5.9	Comparison of contours of the solution $T_1$ in the cross section of $\theta = \frac{\pi}{2}$ at $t = 0.1$ obtained using (a) the 3D first improved CN scheme and (b) the 3D CN scheme with (c) the exact solution .....	72
Figure 5.10	Comparison of contours of the solution of $T_1$ in the cross section of $\theta = 0$ and $\theta = \pi$ at $t = 0.1$ obtained using (a) the 3D first improved CN scheme and (b) the 3D CN scheme with (c) the exact solution.....	73
Figure 5.11	Comparison of contours of the solution $T_2$ in the cross section of $\theta = \frac{\pi}{2}$ at $t = 0.1$ obtained using (a) the 3D first improved CN scheme and (b) the 3D CN scheme with (c) the exact solution .....	74
Figure 5.12	Comparison of contours of the solution of $T_2$ in the cross section of $\theta = 0$ and $\theta = \pi$ at $t = 0.1$ obtained using (a) the 3D first improved CN scheme and (b) the 3D CN scheme with (c) the exact solution.....	75
Figure 5.13	Comparison of contours of the solution $T_3$ in the cross section of $\theta = \frac{\pi}{2}$ at $t = 0.1$ obtained using (a) the 3D first improved CN scheme and (b) the 3D CN scheme with (c) the exact solution .....	76
Figure 5.14	Comparison of contours of the solution of $T_3$ in the cross section of $\theta = 0$ and $\theta = \pi$ at $t = 0.1$ obtained using (a) the 3D first improved CN scheme and (b) the 3D CN scheme with (c) the exact solution.....	77
Figure 5.15	Comparison of $l_2$ -norm errors between the 3D second improved scheme and the 3D CN scheme.....	82
Figure 5.16	Comparison of contours of the solution $T_1$ in the cross section of $\theta = \frac{\pi}{2}$ at $t = 0.1$ obtained using (a) the 3D second improved CN scheme and (b) the 3D CN scheme with (c) the exact solution .....	83
Figure 5.17	Comparison of contours of the solution of $T_1$ in the cross section of $\theta = 0$ and $\theta = \pi$ at $t = 0.1$ obtained using (a) the 3D second improved CN scheme and (b) the 3D CN scheme with (c) the exact solution.....	84

- Figure 5.18 Comparison of contours of the solution  $T_2$  in the cross section of  $\theta = \frac{\pi}{2}$  at  $t = 0.1$  obtained using (a) the 3D second improved CN scheme and (b) the 3D CN scheme with (c) the exact solution ..... 85
- Figure 5.19 Comparison of contours of the solution of  $T_2$  in the cross section of  $\theta = 0$  and  $\theta = \pi$  at  $t = 0.1$  obtained using (a) the 3D second improved CN scheme and (b) the 3D CN scheme with (c) the exact solution..... 86
- Figure 5.20 Comparison of contours of the solution  $T_3$  in the cross section of  $\theta = \frac{\pi}{2}$  at  $t = 0.1$  obtained using (a) the 3D second improved CN scheme and (b) the 3D CN scheme with (c) the exact solution ..... 87
- Figure 5.21 Comparison of contours of the solution of  $T_3$  in the cross section of  $\theta = 0$  and  $\theta = \pi$  at  $t = 0.1$  obtained using (a) the 3D second improved CN scheme and (b) the 3D CN scheme with (c) the exact solution..... 88

## NOMENCLATURE

$a, a^*$	artificial constant for improved CN schemes
$b, b^*$	artificial constant for improved CN schemes
$c, c^*$	artificial constant for improved CN schemes
$C_m$	volumetric heat capacity of carrier $m$
$E$	$l_2$ -norm error
$F$	function
$G$	coupling factor, $W/(m^3K)$
$I$	total number of grid points in $r$ direction of spherical coordinates
$J$	total number of grid points in $\theta$ direction of spherical coordinates
$K$	total number of grid points in $\phi$ direction of 1D spherical coordinates or $\mu$ direction of 3D spherical coordinates
$k_m$	thermal conductivity of carrier $m$ , $W/(mk)$
$L$	length of radius of micro-sphere, $m$
$N$	total number of governing equations
$P$	finite difference operator
$Q_m$	volumetric heat source of carrier $m$ , $W/m^2$
$\bar{q}$	heat flux vector, $W/m^2$
$r$	the radial distance in spherical coordinates

$T$	carrier temperature, $K$
$t$	time, $s$
$t_0$	upper bound for time $t$
$x$	the $x$ distance in Cartesian coordinates
$Z_1, Z_2$	constants in Gronwall's lemma

#### Greek Symbols

$\Delta t$	the time step size, $s$
$\Delta x$	the grid step size in Cartesian coordinates, $m$
$\Delta r$	the grid size in $r$ direction of spherical coordinates
$\Delta \theta$	the grid size in $\theta$ direction of spherical coordinates
$\Delta \phi, \Delta \mu$	the grid size in $\phi$ direction of 1D spherical coordinates or $\mu$ direction of 3D spherical coordinates
$\beta, \beta_1, \beta_2$	artificial parameter of improved CN schemes
$\Phi$	function
$\Omega$	function

#### Subscripts and Superscripts

$i$	grid index in $r$ direction of spherical coordinates
$j$	grid index in $\theta$ direction of spherical coordinates
$k$	grid index in $\phi$ direction of 1D spherical coordinates or $\mu$ direction of 3D spherical coordinates
$m$	index for the carrier $m$
$n$	index for the time step

## **ACKNOWLEDGEMENTS**

I thank my advisor, Dr. Weizhong Dai, for directing my doctoral research. Dr. Dai is an applied mathematician in micro heat transfer modeling, especially in the high-order finite difference method. I thank the faculty of the Computational Analysis and Modeling Program from the Department of Mathematics and Statistics and the Department of Computer Sciences. I thank the members of my academic committee, Dr. Ben Choi, Dr. William Mark Countryman, Dr. Katie Evans and Dr. Songming Hou, for their long-term support and help in improving this dissertation. Also, I thank the friends of the university community for their friendship and help in my five-year doctoral studying.

# CHAPTER ONE

## INTRODUCTION

Chapter One provides the introduction to this dissertation. There are three sections in Chapter One: general overview, research objectives and organization of the dissertation.

### 1.1 General Overview

Energy exchange in metal between the electron and the phonon during the ultrafast transient laser pulse is in non-equilibrium heating. In the range of a few to several tens of picoseconds, heat continuously flows from hot electrons to cold phonons through mutual collisions. When the phonon temperature continuously increases, the electron temperature continuously decreases until thermal equilibrium is reached. Tien developed the well-known parabolic two-step model for describing the non-equilibrium heating in the electron-phonon system in 1992 [1], [2].

Most multi-carrier systems in nature are in thermal non-equilibrium. For instance, non-equilibrium heating may exist in porous media that already involve a more complicated system than the *Two*-carrier system. Also, the phase change in wicked heat pipes may involve non-equilibrium heating and energy dissipation among the solid wick, liquid, and vapor phases.

The *N*-carrier system is the latest progress in micro heat transfer modeling in the past years. The first paper of an *N*-carrier system was published in 2009, and described a

parabolic model in an  $N$ -carrier system in Cartesian coordinates [3]. Dai *et al.* developed a fourth-order finite difference scheme for the parabolic model in Cartesian coordinates [4], and a stable finite difference scheme for thermal analysis in an  $N$ -carrier system [5]. Dai *et al.* also developed a hyperbolic model in an  $N$ -carrier system in Cartesian coordinates [6], and a compact LOD scheme for solving a model in  $N$ -carrier system with the Neumann boundary condition [7].

In the early 1990s, it was discovered that biological tissue, along with a number of other common materials, exhibits a relatively long thermal relaxation (or lag) time before equilibrium heating [8]. Because a biological cell may contain proteins, water, and dissolved minerals, the non-equilibrium heating may also exist in the biological cell when exposed to ultrafast heating.

## 1.2 Research Objectives

The objective of this dissertation is to extend the parabolic two-step model in an  $N$ -carrier system in 1D Cartesian coordinates to the generalized  $N$ -carrier system model in 1D and 3D spherical coordinates. Also, the project will develop numerical schemes to solve the parabolic model in an  $N$ -carrier system in 1D and 3D spherical coordinates.

In detail, research objectives of this dissertation include

- 1) To develop the parabolic model in an  $N$ -carrier system in 1D and 3D spherical coordinates;
- 2) To prove the well-posedness of the parabolic model in 1D and 3D spherical coordinates;
- 3) To develop improved CN schemes for solving the parabolic model in 1D and 3D spherical coordinates;

- 4) To prove the stability of improved CN schemes;
- 5) To provide numerical examples to illustrate the availability of the models and the schemes in 1D and 3D spherical coordinates.

### 1.3 Organization of the Dissertation

Chapter One provides an introduction for this dissertation with a general overview, research objectives and organization of the dissertation.

Chapter Two examines the background and previous work for this dissertation. Macro heat transfer will also be discussed in the chapter, as is the two-step model in a *Two*-carrier system for micro heat transfer in parabolic format. Also reviewed is the latest progress of the model in an *N*-carrier system of recent years.

Chapter Three develops the parabolic model in an *N*-carrier system in 1D and 3D spherical coordinates. The initial condition and the boundary condition for the model will also be discussed. Also, the well-posedness of the model will be proved in Chapter Three.

Chapter Four develops improved CN schemes for solving the model. The 1D improved CN scheme for solving the model in 1D and 3D spherical coordinates is developed. The stability of the 1D improved CN scheme will also be proved in the chapter, and a general algorithm as the solver for the linear system from the scheme. Also, two 3D improved CN schemes for solving the model in 3D spherical coordinates will be provided. The stability of the two second-order schemes will be proved in Chapter Four. Also, a general algorithm as the solver for the linear system from the two schemes is provided.

Chapter Five provides numerical examples for the model and the scheme developed in Chapter Three and in Chapter Four.  $l_2$ -norm errors and convergence rates

will be provided in Chapter Five. Also, numerical solutions and exact solutions will be plotted in Chapter Five.

Chapter Six contains a conclusion of this dissertation. Also, future research is discussed in Chapter Six.

## CHAPTER TWO

### BACKGROUND AND PREVIOUS WORK

Chapter Two provides background and reviews the research done previous to this dissertation. The background section includes a short review of macro heat transfer and micro heat transfer. Also reviewed is the latest progress of the model in an  $N$ -carrier system.

#### 2.1 Macro Heat Transfer

Heat transfer is the process of energy transition from carriers with high temperature to carriers with low temperature [9], [10]. There are three modes of heat transfer: conduction, convection and radiation.

This dissertation will only consider heat conduction. Macro heat conduction describes macroscopic behavior of conduction of thermal energy. Macro heat conduction can be modeled by the macro heat conduction equation. The macro heat conduction equation can be derived from Fourier's law in differential form and the first law of thermodynamics (conservation of energy) [9], [10]

$$C \frac{\partial T}{\partial t} = k \nabla^2 T + Q, \quad (2.1)$$

where  $T$  is the temperature,  $C$  is the volumetric heat capacity,  $k$  is thermal conductivity,  $Q$  is the heat source and  $\nabla^2$  is the Laplace operator. In different coordinates, Laplace

operator  $\nabla^2$  can be expressed in different forms. In Cartesian coordinates  $(x, y, z)$ , Laplace operator can be expressed as

$$\nabla^2 T = \frac{\partial^2 T}{\partial x^2} + \frac{\partial^2 T}{\partial y^2} + \frac{\partial^2 T}{\partial z^2}. \quad (2.2)$$

In spherical coordinates  $(r, \theta, \phi)$ , by substituting the transformation

$$x = r \sin \phi \cos \theta, \quad y = r \sin \phi \sin \theta, \quad z = r \cos \phi, \quad (2.3)$$

into Eq. (2.2), the Laplace operator from Cartesian coordinates to spherical coordinates can be transformed to

$$\nabla^2 T = \frac{1}{r^2} \frac{\partial}{\partial r} \left( r^2 \frac{\partial T}{\partial r} \right) + \frac{1}{r^2 \sin \phi} \frac{\partial}{\partial \phi} \left( \sin \phi \frac{\partial T}{\partial \phi} \right) + \frac{1}{r^2 \sin^2 \phi} \frac{\partial^2 T}{\partial \theta^2}. \quad (2.4a)$$

One can introduce  $\mu = \cos \phi$ , and Eq. (2.4a) can be transformed to an alternative form

$$\nabla^2 T = \frac{1}{r^2} \frac{\partial}{\partial r} \left( r^2 \frac{\partial T}{\partial r} \right) + \frac{1}{r^2 (1 - \mu^2)} \frac{\partial^2 T}{\partial \theta^2} + \frac{1}{r^2} \frac{\partial}{\partial \mu} \left( (1 - \mu^2) \frac{\partial T}{\partial \mu} \right). \quad (2.4b)$$

## 2.2 Micro Heat Transfer

Micro heat transfer modeling is the study of the physical mechanism and mathematical modeling of heat transfer in micro scale. Reviews of micro heat transfer modeling can be seen in [11]-[16].

Micro heat transfer requires collisions among energy carriers. Micro heat transfer by two carriers (*Two-carrier system*), such as phonon-electron interaction in metal, has been well studied for many years. At the micro scale, the process of heat transfer is determined by phonon-electron interaction in metallic films and by phonon scattering in dielectric films, conductors and semiconductors [17]. The general properties of micro heat conduction in phonon-electron system can be found in [1]. A well studied

engineering example of the *Two*-carrier system is the micro heat transfer induced by ultrashort-pulsed lasers during the ultrafast transient [18]-[54].

### 2.2.1 Parabolic Model in a *Two*-carrier System in Cartesian Coordinates

The early version of the two-step model was developed by Kaganov *et al.* in 1957 [55] and by Anisimov *et al.* in 1974 [26]. Qiu and Tien developed the parabolic two-step model in 1992 [1], [2]. In the two-step model, the first step is the heating of electron gas, which can be expressed as

$$C_e \frac{\partial T_e}{\partial t} = k_e \nabla^2 T_e - G(T_e - T_l) + Q, \quad (2.5a)$$

and the second step is the heating of metal lattice, which can be expressed as

$$C_l \frac{\partial T_l}{\partial t} = G(T_e - T_l), \quad (2.5b)$$

where  $T$  is the temperature,  $C_e$  is the volumetric heat capacity for electron,  $C_l$  is the volumetric heat capacity for lattice,  $G$  is the phonon-electron coupling factor and  $k_e$  is the thermal conductivity of electron gas.

In the non-equilibrium heating in the electron-phonon system, which is different from macro heat transfer, the intensity of heat flow is proportional to the temperature difference between the electron and the phonon. To mathematically describe this phenomenon, a coupling factor  $G$  is defined, which is a thermophysical property of carriers in micro heat transfer.

There are applications of the two-step model in Cartesian coordinates, Eq. (2.5), to engineering problems. Wang *et al.* applied a two-dimensional parabolic two-step model to study micro heat transfer in a two-dimensional single-layered thin film exposed to ultrashort-pulsed laser in [14], [56]-[59]. Zhang *et al.* applied a 3D parabolic two-step

model to study micro heat transfer in a two-dimensional single-layered thin film exposed to ultrashort-pulsed laser in [16], [60], [61].

### 2.2.2 Parabolic Model in a *Two*-carrier System in Spherical Coordinates

A parabolic two-step model in a *Two*-carrier system in 3D spherical coordinates  $(r, \theta, \phi)$  is developed in [11], [12], [62], [63]

$$C_e \frac{\partial T_e}{\partial t} = \frac{k_e}{r^2} \frac{\partial}{\partial r} \left( r^2 \frac{\partial T}{\partial r} \right) + \frac{k_e}{r^2 \sin \phi} \frac{\partial}{\partial \phi} \left( \sin \phi \frac{\partial T}{\partial \phi} \right) + \frac{k_e}{r^2 \sin^2 \phi} \frac{\partial^2 T}{\partial \theta^2} - G(T_e - T_l) + Q, \quad (2.6a)$$

$$C_l \frac{\partial T_l}{\partial t} = G(T_e - T_l), \quad (2.6b)$$

where  $T$  is the temperature,  $C_e$  is the volumetric heat capacity for electron,  $C_l$  is the volumetric heat capacity for metal lattice,  $G$  is the coupling factor between phonon and electron and a positive constant, and  $k_e$  is the thermal conductivity of electron gas.

The parabolic two-step model in 3D spherical coordinates, Eq. (2.6), is applied to study a microsphere subjected to an ultrafast laser pulse [12], [63]. A parabolic two-step model in 3D spherical coordinates is developed in [11], [62] to study heat transfer in a microsphere exposed to ultrashort-pulsed lasers.

## 2.3 Previous Work

The  $N$ -carrier system is one of the latest developments of micro heat transfer modeling [3]-[7]. A brief review of current papers of the model in an  $N$ -carrier system is also discussed.

The following assumptions to the  $N$ -carrier system studied are: 1) there is perfect thermal contact among different energy carriers; 2) the coupling factor  $G_{mm}$  is only decided by the physical properties of the carrier; 3) heat convection and radiation is not considered; 4) and all  $N$ -carrier systems are stationary [3]-[7].

### 2.3.1 Parabolic Model in an $N$ -carrier System in Cartesian Coordinates

Tzou developed a parabolic model for a generalized  $N$ -carrier system [3]

$$C_1 \frac{\partial T_1(x,t)}{\partial t} = k_1 \frac{\partial^2 T_1(x,t)}{\partial x^2} - \sum_{m=2}^N G_{1m} [T_1(x,t) - T_m(x,t)] + Q_1(x,t), \quad (2.7a)$$

$$C_m \frac{\partial T_m(x,t)}{\partial t} = k_m \frac{\partial^2 T_m(x,t)}{\partial x^2} + \sum_{m_i=1}^{m-1} G_{m,m_i} [T_{m_i}(x,t) - T_m(x,t)] - \sum_{m_i=m+1}^N G_{mm_i} [T_m(x,t) - T_{m_i}(x,t)] + Q_m(x,t), \quad (2.7b)$$

$$C_N \frac{\partial T_N(x,t)}{\partial t} = k_N \frac{\partial^2 T_N(x,t)}{\partial x^2} + \sum_{m=1}^{N-1} G_{mN} [T_m(x,t) - T_N(x,t)] + Q_N(x,t), \quad (2.7c)$$

where  $T_m$  ( $m=1, \dots, N$ ) are the temperature of carriers,  $C_m$  ( $m=1, \dots, N$ ) are heat capacities and constants,  $k_m$  ( $m=1, \dots, N$ ) are conductivities and constants,  $G_{mm}$  are coupling factors between  $m$ -carrier and  $m_i$ -carrier and positive constants, and  $Q_m$  ( $m=1, \dots, N$ ) are heat sources. In Eq. (2.7), a positive sign denotes energy gain of the

system, and negative sign denotes energy loss from the system. Energy exchange among carriers in Eq. (2.7) can be seen in Figure 2.1 [3].

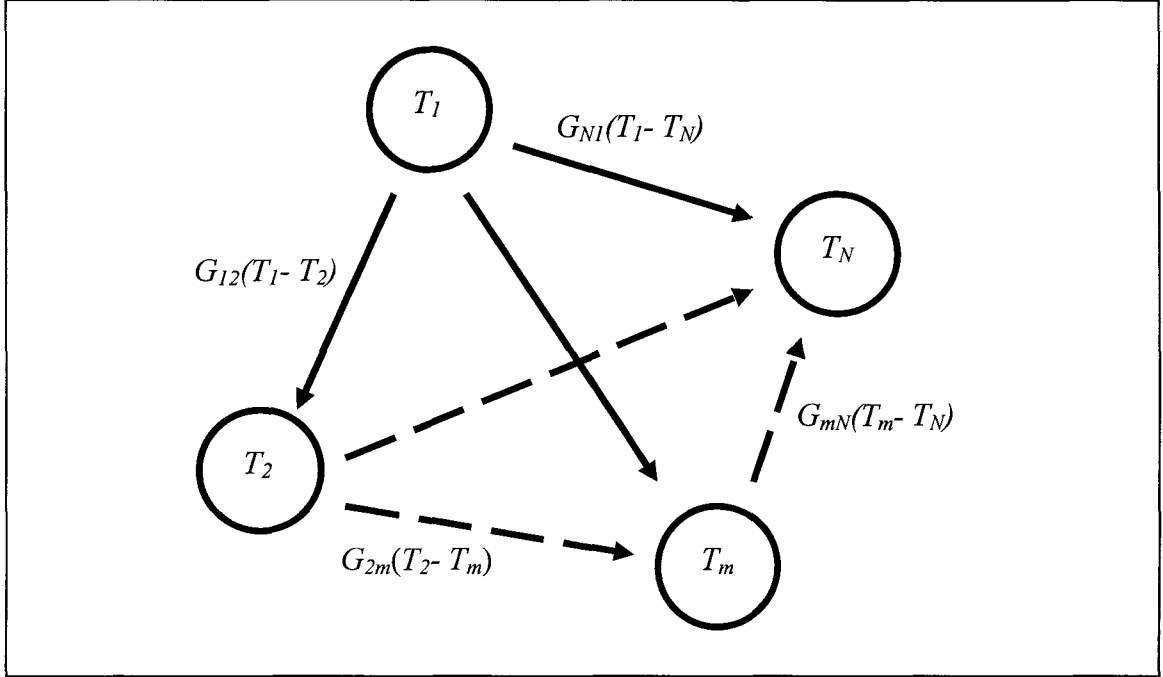


Figure 2.1 Energy exchanges in an  $N$ -carrier system.

If parabolic two-step models for the *Two*-carrier system and the  $N$ -carrier system are solved by finite difference schemes, the order of accuracy of the finite difference scheme depends on the quality of discretization of Laplace operator Eqs. (2.2) and (2.4). The fourth-order finite difference scheme for Laplace operator in Cartesian coordinates is developed in [4]:

$$\frac{1}{10}[(T_m)_{xx}]_{i-1} + [(T_m)_{xx}]_i + \frac{1}{10}[(T_m)_{xx}]_{i+1} = \frac{6}{5} \cdot \frac{[(T_m)_{i-1} - 2(T_m)_i + (T_m)_{i+1}]}{\Delta x^2}, \quad (2.8a)$$

$$\frac{11}{6}[(T_m)_{xx}]_1 - \frac{1}{3}[(T_m)_{xx}]_2 = \frac{[(T_m)_2 - (T_m)_1]}{\Delta x^2}, \quad (2.8b)$$

$$\frac{11}{6}[(T_m)_{xx}]_l - \frac{1}{3}[(T_m)_{xx}]_{l-1} = \frac{[(T_m)_{l-1} - (T_m)_l]}{\Delta x^2}, \quad (2.8c)$$

where  $T_m$  ( $m=1, \dots, N$ ) are the temperature of carriers.

In [4], the authors apply the fourth-order scheme for Laplace operator to the parabolic model in an  $N$ -carrier system in Cartesian coordinates. The stability of the fourth-order scheme in matrix form is proved by discrete energy method. A numerical example of a *Three*-carrier system in 1D Cartesian coordinates shows the match between numerical solution and exact solution with second-order accuracy.

### 2.3.2 Hyperbolic Model in an $N$ -carrier System in Cartesian Coordinates

Dai *et al.* develops a hyperbolic model for micro heat transfer of a generalized  $N$ -carrier system in [6]

$$C_1 \frac{\partial T_1(\bar{x}, t)}{\partial t} = -\nabla \cdot \bar{q}_1 - \sum_{m=2}^N G_{1m} [T_1(\bar{x}, t) - T_m(\bar{x}, t)] + Q_1(\bar{x}, t), \quad (2.9a)$$

$$\tau_1 \frac{\partial \bar{q}_1}{\partial t} + \bar{q}_1 = -k_1 \nabla T_1, \quad (2.9b)$$

$$C_m \frac{\partial T_m(\bar{x}, t)}{\partial t} = -\nabla \cdot \bar{q}_m + \sum_{m_1=1}^{m-1} G_{m, m_1} [T_{m_1}(\bar{x}, t) - T_m(\bar{x}, t)] \\ + \sum_{m_1=m+1}^N G_{m, m_1} [T_{m_1}(\bar{x}, t) - T_m(\bar{x}, t)] + Q_m(\bar{x}, t), \quad (2.9c)$$

$$\tau_m \frac{\partial \bar{q}_m}{\partial t} + \bar{q}_m = -k_m \nabla T_m, \quad (2.9e)$$

$$C_N \frac{\partial T_N(\bar{x}, t)}{\partial t} = -\nabla \cdot \bar{q}_N - \sum_{m=2}^N G_{mN} [T_m(\bar{x}, t) - T_N(\bar{x}, t)] + Q_N(\bar{x}, t), \quad (2.9f)$$

$$\tau_N \frac{\partial \bar{q}_N}{\partial t} + \bar{q}_N = -k_N \nabla T_N, \quad (2.9g)$$

where  $T_m(m=1, \dots, N)$  are temperatures,  $C_m(m=1, \dots, N)$  are heat capacities and constants,  $k_m(m=1, \dots, N)$  are conductivities and constants,  $G_{m_l}$  are coupling factors between  $m$ -carrier and  $m_l$  and positive constants,  $Q_m(m=1, \dots, N)$  are heat sources,  $\bar{q}_m$  are the heat fluxes associated with carriers respectively, and  $\tau_m$  are the relaxation time (the mean free time) for carriers.

Well-posedness of the hyperbolic model is proved. An improved CN scheme is developed, and the stability is proved in the paper. A numerical example of *Three*-carrier system in 1D Cartesian coordinates shows the match between numerical solution and exact solution with second-order accuracy.

## 2.4 Conclusion

Chapter Two discussed the background and previous work for this dissertation. Parabolic models and hyperbolic models for micro heat transfer models are reviewed. This dissertation will consider the parabolic model in an  $N$ -carrier system in 1D and 3D spherical coordinates, and develop an improved scheme to solve the model. The model can then be applied to study the heat transfer in biological cells.

## CHAPTER THREE

### MATHEMATICAL MODEL

The parabolic models in an  $N$ -carrier system in 1D and 3D spherical coordinates are developed in Chapter Three. The initial condition and the boundary condition of the two models are discussed. Also, the well-posedness of the two models is proved in Chapter Three.

#### 3.1 Governing Equations

##### 3.1.1 1D Case

Basing on the micro heat transfer in an  $N$ -carrier system Eq. (2.7) in [3], we develop a parabolic model in 1D spherical coordinates as follows:

$$C_1 \frac{\partial T_1(r,t)}{\partial t} = \frac{k_1}{r^2} \frac{\partial}{\partial r} \left( r^2 \frac{\partial T_1(r,t)}{\partial r} \right) - \sum_{m=2}^N G_{1m} [T_1(r,t) - T_m(r,t)] + Q_1(r,t), \quad (3.1a)$$

$$C_m \frac{\partial T_m(r,t)}{\partial t} = \frac{k_m}{r^2} \frac{\partial}{\partial r} \left( r^2 \frac{\partial T_m(r,t)}{\partial r} \right) + \sum_{m_i=1}^{m-1} G_{m,m_i} [T_{m_i}(r,t) - T_m(r,t)] - \sum_{m_i=m+1}^N G_{m,m_i} [T_m(r,t) - T_{m_i}(r,t)] + Q_m(r,t), \quad (3.1b)$$

$$C_N \frac{\partial T_N(r,t)}{\partial t} = \frac{k_N}{r^2} \frac{\partial}{\partial r} \left( r^2 \frac{\partial T_N(r,t)}{\partial r} \right) + \sum_{m=1}^{N-1} G_{mN} [T_m(r,t) - T_N(r,t)] + Q_N(r,t), \quad (3.1c)$$

where  $T_m$  are temperatures,  $C_m$  are heat capacities and constants,  $k_m$  are conductivities and constants,  $G_{mm_i}$  is the coupling factor between  $m$ -carrier and  $m_i$ -carrier and positive constants, and  $Q_m$  are heat sources.

To further increase accuracy, the initial condition is set as the exact solution of the model when

$$T_m(r, 0) = T_m^0(r), \quad m = 1, \dots, N. \quad (3.2)$$

Also, it is assumed that there is no heat loss in a very short time period, so the boundary condition for  $T_m$  at  $r = L$  is considered as

$$\frac{\partial T_m(L, t)}{\partial r} = 0, \quad m = 1, \dots, N, \quad (3.3)$$

where  $L$  is the right boundary of the radial distance  $r$ .

### 3.1.2 3D Case

Following the International Organization for Standards, the three coordinates  $(r, \theta, \phi)$  for 3D spherical coordinates are defined as follows: for a point in 3D spherical coordinates, the radial distance  $r$ , ranging  $0 \leq r \leq 1$ , is the distance between the point and the origin, the zenith angle  $\theta$ , ranging  $0 \leq \theta \leq 2\pi$ , is the angle between the point and the positive  $z$ -axis, and the azimuth angle  $\phi$  ranging  $0 \leq \phi < \pi$ , is the angle between the point and the positive  $x$ -axis.

In order to analyze the micro non-equilibrium heating in 3D spherical coordinates, similar to Eq. (3.1), parabolic model in an  $N$ -carrier system is developed as:

$$C_1 \frac{\partial T_1(r, \theta, \mu, t)}{\partial t} = \frac{k_1}{r^2} \frac{\partial}{\partial r} \left( r^2 \frac{\partial T_1(r, \theta, \mu, t)}{\partial r} \right)$$

$$\begin{aligned}
& + \frac{k_1}{r^2(1-\mu^2)} \frac{\partial^2 T_1(r, \theta, \mu, t)}{\partial \theta^2} + \frac{k_1}{r^2} \frac{\partial}{\partial \mu} \left( (1-\mu^2) \frac{\partial T_1(r, \theta, \mu, t)}{\partial \mu} \right) \\
& - \sum_{m=2}^N G_{1m} [T_1(r, \theta, \mu, t) - T_m(r, \theta, \mu, t)] + Q_1(r, \theta, \mu, t), \tag{3.4a}
\end{aligned}$$

$$\begin{aligned}
C_m \frac{\partial T_m(r, \theta, \mu, t)}{\partial t} & = \frac{k_m}{r^2} \frac{\partial}{\partial r} \left( r^2 \frac{\partial T_m(r, \theta, \mu, t)}{\partial r} \right) + \frac{k_m}{r^2(1-\mu^2)} \frac{\partial^2 T_m(r, \theta, \mu, t)}{\partial \theta^2} \\
& + \frac{k_m}{r^2} \frac{\partial}{\partial \mu} \left( (1-\mu^2) \frac{\partial T_m(r, \theta, \mu, t)}{\partial \mu} \right) + \sum_{m_i=1}^{m-1} G_{m,m_i} [T_{m_i}(r, \theta, \mu, t) - T_m(r, \theta, \mu, t)] \\
& - \sum_{m_i=m+1}^N G_{mm_i} [T_m(r, \theta, \mu, t) - T_{m_i}(r, \theta, \mu, t)] + Q_m(r, \theta, \mu, t), \tag{3.4b}
\end{aligned}$$

$$\begin{aligned}
C_N \frac{\partial T_N(r, \theta, \mu, t)}{\partial t} & = \frac{k_N}{r^2} \frac{\partial}{\partial r} \left( r^2 \frac{\partial T_N(r, \theta, \mu, t)}{\partial r} \right) \\
& + \frac{k_N}{r^2(1-\mu^2)} \frac{\partial^2 T_N(r, \theta, \mu, t)}{\partial \theta^2} + \frac{k_N}{r^2} \frac{\partial}{\partial \mu} \left( (1-\mu^2) \frac{\partial T_N(r, \theta, \mu, t)}{\partial \mu} \right) \\
& + \sum_{m=1}^{N-1} G_{mN} [T_m(r, \theta, \mu, t) - T_N(r, \theta, \mu, t)] + Q_N(r, \theta, \mu, t), \tag{3.4c}
\end{aligned}$$

where  $0 \leq r \leq L, 0 \leq \theta \leq 2\pi$  and  $\mu = \cos \phi$  with  $0 \leq \phi \leq \pi$ ,  $T_m$  are temperatures,  $C_m$  are heat capacities and constants,  $k_m$  are conductivities and constants,  $G_{mm_i}$  is the coupling factor between  $m$ -carrier and  $m_i$ -carrier and positive constants, and  $Q_m$  are heat sources.

To further increase accuracy, the initial condition is set as the exact solution of the model when  $t = 0$

$$T_m(r, \theta, \mu, 0) = T_m^0(r, \theta, \mu), m = 1, \dots, N. \tag{3.5}$$

It is assumed that there is no heat loss in a very short time period, so the boundary condition for  $T_m$  at  $r = L$  is considered as:

$$\frac{\partial T_m(L, \theta, \mu, t)}{\partial r} = 0, m = 1, \dots, N, \quad (3.6a)$$

where  $L$  is the right boundary of the radial distance  $r$ . Also, it is assumed that:

$$T_m(r, \theta, \mu, t) = T_m(r, \theta + 2\pi, \mu, t), \quad (3.6b)$$

$$T_m(r, \theta, -1, t) = T_m(r, \theta, 1, t) = 0. \quad (3.6c)$$

## 3.2 Well-posedness

### 3.2.1 1D Case

Section 3.2.1 proves the well-posedness of the parabolic model in an  $N$ -carrier system in 1D spherical coordinates Eq. (3.1). Proof is offered that there is a solution for the parabolic model in an  $N$ -carrier system in 1D spherical coordinates. The solution is uniquely decided by the initial condition Eq. (3.2), and the solution depends on the initial condition continuously [64].

In order to simplify the proof of the well-posedness of the parabolic model in an  $N$ -carrier system in 1D spherical coordinates, it is assumed that coefficients  $C_m$  are positive constants, coefficients  $k_m$  are positive constants and the solution  $T_m$  of the parabolic model in an  $N$ -carrier system in 1D spherical coordinates continuously depends on the initial condition.

**Theorem 1.** The parabolic model in an  $N$ -carrier system in 1D spherical coordinates Eq. (3.1) is well-posed with respect to the initial condition Eq. (3.2) and heat source terms.

*Proof.* To analyze the well-posedness of the generalized micro heat transfer model in 1D spherical coordinates for non-equilibrium heating in an  $N$ -carrier system in 1D spherical coordinates, multiplying Eq. (3.1a) by  $r^2 T_1(r, t)$ , Eq. (3.1b) by  $r^2 T_m(r, t)$  and Eq. (3.1c)

by  $r^2 T_N(r, t)$ , summing together over  $m = 2, \dots, N-1$ , rearranging the equation, this gives:

$$\begin{aligned} \sum_{m=1}^N C_m \frac{\partial T_m(r, t)}{\partial t} r^2 T_m(r, t) &= \sum_{m=1}^N k_m \frac{\partial}{\partial r} \left( r^2 \frac{\partial T_m(r, t)}{\partial r} \right) T_m(r, t) \\ &- \sum_{\substack{m, m_1=1 \\ m < m_1}}^N G_{mm_1} [T_m(r, t) - T_{m_1}(r, t)] r^2 T_m(r, t) + \sum_{m=1}^N Q_m(r, t) r^2 T_m(r, t) dr. \end{aligned} \quad (3.7)$$

Integrating both sides of Eq. (3.7) over the interval  $1 \leq r \leq L$  results in

$$\begin{aligned} \int_0^L \sum_{m=1}^N C_m \frac{\partial T_m(r, t)}{\partial t} r^2 T_m(r, t) dr &= \int_0^L \sum_{m=1}^N k_m \frac{\partial}{\partial r} \left( r^2 \frac{\partial T_m(r, t)}{\partial r} \right) T_m(r, t) dr \\ &- \int_0^L \sum_{\substack{m, m_1=1 \\ m < m_1}}^N G_{mm_1} [T_m(r, t) - T_{m_1}(r, t)] r^2 T_m(r, t) dr + \int_0^L \sum_{m=1}^N Q_m(r, t) r^2 T_m(r, t) dr. \end{aligned} \quad (3.8)$$

The term on the left-hand-side (LHS) of Eq. (3.8) can be written as:

$$\int_0^L \sum_{m=1}^N C_m \frac{\partial T_m(r, t)}{\partial t} T_m(r, t) r^2 dr = \frac{\partial}{\partial t} \left( \frac{1}{2} \int_0^L C_m T_m^2(r, t) r^2 dr \right). \quad (3.9)$$

Applying integration by parts (Green's Theorem:  $\iint_D (\Delta f g - f \Delta g) dA = \int_C \left( \frac{\partial f}{\partial n} g - \frac{\partial g}{\partial n} f \right) dS$ )

and the boundary condition Eq. (3.3), the first term of right-hand-side (RHS) of Eq. (3.9)

can be simplified to

$$\begin{aligned} &\int_0^L \sum_{m=1}^N k_m \frac{\partial}{\partial r} \left( r^2 \frac{\partial T_m(r, t)}{\partial r} \right) T_m(r, t) dr \\ &= - \int_0^L \sum_{m=1}^N k_m r^2 \left( \frac{\partial T_m(r, t)}{\partial r} \right)^2 dr + \sum_{m=1}^N k_m r^2 \frac{\partial T_m(r, t)}{\partial r} T_m(r, t) \Big|_0^L \\ &= -k_m \int_0^L \sum_{m=1}^N r^2 \left( \frac{\partial T_m(r, t)}{\partial r} \right)^2 dr. \end{aligned} \quad (3.10)$$

Substituting Eqs. (3.9) and (3.10) into Eq. (3.8), multiplying the result by 2 leads to

$$\begin{aligned} & \frac{\partial}{\partial t} \left( \int_0^L \sum_{m=1}^N C_m T_m^2(r, t) r^2 dr \right) + 2k_m \int_0^L \sum_{m=1}^N r^2 \left( \frac{\partial T_m(r, t)}{\partial r} \right)^2 dr \\ & + 2 \int_0^L \sum_{\substack{m, m_1=1 \\ m < m_1}}^N G_{mm_1} [T_m(r, t) - T_{m_1}(r, t)] r^2 T_m(r, t) = 2 \int_0^L \sum_{m=1}^N Q_m(r, t) r^2 T_m(r, t) dr. \end{aligned} \quad (3.11)$$

After the non-negative term in LHS of Eq. (3.11) is dropped, the result is

$$\frac{\partial}{\partial t} \left( \int_0^L \sum_{m=1}^N C_m T_m^2(r, t) r^2 dr \right) \leq 2 \int_0^L \sum_{m=1}^N Q_m(r, t) r^2 T_m(r, t) dr. \quad (3.12)$$

Using Cauchy-Schwartz's inequality ( $2ab \leq \varepsilon a^2 + \frac{1}{\varepsilon} b^2$  for  $\varepsilon > 0$ ) results in

$$2 \int_0^L \sum_{m=1}^N Q_m(r, t) T_m(r, t) r^2 dr \leq \int_0^L \sum_{m=1}^N C_m T_m^2(r, t) r^2 dr + \int_0^L \sum_{m=1}^N \frac{1}{C_m} Q_m^2(r, t) r^2 dr. \quad (3.13)$$

Linking Eq. (3.12) and Eq. (3.13) provides a result of

$$\begin{aligned} & \frac{\partial}{\partial t} \left( \int_0^L \sum_{m=1}^N C_m T_m^2(r, t) r^2 dr \right) \\ & \leq \int_0^L \sum_{m=1}^N C_m T_m^2(r, t) r^2 dr + \int_0^L \sum_{m=1}^N \frac{1}{C_m} Q_m^2(r, t) r^2 dr. \end{aligned} \quad (3.14)$$

Letting

$$F(t) = \int_0^L \sum_{m=1}^N C_m T_m^2(r, t) r^2 dr \quad (3.15a)$$

and

$$\Phi(t) = \int_0^L \sum_{m=1}^N \frac{1}{C_m} Q_m^2(r, t) r^2 dr, \quad (3.15b)$$

and substituting Eqs. (3.15a) and (3.15b) into Eq. (3.14) leads to

$$\frac{\partial F(t)}{\partial t} \leq F(t) + \Phi(t). \quad (3.16)$$

Integrating Eq. (3.16) with respect to  $t$  results in

$$\int_0^t \frac{\partial F(s)}{\partial s} ds \leq \int_0^t F(s) ds + \int_0^t \Phi(s) ds, \quad (3.17)$$

that is,

$$F(t) - F(0) \leq \int_0^t F(s) ds + \int_0^t \Phi(s) ds. \quad (3.18)$$

Using Gronwall's lemma [64] (If  $\Omega(t) \geq 0$  and  $\psi(t) \geq 0$  are continuous function

such that  $\Omega(t) \leq Z_1 + Z_2 \int_t^t \psi(s) \Omega(s) ds$  holds for all  $t$  in  $[t, t_u]$ , where  $Z_1$  and  $Z_2$  are

positive constants, then  $\Omega(t) \leq Z_1 \exp\left(Z_2 \int_t^t \psi(s) ds\right)$  holds for all  $t$  in  $[t, t_u]$ ) provides

for any time  $t$  on  $0 \leq t \leq t_0$ ,

$$F(t) \leq \int_0^t 1 \cdot F(s) ds + \left[ F(0) + \int_0^t \Phi(s) ds \right] \leq e^t \left[ F(0) + \int_0^t \Phi(s) ds \right]. \quad (3.19)$$

Finally, substituting Eqs. (3.15a) and (3.15b) back into Eq. (3.19) results in an energy estimate for the  $N$ -carrier system in 1D spherical coordinates as follows:

$$\begin{aligned} & \int_0^L \sum_{m=1}^N C_m T_m^2(r, t) r^2 dr \\ & \leq e^t \left[ \int_0^L \sum_{m=1}^N C_m T_m^2(r, 0) r^2 dr + \int_0^t \int_0^L \sum_{m=1}^N \frac{1}{C_m} Q_m^2(r, t) r^2 dr \right], \end{aligned} \quad (3.20)$$

where  $0 \leq t \leq t_0$ , that is, the solution of the parabolic model in an  $N$ -carrier system in 1D spherical coordinates, Eq. (3.1), is unique and is continuously dependent on the initial

condition and heat source terms, implying that the parabolic model in an  $N$ -carrier system in 1D spherical coordinates is well-posed. ■

### 3.2.2 3D Case

This section will prove the well-posedness of the parabolic model in an  $N$ -carrier system in 3D spherical coordinates Eq. (3.4). Before proving that the parabolic model in an  $N$ -carrier system in 3D spherical coordinates is well-posed, the coefficients  $C_m$  are positive constants, the coefficients  $k_m$  are positive constants and the solutions  $T_m(r, \theta, \mu, t)$  of the parabolic model in an  $N$ -carrier system in 3D spherical coordinates continuously depend on the initial condition are assumed.

**Theorem 2.** The parabolic model in an  $N$ -carrier system in 3D spherical coordinates Eq. (3.4) is well-posed with respect to the initial condition Eq (3.5) and heat source terms.

*Proof.* To analyze the well-posedness of the parabolic model in an  $N$ -carrier system in 3D spherical coordinates, multiplying Eq. (3.4a) by  $r^2 T_1(r, \theta, \mu, t)$ , Eq. (3.4b) by  $r^2 T_m(r, \theta, \mu, t)$  and Eq. (3.4c) by  $r^2 T_N(r, \theta, \mu, t)$ , then summing together over  $m = 2, \dots, N-1$  and rearranging the equation, this gives:

$$\begin{aligned}
& \sum_{m=1}^N C_m \frac{\partial T_m(r, \theta, \mu, t)}{\partial t} r^2 T_m(r, \theta, \mu, t) = \sum_{m=1}^N T_m(r, \theta, \mu, t) k_m \frac{\partial}{\partial r} \left( r^2 \frac{\partial T_m(r, \theta, \mu, t)}{\partial r} \right) \\
& + \sum_{m=1}^N k_m \frac{1}{(1-\mu^2)} \frac{\partial^2 T_m(r, \theta, \mu, t)}{\partial \theta^2} T_m(r, \theta, \mu, t) + \sum_{m=1}^N k_m \frac{\partial}{\partial \mu} \left( (1-\mu^2) \frac{\partial T_m(r, \theta, \mu, t)}{\partial \mu} \right) T_m(r, \theta, \mu, t) \\
& \quad + \sum_{\substack{m, m_1=1 \\ m < m_1}}^N G_{mm_1} [T_m(r, \theta, \mu, t) - T_{m_1}(r, \theta, \mu, t)] r^2 T_m(r, \theta, \mu, t) \\
& \quad + \sum_{m=1}^N Q_m(r, \theta, \mu, t) r^2 T_m(r, \theta, \mu, t). \tag{3.21}
\end{aligned}$$

Integrating both sides of Eq. (3.21) over all governing equations in  $1 \leq r \leq L$ ,  $1 \leq \theta \leq 2\pi$  and  $-1 \leq \mu \leq 1$ , this gives:

$$\begin{aligned}
& \int_{-1}^1 \int_0^{2\pi} \int_0^L \sum_{m=1}^N C_m \frac{\partial T_m(r, \theta, \mu, t)}{\partial t} r^2 T_m(r, \theta, \mu, t) dr d\theta d\mu \\
&= \int_{-1}^1 \int_0^{2\pi} \int_0^L \sum_{m=1}^N k_m \frac{\partial}{\partial r} \left( r^2 \frac{\partial T_m(r, \theta, \mu, t)}{\partial r} \right) T_m(r, \theta, \mu, t) dr d\theta d\mu \\
&+ \int_{-1}^1 \int_0^{2\pi} \int_0^L \sum_{m=1}^N \frac{k_m}{(1-\mu^2)} \frac{\partial^2 T_m(r, \theta, \mu, t)}{\partial \theta^2} T_m(r, \theta, \mu, t) dr d\theta d\mu \\
&+ \int_{-1}^1 \int_0^{2\pi} \int_0^L \sum_{m=1}^N k_m \frac{\partial}{\partial \mu} \left( (1-\mu^2) \frac{\partial T_m(r, \theta, \mu, t)}{\partial \mu} \right) T_m(r, \theta, \mu, t) dr d\theta d\mu \\
&+ \int_{-1}^1 \int_0^{2\pi} \int_0^L \sum_{\substack{m, m_1=1 \\ m < m_1}}^N G_{mm_1} [T_m(r, \theta, \mu, t) - T_{m_1}(r, \theta, \mu, t)] r^2 T_m(r, \theta, \mu, t) dr d\theta d\mu \\
&+ \int_{-1}^1 \int_0^{2\pi} \int_0^L \sum_{m=1}^N Q_m(r, \theta, \mu, t) r^2 T_m(r, \theta, \mu, t) dr d\theta d\mu. \tag{3.22}
\end{aligned}$$

The term on the LHS of Eq. (3.22) can be written as:

$$\begin{aligned}
& \int_{-1}^1 \int_0^{2\pi} \int_0^L \sum_{m=1}^N C_m \frac{\partial T_m(r, \theta, \mu, t)}{\partial t} T_m(r, \theta, \mu, t) r^2 dr d\theta d\mu \\
&= \frac{\partial}{\partial t} \left( \int_{-1}^1 \int_0^{2\pi} \int_0^L \sum_{m=1}^N C_m \frac{T_m^2(r, \theta, \mu, t)}{2} r^2 dr d\theta d\mu \right). \tag{3.23}
\end{aligned}$$

By Green's Theorem (  $\iint_D (\Delta f g - f \Delta g) dA = \int_C \left( \frac{\partial f}{\partial n} g - \frac{\partial g}{\partial n} f \right) dS$  ) and the boundary

condition Eq. (3.6), the first term of RHS of Eq. (3.23) can be simplified as:

$$\int_{-1}^1 \int_0^{2\pi} \int_0^L \sum_{m=1}^N k_m \frac{\partial}{\partial r} \left( r^2 \frac{\partial T_m(r, \theta, \mu, t)}{\partial r} \right) T_m(r, \theta, \mu, t) dr d\theta d\mu$$

$$= -\int_{-1}^1 \int_0^{2\pi} \int_0^L \sum_{m=1}^N k_m r^2 \left( \frac{\partial T_m(r, \theta, \mu, t)}{\partial r} \right)^2 dr d\theta d\mu. \quad (3.24a)$$

Similarly, the second and third terms on the RHS of Eq. (3.23) can be simplified as follows:

$$\begin{aligned} & \int_{-1}^1 \int_0^{2\pi} \int_0^L \sum_{m=1}^N \frac{k_m}{(1-\mu^2)} \frac{\partial^2 T_m(r, \theta, \mu, t)}{\partial \theta^2} T_m(r, \theta, \mu, t) dr d\theta d\mu \\ &= -\int_{-1}^1 \int_0^{2\pi} \int_0^L \sum_{m=1}^N \frac{k_m}{(1-\mu^2)} \left( \frac{\partial T_m(r, \theta, \mu, t)}{\partial \theta} \right)^2 dr d\theta d\mu \end{aligned} \quad (3.24b)$$

and

$$\begin{aligned} & \int_{-1}^1 \int_0^{2\pi} \int_0^L \sum_{m=1}^N k_m \frac{\partial}{\partial \mu} \left( (1-\mu^2) \frac{\partial T_m(r, \theta, \mu, t)}{\partial \mu} \right) T_m(r, \theta, \mu, t) dr d\theta d\mu \\ &= -\int_{-1}^1 \int_0^{2\pi} \int_0^L \sum_{m=1}^N k_m (1-\mu^2) \left( \frac{\partial T_m(r, \theta, \mu, t)}{\partial \mu} \right)^2 dr d\theta d\mu. \end{aligned} \quad (3.24c)$$

Substituting Eqs. (3.23) and (3.24) into Eq. (3.22), multiplying both sides by 2 and rearranging, this gives:

$$\begin{aligned} & \frac{\partial}{\partial t} \left( \int_{-1}^1 \int_0^{2\pi} \int_0^L \sum_{m=1}^N C_m T_m^2(r, \theta, \mu, t) r^2 dr d\theta d\mu \right) + 2 \int_{-1}^1 \int_0^{2\pi} \int_0^L \sum_{m=1}^N k_m r^2 \left( \frac{\partial T_m(r, \theta, \mu, t)}{\partial r} \right)^2 dr d\theta d\mu \\ & + 2 \int_{-1}^1 \int_0^{2\pi} \int_0^L \sum_{m=1}^N \frac{k_m}{(1-\mu^2)} \left( \frac{\partial T_m(r, \theta, \mu, t)}{\partial \theta} \right)^2 dr d\theta d\mu \\ & + 2 \int_{-1}^1 \int_0^{2\pi} \int_0^L \sum_{m=1}^N k_m (1-\mu^2) \left( \frac{\partial T_m(r, \theta, \mu, t)}{\partial \mu} \right)^2 dr d\theta d\mu \\ & + 2 \int_{-1}^1 \int_0^{2\pi} \int_0^L \sum_{\substack{m, m_1=1 \\ m < m_1}}^N G_{mm_1} [T_m(r, \theta, \mu, t) - T_{m_1}(r, \theta, \mu, t)]^2 r^2 dr d\theta d\mu \\ & = 2 \int_{-1}^1 \int_0^{2\pi} \int_0^L \sum_{m=1}^N Q_m r^2 T_m(r, \theta, \mu, t) dr d\theta d\mu. \end{aligned} \quad (3.25)$$

After the non-negative term in LHS of Eq. (3.25) is dropped,

$$\frac{\partial}{\partial t} \left( \int_{-1}^1 \int_0^{2\pi} \int_0^L \sum_{m=1}^N C_m T_m^2(r, \theta, \mu, t) r^2 dr d\theta d\mu \right) \leq 2 \int_{-1}^1 \int_0^{2\pi} \int_0^L \sum_{m=1}^N Q_m r^2 T_m(r, \theta, \mu, t) dr d\theta d\mu \quad (3.26)$$

is obtained. Using Cauchy-Schwartz's inequality ( $2ab \leq \varepsilon a^2 + \frac{1}{\varepsilon} b^2$  for  $\varepsilon > 0$ ) results in

$$\begin{aligned} & 2 \int_{-1}^1 \int_0^{2\pi} \int_0^L \sum_{m=1}^N Q_m r^2 T_m(r, \theta, \mu, t) dr d\theta d\mu \\ & \leq \int_{-1}^1 \int_0^{2\pi} \int_0^L \sum_{m=1}^N C_m T_m^2(r, \theta, \mu, t) r^2 dr d\theta d\mu + \int_{-1}^1 \int_0^{2\pi} \int_0^L \sum_{m=1}^N \frac{1}{C_m} Q_m^2(r, \theta, \mu, t) r^2 dr d\theta d\mu. \quad (3.27) \end{aligned}$$

Substituting Eq. (3.26) into Eq. (3.27) leads to

$$\begin{aligned} & \frac{\partial}{\partial t} \left( \int_{-1}^1 \int_0^{2\pi} \int_0^L \sum_{m=1}^N C_m T_m^2(r, \theta, \mu, t) r^2 dr d\theta d\mu \right) \\ & \leq \int_{-1}^1 \int_0^{2\pi} \int_0^L \sum_{m=1}^N C_m T_m^2(r, \theta, \mu, t) r^2 dr d\theta d\mu + \int_{-1}^1 \int_0^{2\pi} \int_0^L \sum_{m=1}^N \frac{1}{C_m} Q_m^2(r, \theta, \mu, t) r^2 dr d\theta d\mu. \quad (3.28) \end{aligned}$$

Denoting

$$F(t) = \int_{-1}^1 \int_0^{2\pi} \int_0^L \sum_{m=1}^N C_m T_m^2(r, \theta, \mu, t) r^2 dr d\theta d\mu \quad (3.29a)$$

and

$$\Phi(t) = \int_{-1}^1 \int_0^{2\pi} \int_0^L \sum_{m=1}^N \frac{1}{C_m} Q_m^2(r, \theta, \mu, t) r^2 dr d\theta d\mu, \quad (3.29b)$$

substituting Eqs. (3.28) and (3.29) into Eq. (3.27), and integrating both sides with respect to  $t$  provides:

$$F(t) - F(0) \leq \int_0^t F(s) ds + \int_0^t \Phi(s) ds. \quad (3.30)$$

Using Gronwall's lemma [64], results in for any time  $t$  in  $[0, t_0]$  leads to

$$F(t) \leq \int_0^t 1 \times F(s) ds + \left[ F(0) + \int_0^t \Phi(s) ds \right] \leq e^t \left[ F(0) + \int_0^t \Phi(s) ds \right]. \quad (3.31)$$

Finally, substituting Eqs. (3.29a) and (3.29b) back into Eq. (3.31) results in

$$\begin{aligned} & \int_{-1}^1 \int_0^{2\pi} \int_0^L \sum_{m=1}^N C_m T_m^2(r, \theta, \mu, t) r^2 dr d\theta d\mu \\ & \leq e^{t_0} \left( \int_{-1}^1 \int_0^{2\pi} \int_0^L \sum_{m=1}^N C_m T_m^2(r, \theta, \mu, 0) r^2 dr d\theta d\mu + \int_0^{t_0} \int_{-1}^1 \int_0^{2\pi} \int_0^L \sum_{m=1}^N \frac{1}{C_m} Q_m^2(r, \theta, \mu, t) r^2 dr d\theta d\mu \right), \end{aligned}$$

that is, the solution to the parabolic model in an  $N$ -carrier system in 3D spherical coordinates is unique and is continuously dependent on the initial condition and heat sources, implying that the parabolic model in an  $N$ -carrier system in 3D spherical coordinates is well-posed. ■

## CHAPTER FOUR

### NUMERICAL METHOD

Improved CN schemes for solving the model in 1D and 3D spherical coordinates are developed in Chapter Four. The stability of improved CN schemes is proved in this chapter. Also provided are general algorithms as the solver for the linear system from the improved schemes.

#### 4.1 Finite Difference Schemes

##### 4.1.1 1D Improved CN Scheme

To develop a finite difference scheme,  $(T_m)_i^n$  is denoted as the numerical approximation of  $(T_m)(i\Delta r)$ , where  $\Delta r$  and  $\Delta t$  are the  $r$  - directional spatial and temporal mesh sizes, respectively, and  $r_i = i\Delta r$ ,  $0 \leq i \leq I+1$ , that  $(I+1)\Delta r = L$ . Also, to briefly describe the 1D improved CN scheme, the following difference operators are defined:

$$P_r \left\{ (T_m)_i^n \right\} = r_{i+\frac{1}{2}}^2 \frac{(T_m)_{i+1}^n - (T_m)_i^n}{\Delta r^2} - r_{i-\frac{1}{2}}^2 \frac{(T_m)_i^n - (T_m)_{i-1}^n}{\Delta r^2}, \quad (4.1a)$$

$$W_i \left[ (T_m)_i^n \right] = \frac{(T_m)_i^{n+1} + (T_m)_i^n}{2}. \quad (4.1b)$$

The generalized micro heat transfer model, Eq. (3.1), can be solved using the well-known second-order accurate and unconditionally stable CN scheme as follows:

$$C_1 \frac{(T_1)_i^{n+1} - (T_1)_i^n}{\Delta t} = \frac{k_1}{r_i^2} P_r \left\{ W_t \left[ (T_1)_i^n \right] \right\} - \sum_{m=2}^N G_{1m} \left\{ W_t \left[ (T_1)_i^n \right] - W_t \left[ (T_m)_i^n \right] \right\} + (Q_1)_m^{n+\frac{1}{2}}, \quad (4.2a)$$

$$C_m \frac{(T_m)_i^{n+1} - (T_m)_i^n}{\Delta t} = \frac{k_m}{r_i^2} P_r \left\{ W_t \left[ (T_m)_i^n \right] \right\} + \sum_{m_1=1}^{m-1} G_{m,m_1} \left\{ W_t \left[ (T_{m_1})_i^n \right] - W_t \left[ (T_m)_i^n \right] \right\} - \sum_{m_2=m+1}^N G_{m,m_2} \left\{ W_t \left[ (T_{m_2})_i^n \right] - W_t \left[ (T_m)_i^n \right] \right\} + (Q_m)_i^{n+\frac{1}{2}}, \quad (4.2b)$$

$$C_N \frac{(T_N)_i^{n+1} - (T_N)_i^n}{\Delta t} = \frac{k_N}{r_i^2} P_r \left\{ W_t \left[ (T_N)_i^n \right] \right\} + \sum_{m=1}^{N-1} G_{mN} \left\{ W_t \left[ (T_m)_i^n \right] - W_t \left[ (T_N)_i^n \right] \right\} + (Q_N)_i^{n+\frac{1}{2}}. \quad (4.2c)$$

To develop a numerical scheme, one usually adds a 1D fictitious boundary condition at the spherical center,  $r = 0$ ,

$$\frac{\partial T_m(0, t)}{\partial r} = 0, \quad m = 1, \dots, N.$$

The boundary condition Eq. (3.3) and the 1D fictitious boundary condition can be discretized by the conventional first-order method as [65]

$$(T_m)_0^n = (T_m)_1^n \quad (4.3a)$$

$$(T_m)_{I+1}^n = (T_m)_I^n. \quad (4.3b)$$

However, the above numerical scheme provides only first-order accuracy with respect to the spatial variable  $r$ , which can be seen in the numerical example in Chapter Five.

The reason why the problem happens is probably the conventional method Eq. (4.3) is a first-order approximation of the Neumann boundary condition Eq. (3.3), although the CN scheme Eq. (4.2) has second-order accuracy. Furthermore, the discretization for the boundary condition Eq. (4.3) needs an additional point for the boundary. Thus, as one of contributions of this dissertation, the conventional method Eq. (4.3) is improved to second-order accuracy. This method shows advantages especially when  $L$  is in micro scale.

A 1D second-order scheme for the boundary condition, Eq. (3.3) and 1D fictitious boundary condition, is obtained by firstly designing a mesh, where the distance between the spherical center  $r = 0$  and the actual left boundary  $r_l$  is set as  $\beta_1 \Delta r$  and the distance between the spherical boundary  $r = L$  and the actual right boundary  $r_r$  is set as  $\beta_2 \Delta r$ , as shown in Figure 4.1.

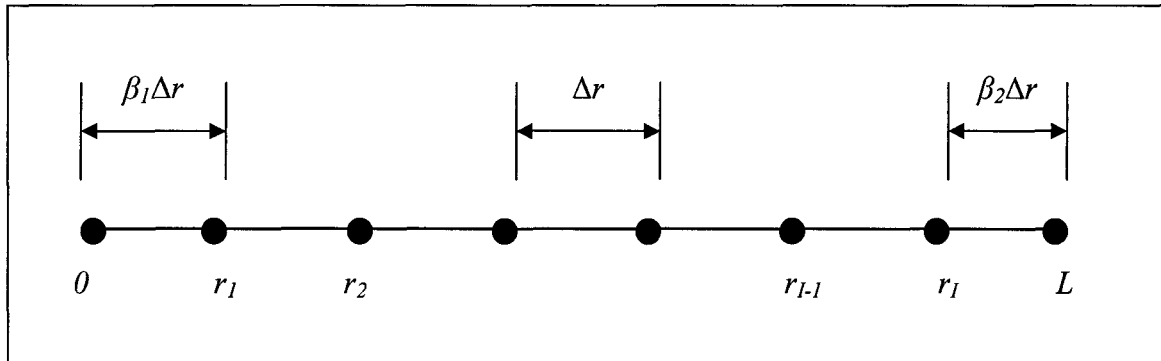


Figure 4.1 Mesh and locations of grid points of the 1D improved CN scheme in spherical coordinates.

The finite difference approximation of  $\frac{\partial}{\partial r} \left( r^2 \frac{\partial T_m(r,t)}{\partial r} \right)$  at the left boundary  $r_l$

is obtained as follows:

$$\begin{aligned}
& b \frac{\partial}{\partial r} \left( r^2 \frac{\partial T_m(r,t)}{\partial r} \right)_1 \\
&= \frac{a}{\Delta r^2} r_{\frac{3}{2}}^2 [T_m(r_2,t) - T_m(r_1,t)] - \frac{1}{\Delta r} r_1^2 \frac{\partial T_m(r_1 - \beta_1 \Delta r, t)}{\partial r}, \tag{4.4}
\end{aligned}$$

where  $a, b, \beta_1$  are constants to be determined and  $r_{\frac{3}{2}} = r_1 + \frac{\Delta r}{2}$ . Expressing each term of

LHS and RHS of Eq. (4.4) into Taylor series at  $r_l$  shows:

$$LHS = br_1^2 (T_m)_{rr}(r_1, t) + 2br_1 (T_m)_r(r_1, t)$$

and

$$\begin{aligned}
RHS &= \frac{a}{\Delta r^2} r_{\frac{3}{2}}^2 \left[ \Delta r (T_m)_r(r_1, t) + \frac{\Delta r^2}{2} (T_m)_{rr}(r_1, t) + \frac{\Delta r^3}{6} (T_m)_{r,r}(r_1, t) \right] \\
&- \frac{1}{\Delta r} r_1^2 \left[ (T_m)_r(r_1, t) - \beta_1 \Delta r (T_m)_{rr}(r_1, t) + \frac{\beta_1^2 \Delta r^2}{2} (T_m)_{r,r}(r_1, t) \right] + O(\Delta r^2) \\
&= \frac{1}{\Delta r} \left[ ar_{\frac{3}{2}}^2 - r_1^2 \right] (T_m)_r(r_1, t) + \left[ \frac{a}{2} r_{\frac{3}{2}}^2 + r_1^2 \beta_1 \right] (T_m)_{rr}(r_1, t) \\
&\quad + \frac{\Delta r}{2} \left[ \frac{a}{3} r_{\frac{3}{2}}^2 - r_1^2 \beta_1^2 \right] (T_m)_{r,r}(r_1, t) + O(\Delta r^2).
\end{aligned}$$

Matching LHS and RHS above, the following equations are obtained:

$$\frac{1}{\Delta r} \left( ar_{\frac{3}{2}}^2 - r_1^2 \right) = 2br_1, \tag{4.5a}$$

$$\frac{a}{2} r_{\frac{3}{2}}^2 + r_1^2 \beta_1 = br_1^2, \tag{4.5b}$$

$$\frac{a}{3} r_{\frac{3}{2}}^2 - r_1^2 \beta_1^2 = 0. \tag{4.5c}$$

Dividing Eq. (4.5a) by Eq. (4.5b) and then replacing  $ar_{\frac{3}{2}}^2$  by  $3r_1^2\beta_1^2$  from Eq. (4.5c)

shows a quadratic equation with respect to  $\beta_1$  as:

$$\beta_1^2 - \beta_1 - 1 = 0. \quad (4.6)$$

Solving the above equations with respect to  $\beta_1$  with  $\beta_1 \geq 0$  results in  $\beta_1 = \frac{\sqrt{5}+1}{2}$ , and

hence

$$\frac{a}{b} = \frac{r_1^2\beta_1}{r_{\frac{3}{2}}^2\left(\frac{\beta_1}{2} + \frac{1}{3}\right)}. \quad (4.7)$$

Thus, after dropping the truncation error  $O(\Delta r^2)$ , a second-order finite difference approximation at  $r_1$  is obtained:

$$\frac{\partial}{\partial r} \left( r^2 \frac{\partial T_m(r,t)}{\partial r} \right)_1 = \frac{a}{b\Delta r^2} r_{\frac{3}{2}}^2 \left[ (T_m)_2 - (T_m)_1 \right] - \frac{1}{b\Delta r} r_1^2 \frac{\partial T_m(r_1 - \beta_1 \Delta r, t)}{\partial r}. \quad (4.8)$$

Symmetrically, the finite difference approximation of  $\frac{\partial}{\partial r} \left( r^2 \frac{\partial T_m(r,t)}{\partial r} \right)$  is expressed at

the right boundary  $r_l$  as follows:

$$b^* \frac{\partial}{\partial r} \left( r^2 \frac{\partial T_m(r,t)}{\partial r} \right)_l = \frac{1}{\Delta r} r_l^2 \frac{\partial T_m(r_l + \beta_2 \Delta r, t)}{\partial r} - \frac{a^*}{\Delta r^2} r_{l-\frac{1}{2}}^2 \left[ T_m(r_l, t) - T_m(r_{l-1}, t) \right], \quad (4.9)$$

where  $a^*, b^*, \beta_2$  are constants to be determined and  $r_{l-\frac{1}{2}} = r_l - \frac{\Delta r}{2}$ . By expressing each

term of LHS and RHS of Eq. (4.9) in Taylor series, and then matching both sides, the following equations are obtained:

$$\frac{1}{\Delta r} \left( r_l^2 - a^* r_{l-\frac{1}{2}}^2 \right) = 2b^* r_l, \quad (4.10a)$$

$$r_i^2 \beta_2 + \frac{a^*}{2} r_{i-\frac{1}{2}}^2 = b^* r_i^2, \quad (4.10b)$$

$$r_i^2 \beta_2 - \frac{a^*}{3} r_{i-\frac{1}{2}}^2 = 0. \quad (4.10c)$$

Dividing Eq. (4.10a) by Eq. (4.10b) and then replacing  $a^* r_{i-\frac{1}{2}}^2$  by  $3r_i^2 \beta_2^2$  from Eq. (4.10c)

results in a quadratic equation with respect to  $\beta_2$  as:

$$(3r_i + 3\Delta r) \beta_2^2 + 2\Delta \beta_2 - r_i = 0. \quad (4.11)$$

If the number of grid points  $I$  is given, then the grid size and the coordinates of the grid points can be determined as follows:

$$\Delta r = \frac{L}{I + \beta_1 + \beta_2 - 1}, \quad r_i = (i - 1 + \beta_1) \Delta r, \quad i = 1, \dots, I. \quad (4.12)$$

Substituting Eq. (4.12) into Eq. (4.11) and then solving above equations respecting to  $\beta_2$

with  $\beta_2 \geq 0$  results in

$$\beta_2 = \frac{\sqrt{4 + 3(\beta_1 + I)(\beta_1 + I - 1)} - 1}{3(\beta_1 + I)}, \quad (4.13a)$$

and

$$\frac{a^*}{b^*} = \frac{r_i^2 \beta_2}{r_{i-\frac{1}{2}}^2 \left( \frac{\beta_2}{2} + \frac{1}{3} \right)}. \quad (4.13b)$$

Thus, after dropping the truncation error  $O(\Delta r^2)$ , a second-order finite difference approximation at  $r_I$  is obtained:

$$\frac{\partial}{\partial r} \left( r^2 \frac{\partial T_m(r, t)}{\partial r} \right)_I = \frac{1}{b^* \Delta r} r_I^2 \frac{\partial T_m(r_I + \beta_2 \Delta r, t)}{\partial r} - \frac{a^*}{b^* \Delta r^2} r_{i-\frac{1}{2}}^2 \left[ (T_m)_I^n - (T_m)_{I-1}^n \right]. \quad (4.14)$$

Using the boundary condition, Eq. (3.3), Eqs. (4.9) and (4.14) can be simplified to

$$\frac{\partial}{\partial r} \left( r^2 \frac{\partial T_m(r,t)}{\partial r} \right)_1 \approx \frac{a}{b \Delta r^2} r_{\frac{3}{2}}^2 \left[ (T_m)_2^n - (T_m)_1^n \right], \quad (4.15a)$$

$$\frac{\partial}{\partial r} \left( r^2 \frac{\partial T_m(r,t)}{\partial r} \right)_I \approx -\frac{a}{b^* \Delta r^2} r_{I-\frac{1}{2}}^2 \left[ (T_m)_I^n - (T_m)_{I-1}^n \right]. \quad (4.15b)$$

It should be pointed out that the boundary condition, Eq. (3.3), is directly substituted into Eqs. (4.9) and (4.14) without discretization. Applying Eq. (4.15a) to Eq. (4.2a) results in the 1D improved CN scheme at  $r_1$ :

$$\begin{aligned} C_1 \frac{(T_1)_1^{n+1} - (T_1)_1^n}{\Delta t} &= \frac{k_1}{r_1^2} \frac{a}{b \Delta r} r_{\frac{3}{2}}^2 \nabla_r \left\{ W_t \left[ (T_m)_2^n \right] \right\} \\ &\quad - \sum_{m=2}^N G_{1m} \left\{ W_t \left[ (T_1)_m^n \right] - W_t \left[ (T_m)_i^n \right] \right\} + (Q_1)_{i_1}^{n+\frac{1}{2}}, \end{aligned} \quad (4.16a)$$

$$\begin{aligned} C_m \frac{(T_m)_1^{n+1} - (T_m)_1^n}{\Delta t} &= \frac{k_m}{r_1^2} \frac{a}{b \Delta r} r_{\frac{3}{2}}^2 \nabla_r W_t \left[ (T_m)_2^n \right] + \sum_{m_i=1}^{m-1} G_{m,m_i} \left\{ W_t \left[ (T_m)_{i_i}^n \right] - W_t \left[ (T_m)_i^n \right] \right\} \\ &\quad - \sum_{m_i=m+1}^N G_{m,m_i} \left\{ W_t \left[ (T_m)_{i_i}^n \right] - W_t \left[ (T_m)_i^n \right] \right\} + (Q_m)_{i_m}^{n+\frac{1}{2}}, \end{aligned} \quad (4.16b)$$

$$\begin{aligned} C_N \frac{(T_N)_i^{n+1} - (T_N)_i^n}{\Delta t} &= \frac{k_N}{r_1^2} \frac{a}{b \Delta r} r_{\frac{3}{2}}^2 \nabla_r W_t \left[ (T_m)_2^n \right] \\ &\quad + \sum_{m=1}^{N-1} G_{mN} \left\{ W_t \left[ (T_m)_i^n \right] - W_t \left[ (T_N)_i^n \right] \right\} + (Q_N)_{i_N}^{n+\frac{1}{2}}. \end{aligned} \quad (4.16c)$$

By keeping Eq. (4.2b) unchanged, and applying Eq. (4.15b) to Eq. (4.2c), the 1D improved CN scheme at  $r_I$  is obtained:

$$\begin{aligned} C_1 \frac{(T_1)_I^{n+1} - (T_1)_I^n}{\Delta t} &= -\frac{k_1}{r_I^2} \frac{a}{b^* \Delta r} r_{I-\frac{1}{2}}^2 \nabla_r W_t \left[ (T_1)_I^n \right] \\ &\quad - \sum_{m=2}^N G_{1m} \left\{ W_t \left[ (T_1)_I^n \right] - W_t \left[ (T_m)_I^n \right] \right\} + (Q_1)_{i_1}^{n+\frac{1}{2}}, \end{aligned} \quad (4.17a)$$

$$\begin{aligned}
C_m \frac{(T_m)_{i}^{n+1} - (T_m)_{i}^n}{\Delta t} &= -\frac{k_m}{r_i^2} \frac{a^*}{b^* \Delta r} r_{i-\frac{1}{2}}^2 \nabla_r \mathcal{W}_i \left[ (T_m)_{i}^n \right] + \sum_{m=1}^{m-1} G_{m,m} \left\{ \mathcal{W}_i \left[ (T_m)_{i}^n \right] - \mathcal{W}_i \left[ (T_m)_{i}^n \right] \right\} \\
&\quad - \sum_{m=m+1}^N G_{m,m} \left\{ \mathcal{W}_i \left[ (T_m)_{i}^n \right] - \mathcal{W}_i \left[ (T_m)_{i}^n \right] \right\} + (Q_m)_{i}^{n+\frac{1}{2}}, \tag{4.17b}
\end{aligned}$$

$$\begin{aligned}
C_N \frac{(T_N)_{i}^{n+1} - (T_N)_{i}^n}{\Delta t} &= -\frac{k_N}{r_i^2} \frac{a^*}{b^* \Delta r} r_{i-\frac{1}{2}}^2 \nabla_r \mathcal{W}_i \left[ (T_N)_{i}^n \right] \\
&\quad + \sum_{m=1}^{N-1} G_{m,N} \left\{ \mathcal{W}_i \left[ (T_m)_{i}^n \right] - \mathcal{W}_i \left[ (T_N)_{i}^n \right] \right\} + (Q_N)_{i}^{n+\frac{1}{2}}. \tag{4.17c}
\end{aligned}$$

Hence, the 1D improved CN scheme is obtained: Eq. (4.2) for interior points  $r_i$  ( $i=2, \dots, I-1$ ) and Eq. (4.16) for grid point  $r_I$  and Eq. (4.17) for grid point  $r_I$  for a second-order discretization of the parabolic model in an  $N$ -carrier system in 1D spherical coordinates. The truncation error of the 1D improved CN scheme is  $(\Delta t^2 + \Delta r^2)$  at all grid points  $\left( r_m, t_{n+\frac{1}{2}} \right), i=1, \dots, I$ .

#### 4.1.2 3D First Improved CN Scheme

A finite difference schemes is developed by denoting  $(T_m)_{ijk}^n$  as the numerical approximation of  $(T_m)(i\Delta r, j\Delta\theta, k\Delta\mu, n\Delta t)$ , where  $\Delta r, \Delta\theta, \Delta\mu$  and  $\Delta t$  are the  $r, \theta, \mu$  - directional spatial and temporal mesh sizes, respectively, and  $r_i = i\Delta r$ ,  $\theta_j = j\Delta\theta$ ,  $\mu_k = k\Delta\mu$ ,  $0 \leq i \leq I+1$ ,  $0 \leq j \leq J+1$ ,  $0 \leq k \leq K$ , so that  $(I+1)\Delta r = L$ ,  $J\Delta\theta = 2\pi$  and  $K\Delta\mu = 2$ . In order to briefly describe the 3D first improved CN scheme, following finite difference operators are defined:

$$P_r \left[ (T_m)_{ijk}^n \right] = r_{i+\frac{1}{2}}^2 \frac{(T_m)_{i+1,jk}^n - (T_m)_{ijk}^n}{\Delta r^2} - r_{i-\frac{1}{2}}^2 \frac{(T_m)_{ijk}^n - (T_m)_{i-1,jk}^n}{\Delta r^2}, \tag{4.18a}$$

$$P_\theta \left[ (T_m)_{ijk}^n \right] = \frac{(T_m)_{ij+1k}^n - 2(T_m)_{ijk}^n + (T_m)_{ij-1k}^n}{(\Delta\theta)^2}, \quad (4.18b)$$

$$P_\mu \left[ (T_m)_{ijk}^n \right] = \left( 1 - \mu_{k+\frac{1}{2}}^2 \right) \frac{(T_m)_{ijk+1}^n - (T_m)_{ijk}^n}{(\Delta\mu)^2} - \left( 1 - \mu_{k-\frac{1}{2}}^2 \right) \frac{(T_m)_{ijk}^n - (T_m)_{ijk-1}^n}{(\Delta\mu)^2}, \quad (4.18c)$$

$$\nabla_r (T_m)_{ijk}^n = \frac{(T_m)_{ijk}^n - (T_m)_{i-1jk}^n}{\Delta r}, \quad (4.18d)$$

$$\nabla_{\bar{\theta}} (T_m)_{ijk}^n = \frac{(T_m)_{ijk}^n - (T_m)_{ij-1k}^n}{\Delta\theta}, \quad (4.18e)$$

$$\nabla_{\bar{\mu}} (T_m)_{ijk}^n = \frac{(T_m)_{ijk}^n - (T_m)_{ijk-1}^n}{\Delta\mu}. \quad (4.18f)$$

Also, the time average of mesh function  $(T_m)_{ijk}^n$  is defined as:

$$W_t \left[ (T_m)_{ijk}^n \right] = \frac{(T_m)_{ijk}^{n+1} + (T_m)_{ijk}^n}{2}.$$

The parabolic model in an  $N$ -carrier system in 3D spherical coordinates Eq. (3.4)

can be solved using the 3D CN scheme as follows:

$$\begin{aligned} C_1 \frac{(T_1)_{ijk}^{n+1} - (T_1)_{ijk}^n}{\Delta t} &= \frac{k_1}{r_i^2} P_r \left\{ W_t \left[ (T_1)_{ijk}^n \right] \right\} + \frac{k_1}{r_i^2 (1 - \mu_k^2)} P_\theta \left\{ W_t \left[ (T_1)_{ijk}^n \right] \right\} \\ &+ \frac{k_1}{r_i^2} P_\mu \left\{ W_t \left[ (T_1)_{ijk}^n \right] \right\} - \sum_{m=2}^N G_{1m} \left\{ W_t \left[ (T_1)_{ijk}^n \right] - W_t \left[ (T_m)_{ijk}^n \right] \right\} + (Q_1)_{ijk}^{n+\frac{1}{2}}, \end{aligned} \quad (4.19a)$$

$$\begin{aligned} C_m \frac{(T_m)_{ijk}^{n+1} - (T_m)_{ijk}^n}{\Delta t} &= \frac{k_m}{r_i^2} P_r \left\{ W_t \left[ (T_m)_{ijk}^n \right] \right\} + \frac{k_m}{r_i^2 (1 - \mu_k^2)} P_\theta \left\{ W_t \left[ (T_m)_{ijk}^n \right] \right\} \\ &+ \frac{k_m}{r_i^2} P_\mu \left\{ W_t \left[ (T_m)_{ijk}^n \right] \right\} + \sum_{m=1}^{m-1} G_{m,m} \left\{ W_t \left[ (T_m)_{ijk}^n \right] - W_t \left[ (T_m)_{ijk}^n \right] \right\} \end{aligned}$$

$$-\sum_{m_i=m+1}^N G_{mm_i} \left\{ W_t \left[ (T_m)^n \right] - W_t \left[ (T_{m_i})^n \right] \right\} + (Q_m)^{n+\frac{1}{2}}, \quad (4.19b)$$

$$C_N \frac{(T_N)^{n+1}_{ijk} - (T_N)^n_{ijk}}{\Delta t} = \frac{k_N}{r_i^2} P_r \left\{ W_t \left[ (T_N)^n \right] \right\} + \frac{k_N}{r_i^2 (1 - \mu_k^2)} P_\theta \left\{ W_t \left[ (T_N)^n \right] \right\} \\ + \frac{k_N}{r_i^2} P_\mu \left\{ W_t \left[ (T_N)^n \right] \right\} + \sum_{m=1}^{N-1} G_{mN} \left\{ W_t \left[ (T_m)^n \right] - W_t \left[ (T_N)^n \right] \right\} + (Q_N)^{n+\frac{1}{2}}. \quad (4.19c)$$

The initial condition is set to be  $(T_m)^0 = (T_m^0)_{ijk}$ . To develop a numerical scheme,

one usually adds a 3D fictitious boundary condition at center,  $r = 0$ :

$$\frac{\partial T_m(0, \theta, \mu, t)}{\partial r} = 0, \quad m = 1, \dots, N.$$

The boundary condition Eq. (3.6) and the 3D fictitious boundary condition can be discretized by the first-order method as:

$$(T_m)^n_{i-1k} = (T_m)^n_{i+1k}, \quad (T_m)^n_{i0k} = (T_m)^n_{ijk}, \quad (4.20a)$$

$$(T_m)^n_{ij0} = (T_m)^n_{ijk} = 0, \quad (4.20b)$$

for any time level  $n$ , where  $m = 1, \dots, N$ . For clarity  $(T_m)^n_{i-1k}$  is the approximation of  $T_m(r_i, -\Delta\theta, \mu_k, n\Delta t)$ . Eqs. (3.6a) and the 3D fictitious boundary condition may be discretized using the conventional first-order method as [65]

$$(T_m)^n_{0jk} = (T_m)^n_{1jk}, \quad m = 1, \dots, N \quad (4.20c)$$

$$(T_m)^n_{I+1,jk} = (T_m)^n_{I,jk}, \quad m = 1, \dots, N. \quad (4.20d)$$

However, the above numerical scheme provides only a first-order accurate solution with respect to the spatial variable  $r$ , which can be seen in Chapter Five. Thus, Chapter Four, we improve the finite difference scheme at the boundary, Eqs. (3.6a) and 3D fictitious

boundary condition, so that both the unconditional stability of schemes and the accurate numerical solutions can be achieved. This is important because the length  $L$  could be in microscale, and a higher-order accurate and unconditionally stable scheme will provide a more accurate solution in a small grid size.

Based on the work in Section 4.1.1 of Chapter Four, the 3D first improved CN scheme for the parabolic model Eq. (3.4) at  $r_l$  and  $r_l$  is developed. At  $r_l$ , the 3D first improved CN scheme can be developed as follows:

$$C_1 \frac{(T_1)_{1jk}^{n+1} - (T_1)_{1jk}^n}{\Delta t} = \frac{k_1 a r_3^2}{r_1^2 b \Delta r} \nabla_{\bar{r}} \left\{ W_t \left[ (T_m)_{2jk}^n \right] \right\} + \frac{k_1}{r_1^2 (1 - \mu_k^2)} P_\theta \left\{ W_t \left[ (T_1)_{1jk}^n \right] \right\} \\ + \frac{k_1}{r_1^2} P_\mu \left\{ W_t \left[ (T_1)_{1jk}^n \right] \right\} - \sum_{m=2}^N G_{1m} \left\{ W_t \left[ (T_1)_{1jk}^n \right] - W_t \left[ (T_m)_{1jk}^n \right] \right\} + (Q_1)_{1jk}^{n+\frac{1}{2}}, \quad (4.21a)$$

$$C_m \frac{(T_m)_{1jk}^{n+1} - (T_m)_{1jk}^n}{\Delta t} = \frac{k_m a r_3^2}{r_1^2 b \Delta r} \nabla_{\bar{r}} \left\{ W_t \left[ (T_m)_{2jk}^n \right] \right\} + \frac{k_m}{r_1^2 (1 - \mu_k^2)} P_\theta \left\{ W_t \left[ (T_m)_{1jk}^n \right] \right\} \\ + \frac{k_m}{r_1^2} P_\mu \left\{ W_t \left[ (T_m)_{1jk}^n \right] \right\} + \sum_{m=1}^{m-1} G_{m,m} \left\{ W_t \left[ (T_m)_{1jk}^n \right] - W_t \left[ (T_m)_{1jk}^n \right] \right\} \\ - \sum_{m=m+1}^N G_{mm} \left\{ W_t \left[ (T_m)_{1jk}^n \right] - W_t \left[ (T_m)_{1jk}^n \right] \right\} + (Q_m)_{1jk}^{n+\frac{1}{2}}, \quad (4.21b)$$

$$C_N \frac{(T_N)_{ijk}^{n+1} - (T_N)_{ijk}^n}{\Delta t} = \frac{k_N a r_3^2}{r_1^2 b \Delta r} \nabla_{\bar{r}} \left\{ W_t \left[ (T_N)_{2jk}^n \right] \right\} + \frac{k_N}{r_1^2 (1 - \mu_k^2)} P_\theta \left\{ W_t \left[ (T_N)_{1jk}^n \right] \right\} \\ + \frac{k_N}{r_1^2} P_\mu \left\{ W_t \left[ (T_N)_{1jk}^n \right] \right\} + \sum_{m=1}^{N-1} G_{mN} \left\{ W_t \left[ (T_m)_{1jk}^n \right] - W_t \left[ (T_N)_{1jk}^n \right] \right\} + (Q_N)_{1jk}^{n+\frac{1}{2}}. \quad (4.21c)$$

Similarly, the 3D first improved CN scheme at  $r_l$  is developed as follows:

$$C_1 \frac{(T_1)_{ijk}^{n+1} - (T_1)_{ijk}^n}{\Delta t} = \frac{k_1 a^* r_{l-1}^2}{r_l^2 b^* \Delta r} \nabla_{\bar{r}} \left\{ W_t \left[ (T_1)_{l-1jk}^n \right] \right\} + \frac{k_1}{r_l^2} P_\theta \left\{ W_t \left[ (T_1)_{ijk}^n \right] \right\}$$

$$+\frac{k_1}{r_1^2}P_\mu\left\{W_t\left[(T_1)_{ijk}^n\right]\right\}-\sum_{m=2}^N G_{1m}\left\{W_t\left[(T_1)_{ijk}^n\right]-W_t\left[(T_m)_{ijk}^n\right]\right\}+(Q_1)_{ijk}^{n+\frac{1}{2}}, \quad (4.22a)$$

$$\begin{aligned} C_m \frac{(T_m)_{ijk}^{n+1}-(T_m)_{ijk}^n}{\Delta t} &= \frac{k_m \alpha^* r_{i-1}^2}{r_i^2 b^* \Delta r} \nabla_{\bar{r}} \left\{ W_t \left[ (T_m)_{i-1,jk}^n \right] \right\} + \frac{k_m}{r_i^2} P_\theta \left\{ W_t \left[ (T_m)_{ijk}^n \right] \right\} \\ &+ \frac{k_m}{r_i^2} P_\mu \left\{ W_t \left[ (T_m)_{ijk}^n \right] \right\} + \sum_{m=1}^{m-1} G_{m,m} \left\{ W_t \left[ (T_m)_{ijk}^n \right] - W_t \left[ (T_m)_{ijk}^n \right] \right\} \\ &- \sum_{m=m+1}^N G_{mm} \left\{ W_t \left[ (T_m)_{ijk}^n \right] - W_t \left[ (T_m)_{ijk}^n \right] \right\} + (Q_m)_{ijk}^{n+\frac{1}{2}}, \end{aligned} \quad (4.22b)$$

$$\begin{aligned} C_N \frac{(T_N)_{ijk}^{n+1}-(T_N)_{ijk}^n}{\Delta t} &= \frac{k_N \alpha^* r_{i-1}^2}{r_i^2 b^* \Delta r} \nabla_{\bar{r}} \left\{ W_t \left[ (T_N)_{i-1,jk}^n \right] \right\} + \frac{k_N}{r_i^2} P_\theta \left\{ W_t \left[ (T_N)_{ijk}^n \right] \right\} \\ &+ \frac{k_N}{r_i^2} P_\mu \left\{ W_t \left[ (T_N)_{ijk}^n \right] \right\} + \sum_{m=1}^{N-1} G_{mN} \left\{ W_t \left[ (T_m)_{ijk}^n \right] - W_t \left[ (T_N)_{ijk}^n \right] \right\} + (Q_N)_{ijk}^{n+\frac{1}{2}}. \end{aligned} \quad (4.22c)$$

Hence, the 3D first improved CN scheme consists of Eq. (4.19) for interior grid point  $r_i$  where  $i = 2, \dots, I-1$ , and Eq. (4.21) for the left boundary  $r_l$  and Eq. (4.22) for the right boundary  $r_I$ . It can be seen that the truncation error for the scheme with respect to  $r$  has the order of  $\Delta r^2$  at all grid points  $\left( r_i, \theta_j, \mu_k, t_{n+\frac{1}{2}} \right)$ .

### 4.1.3 3D Second Improved CN Scheme

It is noted that that the above improved finite difference scheme consists of the 3D fictitious boundary condition. If the fictitious condition is noted, the value of  $(T_m)_{ijk}^{n-1}$  at the center is needed to determine in Eq. (4.19) when  $i = 1$ . To this end, the mesh in Figure 4.1 is first modified as shown in Figure 4.2.

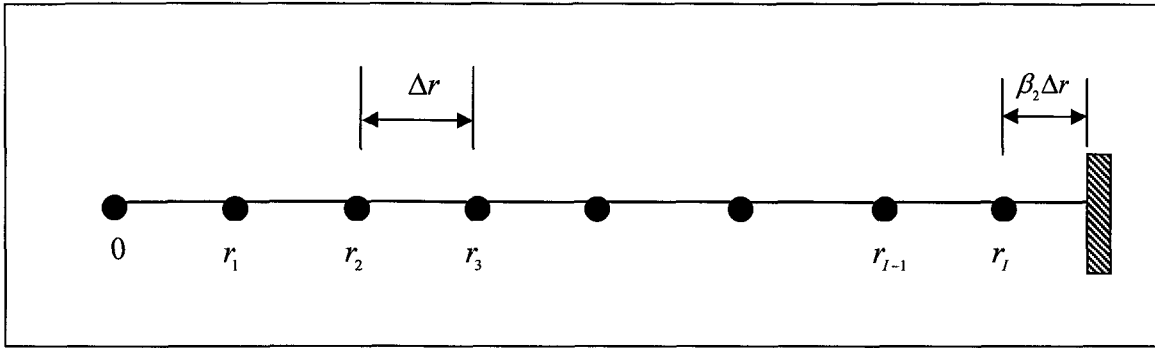


Figure 4.2 Mesh and locations of grid points of the 3D second improved CN scheme in spherical coordinates.

Following the idea in [65], multiplying both sides of Eq. (3.4a) by  $r^2$ , and then integrating both sides over  $0 \leq r \leq \varepsilon, 0 \leq \theta \leq 2\pi$ , and  $-1 \leq \mu \leq 1$  with respect to  $r, \theta, \mu$  results in:

$$\begin{aligned}
 & \int_{-1}^1 \int_0^{2\pi} \int_0^\varepsilon C r^2 \frac{\partial T_1(r, \theta, \mu, t)}{\partial t} dr d\theta d\mu \\
 &= \int_{-1}^1 \int_0^{2\pi} \int_0^\varepsilon k_1 \frac{\partial}{\partial r} \left( r^2 \frac{\partial T_1(r, \theta, \mu, t)}{\partial r} \right) dr d\theta d\mu \\
 &+ \int_{-1}^1 \int_0^{2\pi} \int_0^\varepsilon \frac{k_1}{(1-\mu^2)} \frac{\partial^2 T_1(r, \theta, \mu, t)}{\partial \theta^2} dr d\theta d\mu + \int_{-1}^1 \int_0^{2\pi} \int_0^\varepsilon k_1 \frac{\partial}{\partial \mu} \left( (1-\mu^2) \frac{\partial T_1(r, \theta, \mu, t)}{\partial \mu} \right) dr d\theta d\mu \\
 &- \int_{-1}^1 \int_0^{2\pi} \int_0^\varepsilon r_i^2 \sum_{m=2}^N G_{1m} [T_1(r, \theta, \mu, t) - T_m(r, \theta, \mu, t)] dr d\theta d\mu \\
 &+ \int_{-1}^1 \int_0^{2\pi} \int_0^\varepsilon Q_1(r, \theta, \mu, t) dr d\theta d\mu. \tag{4.23}
 \end{aligned}$$

Replacing  $\frac{\partial T_1(r, \theta, \mu, t)}{\partial t}$ ,  $[T_1(r, \theta, \mu, t) - T_m(r, \theta, \mu, t)]$  and  $Q_1(r, \theta, \mu, t)$  with those values at the spherical center  $r = 0$ , calculating integrals in Eq. (4.23) and using boundary condition Eq. (3.6b) leads to

$$\begin{aligned} & \frac{4\pi\varepsilon^3}{3} C_1 \frac{\partial(T_1)_0}{\partial t} \\ = & \int_{-1}^1 \int_0^{2\pi} k_1 \varepsilon^2 \frac{\partial T_1(r, \theta, \mu, t)}{\partial r} d\theta d\mu - \frac{4\pi\varepsilon^3}{3} \sum_{m=2}^N G_{1m} [(T_1)_0 - (T_m)_0] + \frac{4\pi\varepsilon^3}{3} (Q_1)_0. \end{aligned}$$

Here, denote  $(T_m)_0 = T_m(0, \theta, \mu, t)$ ,  $m=1, \dots, N$ , and  $(Q_1)_0 = Q_1(0, \theta, \mu, t)$ . Deriving the

equation and setting  $\varepsilon = \frac{\Delta r}{2}$  results in the 3D second improved CN scheme at spherical

center  $r = 0$ :

$$\begin{aligned} C_1 \frac{(T_1)_0^{n+1} - (T_1)_0^n}{\Delta t} &= \frac{3k_1}{2\pi\Delta r} \Delta\theta\Delta\mu \sum_{j=0}^{J-1} \sum_{k=1}^{K-1} \nabla_{\vec{r}} \left\{ W_t \left[ (T_1)_{1,jk}^n \right] \right\} \\ &\quad - \sum_{m=2}^N G_{1m} \left\{ W_t \left[ (T_1)_0^n \right] - W_t \left[ (T_m)_0^n \right] \right\} + (Q_1)_0^{n+\frac{1}{2}}. \end{aligned} \quad (4.24a)$$

Using a similar process for Eq. (3.4b) and (3.4c) leads to

$$\begin{aligned} & C_m \frac{(T_m)_0^{n+1} - (T_m)_0^n}{\Delta t} \\ = & \frac{3k_m}{2\pi\Delta r} \Delta\theta\Delta\mu \sum_{j=0}^{J-1} \sum_{k=1}^{K-1} \nabla_{\vec{r}} W_t \left[ (T_m)_{1,jk}^n \right] + \sum_{m_1=1}^{m-1} G_{m,m_1} \left\{ W_t \left[ (T_{m_1})_0^n \right] - W_t \left[ (T_m)_0^n \right] \right\} \\ & \quad - \sum_{m_2=m+1}^N G_{m,m_2} \left\{ W_t \left[ (T_m)_0^n \right] - W_t \left[ (T_{m_2})_0^n \right] \right\} + (Q_m)_0^{n+\frac{1}{2}}, \end{aligned} \quad (4.24b)$$

$$\begin{aligned} & C_N \frac{(T_N)_0^{n+1} - (T_N)_0^n}{\Delta t} \\ = & \frac{3k_N}{2\pi\Delta r} \Delta\theta\Delta\mu \sum_{j=0}^{J-1} \sum_{k=1}^{K-1} \nabla_{\vec{r}} W_t \left[ (T_N)_{1,jk}^n \right] \\ & \quad + \sum_{m=1}^{N-1} G_{mN} \left\{ W_t \left[ (T_m)_0^n \right] - W_t \left[ (T_N)_0^n \right] \right\} + (Q_N)_0^{n+\frac{1}{2}}. \end{aligned} \quad (4.24c)$$

Hence, the 3D second improved CN scheme consists of Eq. (4.19) for interior grid point  $r_i$  where  $i = 2, \dots, I-1$ , and Eq. (4.24) for the left boundary  $r_l$  and Eq. (4.22) for the right boundary  $r_I$ . Again, it can be seen that the truncation error for the scheme with respect to  $r$  has an order of  $\Delta r^2$  at all grid points  $\left(r_i, \theta_j, \mu_k, t_{n+\frac{1}{2}}\right)$ .

## 4.2 Stability

### 4.2.1 Stability of 1D Improved CN Scheme

Proving the stability of the 1D improved CN scheme requires firstly building two lemmas, Lemma 1 and Lemma 2. The stability is proved basing on the two lemmas. The key to prove the stability of the 1D improved CN scheme is to consider the left boundary  $r_l$ , interior points  $r_i$  ( $i = 2, \dots, I-1$ ) and the right boundary  $r_I$  separately.

**Lemma 1.** For any mesh function  $(T_m)_i^n$ ,

$$\left[(T_m)_i^{n+1} + (T_m)_i^n\right] \cdot \left[(T_m)_i^{n+1} - (T_m)_i^n\right] = \left\{ \left[(T_m)_i^{n+1}\right]^2 - \left[(T_m)_i^n\right]^2 \right\}, \quad (4.25)$$

where  $1 \leq m \leq N$ .

**Lemma 2.** For any mesh function  $(T_m)_i^n$ ,

$$\begin{aligned} \Delta r \sum_{m=2}^{N-1} P_r \left[ (T_m)_i^n \right] \cdot (T_m)_i^n + r_{\frac{3}{2}}^2 \nabla_{\bar{r}} (T_m)_2^n \cdot (T_m)_1^n - r_{I-\frac{1}{2}}^2 \nabla_{\bar{r}} (T_m)_I^n \cdot (T_m)_I^n \\ = -\Delta r \sum_{m=2}^N r_{m-\frac{1}{2}}^2 \left[ \nabla_{\bar{r}} (T_m)_I^n \right]^2. \end{aligned} \quad (4.26)$$

*Proof.*

$$LHS = \Delta r \sum_{i=2}^{I-1} \left\{ r_{i+\frac{1}{2}}^2 \left[ (T_m)_{i+1}^n - (T_m)_i^n \right] - r_{i-\frac{1}{2}}^2 \left[ (T_m)_i^n - (T_m)_{i-1}^n \right] \right\} \cdot (T_m)_i^n$$

$$\begin{aligned}
& +r\frac{2}{3}\nabla_{\bar{r}}(T_m)_2^n \cdot (T_m)_1^n - r_{l-\frac{1}{2}}^2 \nabla_{\bar{r}}(T_m)_l^n \cdot (T_m)_l^n \\
& = \sum_{i=3}^l r_{i-\frac{1}{2}}^2 \nabla_{\bar{r}}(T_m)_i^n \cdot (T_m)_{i-1}^n - \sum_{i=1}^{l-1} r_{l-\frac{1}{2}}^2 \nabla_{\bar{r}}(T_m)_i^n \cdot (T_m)_i^n \\
& \quad + r\frac{2}{3}\nabla_{\bar{r}}(T_m)_2^n \cdot (T_m)_1^n - r_{l-\frac{1}{2}}^2 \nabla_{\bar{r}}(T_m)_l^n \cdot (T_m)_l^n \\
& = \sum_{i=2}^l r_{i-\frac{1}{2}}^2 \nabla_{\bar{r}}(T_m)_i^n \cdot (T_m)_{i-1}^n - \sum_{i=1}^l r_{i-\frac{1}{2}}^2 \nabla_{\bar{r}}(T_m)_i^n \cdot (T_m)_i^n = -\Delta r \sum_{i=2}^l r_{i-\frac{1}{2}}^2 \left[ \nabla_{\bar{r}}(T_m)_{ijk}^n \right]^2. \quad \blacksquare
\end{aligned}$$

**Theorem 3.** The 1D improved CN scheme, Eqs. (4.2), (4.16) and (4.17), is unconditionally stable with respect to the initial condition  $(T_m)_i^0 = (T_m^0)_i$  and source terms.

*Proof.* By multiplying Eq. (4.2a) by  $r_i^2 \Delta r W_i \left[ (T_1)_i^n \right]$ , Eq. (4.2b) by  $r_i^2 \Delta r W_i \left[ (T_m)_i^n \right]$ ,

$1 \leq m \leq N$ , Eq. (4.2c) by  $r_i^2 \Delta r W_i \left[ (T_N)_i^n \right]$ , Eq. (4.6a) by  $r_i^2 \Delta r \frac{b}{a} W_i \left[ (T_1)_i^n \right]$ , Eq. (4.6b) by

$r_i^2 \Delta r \frac{b}{a} W_i \left[ (T_m)_i^n \right]$ , Eq. (4.6c) by  $r_i^2 \Delta r \frac{b}{a} W_i \left[ (T_N)_i^n \right]$ , Eq. (4.7a) by  $r_i^2 \Delta r \frac{b^*}{a} W_i \left[ (T_1)_i^n \right]$ , Eq.

(4.7b) by  $r_i^2 \Delta r \frac{b^*}{a} W_i \left[ (T_m)_i^n \right]$ , Eq. (4.7c) by  $r_i^2 \Delta r \frac{b^*}{a} W_i \left[ (T_N)_i^n \right]$ , adding them together over

$1 \leq m \leq N$ , and using Lemma 1 and Lemma 2, this gives:

$$\begin{aligned}
& \frac{2\Delta r}{\Delta t} \sum_{m=1}^N C_m \left\{ \frac{b}{a} r_1^2 \left\{ \left[ (T_m)_1^{n+1} \right]^2 - \left[ (T_m)_1^n \right]^2 \right\} + \sum_{i=2}^{l-1} r_i^2 \left\{ \left[ (T_m)_i^{n+1} \right]^2 - \left[ (T_m)_i^n \right]^2 \right\} \right. \\
& \quad \left. + \frac{b^*}{a} r_l^2 \left\{ \left[ (T_m)_l^{n+1} \right]^2 - \left[ (T_m)_l^n \right]^2 \right\} \right\} = -\Delta r \sum_{m=1}^N k_m \sum_{i=2}^l r_{i-\frac{1}{2}}^2 \left\{ \nabla_{\bar{r}} W_i \left[ (T_m)_i^n \right] \right\}^2 \\
& - \Delta r \sum_{\substack{m, n_1=1 \\ m < n_1}}^{N-1} G_{m,m} \left\{ \frac{b}{a} r_1^2 \left\{ W_i \left[ (T_m)_1^n \right] - W_i \left[ (T_{m_1})_1^n \right] \right\}^2 + \sum_{i=2}^{l-1} r_i^2 \left\{ W_i \left[ (T_m)_i^n \right] - W_i \left[ (T_{m_1})_i^n \right] \right\}^2 \right. \\
& \quad \left. + \frac{b^*}{a} r_l^2 \left\{ W_i \left[ (T_m)_l^n \right] - W_i \left[ (T_{m_1})_l^n \right] \right\}^2 \right\} + 2\Delta r \sum_{m=1}^N \left\{ \frac{b}{a} r_1^2 W_i \left[ (T_m)_1^n \right] (Q_m)_1^{n+\frac{1}{2}} \right.
\end{aligned}$$

$$+ \sum_{i=2}^{l-1} r_i^2 \mathcal{W}_i \left[ (T_m)_i^n \right] (Q_m)_i^{n+\frac{1}{2}} + \frac{b^*}{a} r_l^2 \mathcal{W}_l \left[ (T_m)_l^n \right] (Q_m)_l^{n+\frac{1}{2}} \}. \quad (4.27)$$

Dropping negative terms in RHS of Eq. (4.27) provides the result:

$$\begin{aligned} & \frac{2\Delta r}{\Delta t} \sum_{m=1}^N C_m \left\{ \frac{b}{a} r_1^2 \left\{ \left[ (T_m)_1^{n+1} \right]^2 - \left[ (T_m)_1^n \right]^2 \right\} + \sum_{i=2}^{l-1} r_i^2 \left\{ \left[ (T_m)_i^{n+1} \right]^2 - \left[ (T_m)_i^n \right]^2 \right\} \right. \\ & \left. + \frac{b^*}{a} r_l^2 \left\{ \left[ (T_m)_l^{n+1} \right]^2 - \left[ (T_m)_l^n \right]^2 \right\} \right\} \leq 2\Delta r \sum_{m=1}^N \left\{ \frac{b}{a} r_1^2 \mathcal{W}_1 \left[ (T_m)_1^n \right] (Q_m)_1^{n+\frac{1}{2}} \right. \\ & \left. + \sum_{i=2}^{l-1} r_i^2 \mathcal{W}_i \left[ (T_m)_i^n \right] (Q_m)_i^{n+\frac{1}{2}} + \frac{b^*}{a} r_l^2 \mathcal{W}_l \left[ (T_m)_l^n \right] (Q_m)_l^{n+\frac{1}{2}} \right\}. \end{aligned} \quad (4.28)$$

Using Cauchy-Schwartz's inequality leads to

$$\begin{aligned} 2(Q_m)_i^{n+\frac{1}{2}} \cdot \left[ (T_m)_i^{n+1} + (T_m)_i^n \right] & \leq C_m \left[ (T_m)_i^{n+1} + (T_m)_i^n \right]^2 + \frac{1}{C_m} \left[ (Q_m)_i^{n+\frac{1}{2}} \right]^2 \\ & \leq 2C_m \left\{ \left[ (T_m)_i^{n+1} \right]^2 + \left[ (T_m)_i^n \right]^2 \right\} + \frac{1}{C_m} \left[ (Q_m)_i^{n+\frac{1}{2}} \right]^2. \end{aligned} \quad (4.29)$$

Substituting Eq. (4.29) into Eq. (4.28), and multiplying both sides by  $\Delta t$  results in

$$\begin{aligned} & 2\Delta r \sum_{m=1}^N C_m \left\{ \frac{b}{a} r_1^2 \left\{ \left[ (T_m)_1^{n+1} \right]^2 - \left[ (T_m)_1^n \right]^2 \right\} + \sum_{i=2}^{l-1} r_i^2 \left\{ \left[ (T_m)_i^{n+1} \right]^2 - \left[ (T_m)_i^n \right]^2 \right\} \right. \\ & \left. + \frac{b^*}{a} r_l^2 \left\{ \left[ (T_m)_l^{n+1} \right]^2 - \left[ (T_m)_l^n \right]^2 \right\} \right\} \leq 2\Delta r \Delta t \sum_{m=1}^N C_m \left\{ \frac{b}{a} r_1^2 \left\{ \left[ (T_m)_1^{n+1} \right]^2 + \left[ (T_m)_1^n \right]^2 \right\} \right. \\ & \left. + \sum_{i=2}^{l-1} r_i^2 \left\{ \left[ (T_m)_i^{n+1} \right] + \left[ (T_m)_i^n \right] \right\}^2 + \frac{b^*}{a} r_l^2 \left\{ \left[ (T_m)_l^{n+1} \right] + \left[ (T_m)_l^n \right] \right\}^2 \right\} \\ & + \Delta r \Delta t \sum_{m=1}^N \frac{1}{C_m} \left\{ \frac{b}{a} r_1^2 \left[ (Q_m)_1^{n+\frac{1}{2}} \right]^2 + \sum_{i=2}^{l-1} r_i^2 \left[ (Q_m)_i^{n+\frac{1}{2}} \right]^2 + \frac{b^*}{a} r_l^2 \left[ (Q_m)_l^{n+\frac{1}{2}} \right]^2 \right\}. \end{aligned} \quad (4.30)$$

Denoting

$$F(n) = 2\Delta r \sum_{m=1}^N C_m \left\{ \frac{b}{a} r_1^2 \left[ (T_m)_1^n \right]^2 + \sum_{i=2}^{l-1} r_i^2 \left[ (T_m)_i^n \right]^2 + \frac{b^*}{a} r_l^2 \left[ (T_m)_l^n \right]^2 \right\}, \quad (4.31a)$$

and

$$\Phi(n) = \Delta r \sum_{m=1}^N \frac{1}{C_m} \left\{ \frac{b}{a} r_1^2 \left[ (\mathcal{Q}_m)_{1_1}^{n+\frac{1}{2}} \right]^2 + \sum_{i=2}^{I-1} r_i^2 \left[ (\mathcal{Q}_m)_i^{n+\frac{1}{2}} \right]^2 + \frac{b^*}{a} r_I^2 \left[ (\mathcal{Q}_m)_{I_1}^{n+\frac{1}{2}} \right]^2 \right\}, \quad (4.31b)$$

and substituting Eq. (4.31a) and Eq. (4.31b) into Eq. (4.30), this gives:

$$\begin{aligned} & F(n+1) \\ & \leq \frac{(1+\Delta t)}{(1-\Delta t)} F(n) + \frac{\Delta t}{(1-\Delta t)} \Phi(n) \\ & \leq \frac{(1+\Delta t)}{(1-\Delta t)} \left[ \frac{(1+\Delta t)}{(1-\Delta t)} F(n-1) + \frac{\Delta t}{(1-\Delta t)} \Phi(n-1) \right] + \frac{\Delta t}{(1-\Delta t)} \Phi(n) \\ & \leq \left( \frac{(1+\Delta t)}{(1-\Delta t)} \right)^{n+1} F(0) + \frac{(1+\Delta t)}{(1-\Delta t)} \left[ 1 + \frac{(1+\Delta t)^1}{(1-\Delta t)} + \dots + \frac{(1+\Delta t)^n}{(1-\Delta t)} \right] \max_{0 \leq n_1 \leq n} \Phi(n_1) \\ & \leq \left( \frac{(1+\Delta t)}{(1-\Delta t)} \right)^{n+1} \left( F(0) + \max_{0 \leq n_1 \leq n} \Phi(n_1) \right). \end{aligned} \quad (4.32)$$

Using the inequalities  $(1+\varepsilon)^n \leq e^{n\varepsilon}$  for  $\varepsilon > 0$  and  $(1-\varepsilon)^{-1} \leq e^{2\varepsilon}$  for  $0 < \varepsilon < \frac{1}{2}$  results in

$(1+\Delta t)^{n+1} \leq e^{(n+1)\Delta t}$  and  $(1-\Delta t)^{-1} \leq e^{2\Delta t}$ . Multiplying the two inequalities together results in

$$\begin{aligned} & (1+\Delta t)^{n+1} (1-\Delta t)^{-(n+1)} \\ & \leq e^{(n+1)\Delta t} \cdot e^{2(n+1)\Delta t} = e^{3(n+1)\Delta t}. \end{aligned} \quad (4.33)$$

Substituting Eq. (4.33) into Eq. (4.32) leads to

$$F(n+1) \leq e^{3(n+1)\Delta t} \left( F(0) + \max_{0 \leq n_1 \leq n} \Phi(n_1) \right) \leq e^{3t_0} \left( F(0) + \max_{0 \leq n_1 \leq n} \Phi(n_1) \right),$$

that is, for any  $0 \leq (n+1)\Delta t \leq t_0$ , the scheme is unconditionally stable with respect to the

initial condition and heat source terms. ■

### 4.2.2 Stability of 3D First Improved CN Scheme

Proving the stability of the 3D first improved CN scheme requires building Lemma 3. Next, the stability will be proved basing on Lemma 1 and Lemma 3.

**Lemma 3.** For any mesh function  $(T_m)_{ijk}^n$  with satisfying the boundary condition, Eq. (3.6) has

$$\begin{aligned} \Delta r \sum_{i=2}^{I-1} P_r \left[ (T_m)_{ijk}^n \right] \cdot (T_m)_{ijk}^n + r_{\frac{3}{2}}^2 \nabla_{\bar{r}} (T_m)_{2,jk}^n \cdot (T_m)_{1,jk}^n - r_{I-\frac{1}{2}}^2 \nabla_{\bar{r}} (T_m)_{I,jk}^n \cdot (T_m)_{I,jk}^n \\ = -\Delta r \sum_{i=2}^I r_{i-\frac{1}{2}}^2 \left[ \nabla_{\bar{r}} (T_m)_{ijk}^n \right]^2, \end{aligned} \quad (4.34a)$$

$$\Delta \theta \sum_{j=0}^{J-1} P_\theta \left[ (T_m)_{ijk}^n \right] \cdot (T_m)_{ijk}^n = -\Delta \theta \sum_{j=1}^J \left[ \nabla_{\bar{\theta}} (T_m)_{ijk}^n \right]^2, \quad (4.34b)$$

$$\Delta \mu \sum_{k=0}^{K-1} P_\mu \left[ (T_m)_{ijk}^n \right] \cdot (T_m)_{ijk}^n = -\Delta \mu \sum_{k=1}^K \left[ \left( 1 - \mu_{k-\frac{1}{2}}^2 \right) \nabla_{\bar{\mu}} (T_m)_{ijk}^n \right]^2 \quad (4.34c)$$

for any  $1 \leq i \leq I$ .

*Proof.* The LHS of Eq. (4.34a) can be changed to

$$\begin{aligned} LHS &= \frac{1}{\Delta r} \sum_{i=2}^{I-1} \left\{ r_{i+\frac{1}{2}}^2 \left[ (T_m)_{i+1,jk}^n - (T_m)_{ijk}^n \right] - r_{i-\frac{1}{2}}^2 \left[ (T_m)_{ijk}^n - (T_m)_{i-1,jk}^n \right] \right\} \cdot (T_m)_{ijk}^n \\ &\quad + r_{\frac{3}{2}}^2 \nabla_{\bar{r}} (T_m)_{2,jk}^n \cdot (T_m)_{1,jk}^n - r_{I-\frac{1}{2}}^2 \nabla_{\bar{r}} (T_m)_{I,jk}^n \cdot (T_m)_{I,jk}^n \\ &= \sum_{i=3}^I r_{i-\frac{1}{2}}^2 \nabla_{\bar{r}} (T_m)_{ijk}^n \cdot (T_m)_{i-1,jk}^n - \sum_{i=2}^{I-1} r_{i-\frac{1}{2}}^2 \nabla_{\bar{r}} (T_m)_{ijk}^n \cdot (T_m)_{ijk}^n \\ &\quad + r_{\frac{3}{2}}^2 \nabla_{\bar{r}} (T_m)_{2,jk}^n \cdot (T_m)_{1,jk}^n - r_{I-\frac{1}{2}}^2 \nabla_{\bar{r}} (T_m)_{I,jk}^n \cdot (T_m)_{I,jk}^n \\ &= \sum_{i=2}^I r_{i-\frac{1}{2}}^2 \nabla_{\bar{r}} (T_m)_{ijk}^n \cdot (T_m)_{i-1,jk}^n - \sum_{i=2}^I r_{i-\frac{1}{2}}^2 \nabla_{\bar{r}} (T_m)_{ijk}^n \cdot (T_m)_{ijk}^n \end{aligned}$$

$$= -\Delta r \sum_{i=2}^I r_{i-\frac{1}{2}}^2 \left[ \nabla_r (T_m)_{ijk}^n \right]^2. \quad \blacksquare$$

Proof of Eq. (4.34b) and Eq. (4.34c) is similar to Eq. (4.26a). Now the stability of the 3D first improved CN scheme can be proved.

**Theorem 4.** The 3D first improved CN scheme, Eqs. (4.19), (4.21) and (4.22), is unconditionally stable with respect to the initial condition  $(T_m)_{ijk}^0 = (T_m^0)_{ijk}$  and source terms.

*Proof.* Multiplying Eq. (4.19a) by  $r_i^2 \Delta r \Delta \theta \Delta \mu \Delta t W_i \left[ (T_1)_{ijk}^n \right]$ , Eq. (4.19b) by  $r_i^2 \Delta r \Delta \theta \Delta \mu \Delta t W_i \left[ (T_m)_{ijk}^n \right]$ , Eq. (4.19c) by  $r_i^2 \Delta r \Delta \theta \Delta \mu \Delta t W_i \left[ (T_N)_{ijk}^n \right]$  for interior points  $i = 2, \dots, I-1$ ; multiplying Eq. (4.21a) by  $r_1^2 \frac{b}{a} \Delta r \Delta \theta \Delta \mu \Delta t W_i \left[ (T_1)_{1jk}^n \right]$ , Eq. (4.21b) by  $r_1^2 \frac{b}{a} \Delta r \Delta \theta \Delta \mu \Delta t W_i \left[ (T_m)_{1jk}^n \right]$ , Eq. (4.21c) by  $r_1^2 \frac{b}{a} \Delta r \Delta \theta \Delta \mu \Delta t W_i \left[ (T_N)_{1jk}^n \right]$  for the left boundary; multiplying Eq. (4.22a) by  $r_i^2 \frac{b^*}{a} \Delta r \Delta \theta \Delta \mu \Delta t W_i \left[ (T_1)_{ijk}^n \right]$  Eq. (4.22b) by  $r_i^2 \frac{b^*}{a} \Delta r \Delta \theta \Delta \mu \Delta t W_i \left[ (T_m)_{ijk}^n \right]$ , Eq. (4.22c) by  $r_i^2 \Delta r \Delta \theta \Delta \mu \Delta t W_i \left[ (T_N)_{ijk}^n \right]$ , adding all equations together over  $1 \leq m \leq N, 1 \leq i \leq I, 1 \leq j \leq J-1, 1 \leq k \leq K-1$ , and applying Lemma 3 and Lemma 4, this gives:

$$\begin{aligned} & \frac{1}{2} \Delta r \Delta \theta \Delta \mu \sum_{m=1}^N C_m \sum_{j=0}^{J-1} \sum_{k=1}^{K-1} \left\{ \frac{b}{a} \left[ \left[ (T_m)_{1jk}^{n+1} \right]^2 - \left[ (T_m)_{1jk}^n \right]^2 \right] r_1^2 + \sum_{i=2}^{I-1} \left\{ \left[ (T_m)_{ijk}^{n+1} \right]^2 - \left[ (T_m)_{ijk}^n \right]^2 \right\} r_i^2 \right. \\ & \left. + \frac{b^*}{a} \left\{ \left[ (T_m)_{ijk}^{n+1} \right]^2 - \left[ (T_m)_{ijk}^n \right]^2 \right\} r_i^2 \right\} + \Delta r \Delta \theta \Delta \mu \Delta t \sum_{m=1}^N k_m \sum_{j=0}^{J-1} \sum_{k=1}^{K-1} \sum_{i=2}^I r_{i-\frac{1}{2}}^2 \left\{ \nabla_r W_i \left[ (T_m)_{ijk}^n \right] \right\}^2 \\ & + \Delta r \Delta \theta \Delta \mu \Delta t \sum_{m=1}^N k_m \sum_{i=2}^I \sum_{j=0}^{J-1} \sum_{k=1}^{K-1} r_{i-\frac{1}{2}}^2 \left\{ \nabla_r W_i \left[ (T_m)_{ijk}^n \right] \right\}^2 \end{aligned}$$

$$\begin{aligned}
& + \sum_{i=2}^{I-1} \left\{ \nabla_{\partial} \mathcal{W}_i \left[ (T_m)_{ijk}^n \right] \right\}^2 + \frac{b^*}{a} \left\{ \nabla_{\partial} \mathcal{W}_i \left[ (T_m)_{ijk}^n \right] \right\}^2 \\
& + \Delta r \Delta \theta \Delta \mu \Delta t \sum_{m=1}^N k_m \sum_{j=0}^{J-1} \sum_{k=1}^K \left( 1 - \mu_{k-\frac{1}{2}}^2 \right) \left\{ \frac{b}{a} \left\{ \nabla_{\mu} \mathcal{W}_i \left[ (T_m)_{1jk}^n \right] \right\}^2 \right. \\
& \quad \left. + \sum_{i=2}^{I-1} \left\{ \nabla_{\mu} \mathcal{W}_i \left[ (T_m)_{ijk}^n \right] \right\}^2 + \frac{b^*}{a} \left\{ \nabla_{\mu} \mathcal{W}_i \left[ (T_m)_{ijk}^n \right] \right\}^2 \right\} \\
& + \Delta r \Delta \theta \Delta \mu \Delta t \sum_{\substack{m, m_1=1 \\ m < m_1}}^N G_{mm_1} \sum_{j=0}^{J-1} \sum_{k=1}^{K-1} \left\{ \frac{b}{a} r_i^2 \left\{ \mathcal{W}_i \left[ (T_m)_{1jk}^n \right] - \mathcal{W}_i \left[ (T_{m_1})_{1jk}^n \right] \right\}^2 \right. \\
& \quad \left. + \sum_{i=2}^{I-1} r_i^2 \left\{ \mathcal{W}_i \left[ (T_m)_{ijk}^n \right] - \mathcal{W}_i \left[ (T_{m_1})_{ijk}^n \right] \right\}^2 + \frac{b^*}{a} r_i^2 \left\{ \mathcal{W}_i \left[ (T_m)_{ijk}^n \right] - \mathcal{W}_i \left[ (T_{m_1})_{ijk}^n \right] \right\}^2 \right\} \\
& = \frac{1}{2} \Delta r \Delta \theta \Delta \mu \Delta t \sum_{m=1}^N \sum_{j=0}^{J-1} \sum_{k=1}^{K-1} \left\{ \frac{b}{a} r_i^2 \mathcal{W}_i \left[ (T_m)_{1jk}^n \right] (\mathcal{Q}_m)_{1jk}^{n+\frac{1}{2}} \right. \\
& \quad \left. + \sum_{i=2}^I r_i^2 \mathcal{W}_i \left[ (T_m)_{ijk}^n \right] (\mathcal{Q}_m)_{ijk}^{n+\frac{1}{2}} + \frac{b^*}{a} r_i^2 \mathcal{W}_i \left[ (T_m)_{ijk}^n \right] (\mathcal{Q}_m)_{ijk}^{n+\frac{1}{2}} \right\}. \tag{4.35}
\end{aligned}$$

Since  $\frac{1}{(1-\mu_k^2)} \geq 0$ ,  $\left(1 - \mu_{k-\frac{1}{2}}^2\right) \geq 0$  and  $G_{mm_1} \geq 0$ , dropping non-negative terms in LHS of

Eq. (4.35) leads to

$$\begin{aligned}
& \frac{1}{2} \Delta r \Delta \theta \Delta \mu \sum_{m=1}^N C_m \sum_{j=0}^{J-1} \sum_{k=1}^{K-1} \left\{ \frac{b}{a} \left[ \left[ (T_m)_{1jk}^{n+1} \right]^2 - \left[ (T_m)_{1jk}^n \right]^2 \right] r_i^2 \right. \\
& \quad \left. + \sum_{i=2}^{I-1} \left\{ \left[ (T_m)_{ijk}^{n+1} \right]^2 - \left[ (T_m)_{ijk}^n \right]^2 \right\} r_i^2 + \frac{b^*}{a} \left\{ \left[ (T_m)_{ijk}^{n+1} \right]^2 - \left[ (T_m)_{ijk}^n \right]^2 \right\} r_i^2 \right\} \\
& \leq \Delta r \Delta \theta \Delta \mu \Delta t \sum_{m=1}^N \sum_{j=0}^{J-1} \sum_{k=1}^{K-1} \left\{ \frac{b}{a} r_i^2 \mathcal{W}_i \left[ (T_m)_{1jk}^n \right] (\mathcal{Q}_m)_{1jk}^{n+\frac{1}{2}} \right. \\
& \quad \left. + \sum_{i=2}^I r_i^2 \mathcal{W}_i \left[ (T_m)_{ijk}^n \right] (\mathcal{Q}_m)_{ijk}^{n+\frac{1}{2}} + \frac{b^*}{a} r_i^2 \mathcal{W}_i \left[ (T_m)_{ijk}^n \right] (\mathcal{Q}_m)_{ijk}^{n+\frac{1}{2}} \right\}. \tag{4.36}
\end{aligned}$$

Applying Cauchy-Schwartz's inequality provides the result of

$$(\mathcal{Q}_m)_{ijk}^{n+\frac{1}{2}} \cdot [(T_m)_{ijk}^{n+1} + (T_m)_{ijk}^n] \leq \frac{1}{2C_m} \left[ (\mathcal{Q}_m)_{ijk}^{n+\frac{1}{2}} \right]^2 + C_m \left\{ [(T_m)_{ijk}^{n+1}]^2 + [(T_m)_{ijk}^n]^2 \right\}. \quad (4.37)$$

Substituting Eq. (4.37) into Eq. (4.36) leads to

$$\begin{aligned} & \Delta r \Delta \theta \Delta \mu \sum_{m=1}^N C_m \sum_{j=0}^{J-1} \sum_{k=1}^{K-1} \left\{ \frac{b}{a} \left[ [(T_m)_{1jk}^{n+1}]^2 - [(T_m)_{1jk}^n]^2 \right] r_1^2 \right. \\ & \left. + \sum_{i=2}^{I-1} \left\{ [(T_m)_{ijk}^{n+1}]^2 - [(T_m)_{ijk}^n]^2 \right\} r_i^2 + \frac{b^*}{a^*} \left\{ [(T_m)_{ijk}^{n+1}]^2 - [(T_m)_{ijk}^n]^2 \right\} r_i^2 \right\} \\ & \leq \Delta r \Delta \theta \Delta \mu \Delta t \sum_{m=1}^N \frac{1}{2C_m} \sum_{j=0}^{J-1} \sum_{k=1}^{K-1} \left\{ \frac{b}{a} r_1^2 \left[ (\mathcal{Q}_m)_{1jk}^{n+\frac{1}{2}} \right]^2 + \sum_{i=2}^{I-1} r_i^2 \left[ (\mathcal{Q}_m)_{ijk}^{n+\frac{1}{2}} \right]^2 + \frac{b^*}{a^*} r_i^2 \left[ (\mathcal{Q}_m)_{ijk}^{n+\frac{1}{2}} \right]^2 \right\} \\ & \quad + \Delta r \Delta \theta \Delta \mu \Delta t \sum_{m=1}^N C_m \sum_{j=0}^{J-1} \sum_{k=1}^{K-1} \left\{ \frac{b}{a} r_1^2 \left\{ [(T_m)_{1jk}^{n+1}]^2 + [(T_m)_{1jk}^n]^2 \right\} \right. \\ & \quad \left. + \sum_{i=2}^{I-1} r_i^2 \left\{ [(T_m)_{ijk}^n]^2 + [(T_m)_{ijk}^{n+1}]^2 \right\} + \frac{b^*}{a^*} r_i^2 \left\{ [(T_m)_{ijk}^{n+1}]^2 + [(T_m)_{ijk}^n]^2 \right\} \right\}. \quad (4.38) \end{aligned}$$

Denoting

$$F(n) = \Delta r \Delta \theta \Delta \mu \Delta t \sum_{m=1}^N C_m \left\{ \frac{b}{a} [(T_m)_{1jk}^n]^2 r_1^2 + \sum_{i=2}^{I-1} [(T_m)_{ijk}^n]^2 r_i^2 + \frac{b^*}{a^*} [(T_m)_{ijk}^n]^2 r_i^2 \right\} \quad (4.39a)$$

and

$$\Phi(n) = \frac{\Delta r \Delta \theta \Delta \mu}{2C_m} \sum_{m=1}^N \sum_{j=0}^{J-1} \sum_{k=1}^{K-1} \left\{ \frac{b r_1^2}{a} \left[ (\mathcal{Q}_m)_{1jk}^{n+\frac{1}{2}} \right]^2 + \sum_{i=2}^{I-1} r_i^2 \left[ (\mathcal{Q}_m)_{ijk}^{n+\frac{1}{2}} \right]^2 + \frac{b^* r_i^2}{a^*} \left[ (\mathcal{Q}_m)_{ijk}^{n+\frac{1}{2}} \right]^2 \right\}, \quad (4.39b)$$

and substituting Eq. (4.39a) and Eq. (4.39b) into Eq. (4.38), this gives:

$$F(n+1)$$

$$\leq \frac{(1+\Delta t)}{(1-\Delta t)} F(n) + \frac{\Delta t}{(1-\Delta t)} \Phi(n)$$

$$\leq \frac{(1+\Delta t)}{(1-\Delta t)} \left[ \frac{(1+\Delta t)}{(1-\Delta t)} F(n-1) + \frac{\Delta t}{(1-\Delta t)} \Phi(n-1) \right] + \frac{\Delta t}{(1-\Delta t)} \Phi(n)$$

$$\begin{aligned}
&\leq \left( \frac{(1+\Delta t)}{(1-\Delta t)} \right)^{n+1} F(0) + \frac{(1+\Delta t)}{(1-\Delta t)} \left[ 1 + \frac{(1+\Delta t)}{(1-\Delta t)} + \cdots + \frac{(1+\Delta t)^{n+1}}{(1-\Delta t)^{n+1}} \right] \max_{0 \leq n_1 \leq n} \Phi(n_1) \\
&\leq \left( \frac{(1+\Delta t)}{(1-\Delta t)} \right)^{n+1} \left( F(0) + \max_{0 \leq n_1 \leq n} \Phi(n_1) \right). \tag{4.40}
\end{aligned}$$

Using the inequalities  $(1+\varepsilon)^n \leq e^{n\varepsilon}$  for  $\varepsilon > 0$  and  $(1-\varepsilon)^{-1} \leq e^{2\varepsilon}$  for  $0 < \varepsilon < \frac{1}{2}$  results in

$(1+\Delta t)^{n+1} \leq e^{(n+1)\Delta t}$  and  $(1-\Delta t)^{-1} \leq e^{2\Delta t}$ . Multiplying the two inequalities together leads to

$$(1+\Delta t)^{n+1} (1-\Delta t)^{-(n+1)} \leq e^{(n+1)\Delta t} \cdot e^{2(n+1)\Delta t} = e^{3(n+1)\Delta t}. \tag{4.41}$$

Substituting Eq. (4.41) into Eq. (4.40) results in

$$F(n+1) \leq e^{3n\Delta t} \left( F(0) + \max_{0 \leq n_1 \leq n} \Phi(n_1) \right) \leq e^{3t_0} \left( F(0) + \max_{0 \leq n_1 \leq n} \Phi(n_1) \right),$$

that is, for any  $0 \leq (n+1)\Delta t \leq t_0$ , the scheme is unconditionally stable with respect to the initial condition and source terms. ■

### 4.2.3 Stability of 3D Second Improved CN Scheme

Proving the stability of the 3D second improved CN scheme requires building Lemma 4. The stability will be proved basing on Lemma 1 and Lemma 4.

**Lemma 4.** For any mesh function  $(T_m)_{ijk}^n$ ,

$$\begin{aligned}
&\sum_{j=0}^{J-1} \sum_{k=1}^{K-1} \left\{ \Delta r \sum_{i=2}^{I-1} P_r \left[ (T_m)_{ijk}^n \right] \cdot (T_m)_{ijk}^n + r_{\frac{1}{2}}^2 \nabla_{\bar{r}} (T_m)_{1jk}^n \cdot (T_m)_{0jk}^n - r_{I-\frac{1}{2}}^2 \nabla_{\bar{r}} (T_m)_{Ijk}^n \cdot (T_m)_{Ijk}^n \right\} \\
&= -\Delta r \sum_{i=2}^I \sum_{j=0}^{J-1} \sum_{k=1}^K r_{i-\frac{1}{2}}^2 \left[ \nabla_{\bar{r}} (T_m)_{ijk}^n \right]^2. \tag{4.42a}
\end{aligned}$$

$$\Delta \theta \sum_{j=0}^{J-1} P_\theta \left[ (T_m)_{ijk}^n \right] \cdot (T_m)_{ijk}^n = -\Delta \theta \sum_{j=1}^J \left[ \nabla_{\bar{\theta}} (T_m)_{ijk}^n \right]^2, i = 1, \dots, I. \tag{4.42b}$$

$$\Delta\mu \sum_{k=0}^{K-1} P_\mu \left[ (T_m)_{ijk}^n \right] \cdot (T_m)_{ijk}^n = -\Delta\mu \sum_{k=1}^K \left[ \left( 1 - \mu^2_{k-\frac{1}{2}} \right) \nabla_{\bar{\mu}} (T_m)_{ijk}^n \right]^2, i=1, \dots, I. \quad (4.42c)$$

*Proof.*

$$\begin{aligned} LHS &= \sum_{j=0}^{J-1} \sum_{k=1}^{K-1} \left\{ \Delta r \sum_{i=1}^{I-1} \left[ r_{i+\frac{1}{2}}^2 \left[ (T_m)_{i+1,jk}^n - (T_m)_{ijk}^n \right] - r_{i-\frac{1}{2}}^2 \left[ (T_m)_{ijk}^n - (T_m)_{i-1,jk}^n \right] \right] \cdot (T_m)_{ijk}^n \right. \\ &\quad \left. + r_{\frac{1}{2}}^2 \nabla_{\bar{r}} (T_m)_{1,jk}^n \cdot (T_m)_{0,jk}^n - r_{I-\frac{1}{2}}^2 \nabla_{\bar{r}} (T_m)_{I,jk}^n \cdot (T_m)_{I,jk}^n \right\} \\ &= \sum_{j=0}^{J-1} \sum_{k=1}^{K-1} \left\{ \sum_{i=2}^I r_{i-\frac{1}{2}}^2 \nabla_{\bar{r}} (T_m)_{ijk}^n \cdot (T_m)_{i-1,jk}^n - \sum_{i=1}^{I-1} r_{i-\frac{1}{2}}^2 \nabla_{\bar{r}} (T_m)_{ijk}^n \cdot (T_m)_{ijk}^n \right. \\ &\quad \left. + r_{\frac{1}{2}}^2 \nabla_{\bar{r}} (T_m)_{1,jk}^n \cdot (T_m)_{0,jk}^n - r_{I-\frac{1}{2}}^2 \nabla_{\bar{r}} (T_m)_{I,jk}^n \cdot (T_m)_{I,jk}^n \right\} \\ &= \sum_{j=0}^{J-1} \sum_{k=1}^{K-1} \left\{ \sum_{i=1}^I r_{i-\frac{1}{2}}^2 \nabla_{\bar{r}} (T_m)_{ijk}^n \cdot (T_m)_{i-1,jk}^n - \sum_{i=1}^{I-1} r_{i-\frac{1}{2}}^2 \nabla_{\bar{r}} (T_m)_{ijk}^n \cdot (T_m)_{ijk}^n \right\} \\ &= -\Delta r \sum_{i=1}^I \sum_{j=0}^{J-1} \sum_{k=1}^{K-1} r_{i-\frac{1}{2}}^2 \left[ \nabla_{\bar{r}} (T_m)_{ijk}^n \right]^2. \quad \blacksquare \end{aligned}$$

Proof of Eq. (4.42b) and Eq. (4.42c) is similar to Eq. (4.42a). The stability of the 3D second improved CN scheme is proved.

**Theorem 5.** The 3D second improved CN scheme, Eqs. (4.19), (4.22) and (4.24), is unconditionally stable with respect to the initial condition  $(T_m)_{ijk}^0 = (T_m^0)_{ijk}$  and source terms.

*Proof.* Multiplying Eq. (4.19a) by  $r_i^2 \Delta r \Delta \theta \Delta \mu \Delta t W_i \left[ (T_1)_{ijk}^n \right]$ , Eq. (4.19b) by  $r_i^2 \Delta r \Delta \theta \Delta \mu \Delta t W_i \left[ (T_m)_{ijk}^n \right]$ , Eq. (4.19c) by  $r_i^2 \Delta r \Delta \theta \Delta \mu \Delta t W_i \left[ (T_N)_{ijk}^n \right]$  for interior points  $i=1, \dots, I-1$ ; multiplying Eq. (4.24a) by  $\frac{2\pi}{3} r_{\frac{1}{2}}^2 \Delta r \Delta t W_i \left[ (T_1)_{1,jk}^n \right]$ , Eq. (4.24b) by

$\frac{2\pi}{3}r_1^2\Delta r\Delta tW_t\left[(T_m)_{1,jk}^n\right]$ , Eq. (4.24c) by  $\frac{2\pi}{3}r_1^2\Delta r\Delta tW_t\left[(T_N)_{1,jk}^n\right]$  for the left boundary;

multiplying Eq. (4.22a) by  $r_i^2\frac{b^*}{a^*}\Delta r\Delta\theta\Delta\mu\Delta tW_t\left[(T_1)_{ijk}^n\right]$ , Eq. (4.22b) by

$r_i^2\frac{b^*}{a^*}\Delta r\Delta\theta\Delta\mu\Delta tW_t\left[(T_m)_{ijk}^n\right]$ , Eq. (4.22c) by  $r_i^2\Delta r\Delta\theta\Delta\mu\Delta tW_t\left[(T_N)_{ijk}^n\right]$  for the right

boundary, adding together over  $1\leq m\leq N$ ,  $0\leq i\leq I$ ,  $0\leq j\leq J-1$ ,  $1\leq k\leq K-1$  and

applying Lemma 1 and Lemma 4, this gives:

$$\begin{aligned}
& \frac{1}{2}\Delta r\sum_{m=1}^N C_m\sum_{j=0}^{J-1}\sum_{k=1}^{K-1}\left\{\frac{2\pi}{3}\left\{\left[(T_m)_0^{n+1}\right]^2-\left[(T_m)_0^n\right]^2\right\}r_1^2\right. \\
& +\Delta\theta\Delta\mu\sum_{i=1}^{I-1}\left\{\left[(T_m)_{ijk}^{n+1}\right]^2-\left[(T_m)_{ijk}^n\right]^2\right\}r_i^2+\Delta\theta\Delta\mu\frac{b^*}{a^*}\left\{\left[(T_m)_{ijk}^{n+1}\right]^2-\left[(T_m)_{ijk}^n\right]^2\right\}r_i^2\left. \right\} \\
& +\Delta r\Delta\theta\Delta\mu\Delta t\sum_{m=1}^N k_m\sum_{i=1}^I\sum_{j=0}^{J-1}\sum_{k=1}^{K-1}r_{i-\frac{1}{2}}^2\left\{\nabla_{\theta}W_t\left[(T_m)_{ijk}^n\right]\right\}^2 \\
& +\Delta r\Delta\theta\Delta\mu\Delta t\sum_{m=1}^N k_m\sum_{j=1}^J\sum_{k=1}^{K-1}\frac{1}{(1-\mu_k^2)}\left\{\sum_{i=1}^{I-1}\left\{\nabla_{\theta}W_t\left[(T_m)_{ijk}^n\right]\right\}^2+\frac{b^*}{a^*}\left\{\nabla_{\theta}W_t\left[(T_m)_{ijk}^n\right]\right\}^2\right\} \\
& +\Delta r\Delta\theta\Delta\mu\Delta t\sum_{m=1}^N k_m\sum_{j=0}^{J-1}\sum_{k=1}^K\left(1-\mu_{k-\frac{1}{2}}^2\right)\left\{\sum_{i=1}^{I-1}\left\{\nabla_{\theta}W_t\left[(T_m)_{ijk}^n\right]\right\}^2+\frac{b^*}{a^*}\left\{\nabla_{\theta}W_t\left[(T_m)_{ijk}^n\right]\right\}^2\right\} \\
& +\Delta r\Delta t\sum_{\substack{m,m_1=1 \\ m<m_1}}^N\sum_{j=0}^{J-1}\sum_{k=1}^{K-1}G_{mm_1}\left\{\frac{2\pi}{3}r_1^2\left\{W_t\left[(T_m)_0^n\right]-W_t\left[(T_{m_1})_0^n\right]\right\}\right\}^2 \\
& +\Delta\theta\Delta\mu\sum_{i=1}^{I-1}r_i^2\left\{W_t\left[(T_m)_{ijk}^n\right]-W_t\left[(T_{m_1})_{ijk}^n\right]\right\}^2+\Delta\theta\Delta\mu\frac{b^*}{a^*}r_i^2\left\{W_t\left[(T_m)_{ijk}^n\right]-W_t\left[(T_{m_1})_{ijk}^n\right]\right\}^2\left. \right\} \\
& =\Delta r\Delta t\sum_{m=1}^N\sum_{j=0}^{J-1}\sum_{k=1}^{K-1}\left\{\frac{2\pi}{3}r_1^2W_t\left[(T_m)_0^n\right](Q_m)_0^{n+\frac{1}{2}}+\Delta\theta\Delta\mu\sum_{i=1}^{I-1}r_i^2W_t\left[(T_m)_{ijk}^n\right](Q_m)_{ijk}^{n+\frac{1}{2}}\right. \\
& \left. +\Delta\theta\Delta\mu\frac{b^*}{a^*}r_i^2W_t\left[(T_m)_{ijk}^n\right](Q_m)_{ijk}^{n+\frac{1}{2}}\right\}. \tag{4.43}
\end{aligned}$$

Since  $\frac{1}{(1-\mu_k^2)} \geq 0$ ,  $\left(1-\mu_{k-\frac{1}{2}}^2\right) \geq 0$  and  $G_{mm} \geq 0$ , the positive terms in LHS of Eq. (4.43)

can be dropped, and this gives:

$$\begin{aligned}
& \frac{1}{2} \Delta r \sum_{m=1}^N C_m \sum_{j=0}^{J-1} \sum_{k=1}^{K-1} \left\{ \frac{2\pi}{3} \left\{ \left[ (T_m)_0^{n+1} \right]^2 - \left[ (T_m)_0^n \right]^2 \right\} r_i^2 \right. \\
& + \Delta \theta \Delta \mu \sum_{i=1}^{I-1} \left\{ \left[ (T_m)_{ijk}^{n+1} \right]^2 - \left[ (T_m)_{ijk}^n \right]^2 \right\} r_i^2 + \Delta \theta \Delta \mu \frac{b^*}{a} \left\{ \left[ (T_m)_{ijk}^{n+1} \right]^2 - \left[ (T_m)_{ijk}^n \right]^2 \right\} r_i^2 \left. \right\} \\
& \leq \Delta r \Delta t \sum_{m=1}^N \sum_{j=0}^{J-1} \sum_{k=1}^{K-1} \left\{ \frac{2\pi}{3} r_i^2 W_i \left[ (T_m)_0^n \right] (Q_m)_0^{n+\frac{1}{2}} + \Delta \theta \Delta \mu \sum_{i=1}^{I-1} r_i^2 W_i \left[ (T_m)_{ijk}^n \right] (Q_m)_{ijk}^{n+\frac{1}{2}} \right. \\
& \quad \left. + \Delta \theta \Delta \mu \frac{b^*}{a} r_i^2 W_i \left[ (T_m)_{ijk}^n \right] (Q_m)_{ijk}^{n+\frac{1}{2}} \right\}. \tag{4.44}
\end{aligned}$$

Using Cauchy-Schwartz's inequality results in

$$(Q_m)_{ijk}^{n+\frac{1}{2}} \cdot \left[ (T_m)_{ijk}^{n+1} + (T_m)_{ijk}^n \right] \leq \frac{1}{2C_m} \left[ (Q_m)_{ijk}^{n+\frac{1}{2}} \right]^2 + C_m \left\{ \left[ (T_m)_{ijk}^{n+1} \right]^2 + \left[ (T_m)_{ijk}^n \right]^2 \right\}. \tag{4.45}$$

Substituting Eq. (4.45) into Eq. (4.44) leads to

$$\begin{aligned}
& \frac{1}{2} \Delta r \sum_{m=1}^N C_m \sum_{j=0}^{J-1} \sum_{k=1}^{K-1} \left\{ \frac{2\pi}{3} \left\{ \left[ (T_m)_0^{n+1} \right]^2 - \left[ (T_m)_0^n \right]^2 \right\} r_i^2 \right. \\
& + \Delta \theta \Delta \mu \sum_{i=1}^{I-1} \left\{ \left[ (T_m)_{ijk}^{n+1} \right]^2 - \left[ (T_m)_{ijk}^n \right]^2 \right\} r_i^2 + \Delta \theta \Delta \mu \frac{b^*}{a} \left\{ \left[ (T_m)_{ijk}^{n+1} \right]^2 - \left[ (T_m)_{ijk}^n \right]^2 \right\} r_i^2 \left. \right\} \\
& \leq \Delta r \Delta t \sum_{m=1}^N \frac{1}{2C_m} \sum_{j=0}^{J-1} \sum_{k=1}^{K-1} \left\{ \frac{2\pi}{3} \left[ (Q_m)_0^{n+\frac{1}{2}} \right]^2 + \Delta \theta \Delta \mu \sum_{i=1}^{I-1} r_i^2 \left[ (Q_m)_{ijk}^{n+\frac{1}{2}} \right]^2 + \Delta \theta \Delta \mu \frac{b^*}{a} r_i^2 \left[ (Q_m)_{ijk}^{n+\frac{1}{2}} \right]^2 \right\} \\
& + \Delta r \Delta t \sum_{m=1}^N C_m \sum_{j=0}^{J-1} \sum_{k=1}^{K-1} \left\{ \frac{2\pi}{3} r_i^2 \left\{ \left[ (T_m)_0^{n+1} \right]^2 + \left[ (T_m)_0^n \right]^2 \right\} + \Delta \theta \Delta \mu \sum_{i=1}^{I-1} r_i^2 \left\{ \left[ (T_m)_{ijk}^{n+1} \right]^2 + \left[ (T_m)_{ijk}^n \right]^2 \right\} \right. \\
& \quad \left. + \Delta \theta \Delta \mu \frac{b^*}{a} r_i^2 \left\{ \left[ (T_m)_{ijk}^{n+1} \right]^2 + \left[ (T_m)_{ijk}^n \right]^2 \right\} \right\}. \tag{4.46}
\end{aligned}$$

Denoting

$$F(n) = \Delta r \Delta t \sum_{m=1}^N C_m \sum_{j=0}^{J-1} \sum_{k=1}^{K-1} \left\{ \frac{3\pi}{2} r_{\frac{1}{2}}^2 \left[ (T_m)_0^n \right]^2 + \sum_{i=1}^{I-1} r_i^2 \left[ (T_m)_{ijk}^n \right]^2 + \frac{b^*}{a} r_i^2 \left[ (T_m)_{ijk}^n \right]^2 \right\} \quad (4.47a)$$

and

$$\begin{aligned} \Phi(n) = & \Delta r \Delta t \sum_{m=1}^N \frac{1}{2C_m} \sum_{j=0}^{J-1} \sum_{k=1}^{K-1} \left\{ \frac{2\pi}{3} \left[ (Q_m)_0^{n+\frac{1}{2}} \right]^2 \right. \\ & \left. + \Delta \theta \Delta \mu \sum_{i=1}^{I-1} r_i^2 \left[ (Q_m)_{ijk}^{n+\frac{1}{2}} \right]^2 + \Delta \theta \Delta \mu \frac{b^*}{a} r_i^2 \left[ (Q_m)_{ijk}^{n+\frac{1}{2}} \right]^2 \right\}, \end{aligned} \quad (4.47b)$$

and substituting Eq. (4.47) into Eq. (4.46), this gives:

$$\begin{aligned} & F(n+1) \\ & \leq \frac{(1+\Delta t)}{(1-\Delta t)} F(n) + \frac{\Delta t}{(1-\Delta t)} \Phi(n) \\ & \leq \frac{(1+\Delta t)}{(1-\Delta t)} \left[ \frac{(1+\Delta t)}{(1-\Delta t)} F(n-1) + \frac{\Delta t}{(1-\Delta t)} \Phi(n-1) \right] + \frac{2\Delta t}{(1-\Delta t)} \Phi(n) \\ & \leq \left( \frac{(1+\Delta t)}{(1-\Delta t)} \right)^{n+1} F(0) + \frac{(1+\Delta t)}{(1-\Delta t)} \left[ 1 + \frac{(1+\Delta t)}{(1-\Delta t)} + \dots + \frac{(1+\Delta t)^{n+1}}{(1-\Delta t)} \right] \max_{0 \leq n_1 \leq n} \Phi(n_1) \\ & \leq \left( \frac{(1+\Delta t)}{(1-\Delta t)} \right)^{n+1} \left( F(0) + \max_{0 \leq n_1 \leq n} \Phi(n_1) \right). \end{aligned} \quad (4.48)$$

Using the inequalities  $(1+\varepsilon)^n \leq e^{n\varepsilon}$  for  $\varepsilon > 0$  and  $(1-\varepsilon)^{-1} \leq e^{2\varepsilon}$  for  $0 < \varepsilon < \frac{1}{2}$  results in

$(1+\Delta t)^{n+1} \leq e^{(n+1)\Delta t}$  and  $(1-\Delta t)^{-1} \leq e^{2\Delta t}$ . Multiplying the two inequalities together leads to

$$(1+\Delta t)^{n+1} (1-\Delta t)^{-(n+1)} \leq e^{(n+1)\Delta t} \cdot e^{2(n+1)\Delta t} = e^{3(n+1)\Delta t}. \quad (4.49)$$

After substituting Eq. (4.49) into Eq. (4.48),

$$F(n+1) \leq e^{3n\Delta t} \left( F(0) + \max_{0 \leq n_1 \leq n} \Phi(n_1) \right) \leq e^{3n} \left( F(0) + \max_{0 \leq n_1 \leq n} \Phi(n_1) \right)$$

is obtained, that is, for any  $0 \leq (n+1)\Delta t \leq t_0$ , the scheme is unconditionally stable with respect to the initial condition and heat source terms. ■

### 4.3 General Algorithms

#### 4.3.1 1D Case

In Section 4.3.1, an algorithm for the 1D improved CN scheme with temperature  $T_l$ ,  $T_m$  and  $T_N$  is developed for the purpose of coding. A Gauss-Seidel method is used to solve the linear system from the 1D improved CN scheme. In detail, the algorithm work through following steps:

Step 1. Set the initial value for  $(T_l)_i^n$ ,  $(T_m)_i^n$  and  $(T_N)_i^n$  by Eq. (3.2);

Step 2. Solve  $(T_l)_i^{n+1}$  through Eqs. (4.2a), (4.16a) and (4.17a);

Step 3. Substitute the value of  $(T_l)_i^{n+1}$  into Eqs. (4.2b), (4.16b) and (4.17b), solve  $(T_m)_i^{n+1}$  through Eqs. (4.2b), (4.16b) and (4.17b);

Step 5. Substitute new value of  $(T_m)_i^{n+1}$  into Eqs. (4.2c), (4.16c) and (4.17c), solve  $(T_N)_i^{n+1}$  through Eqs. (4.2c), (4.16c) and (4.17c);

Step 6. Check the convergence of Gauss-Seidel iteration, with a tolerance and a small number  $tol$ , if the following condition:

$$\max \left\| (T_l)_i^{n+1(new)} - (T_l)_i^{n+1(old)} \right\| \leq tol ,$$

$$\max \left\| (T_m)_i^{n+1(new)} - (T_m)_i^{n+1(old)} \right\| \leq tol ,$$

$$\max \left\| (T_N)_i^{n+1(new)} - (T_N)_i^{n+1(old)} \right\| \leq tol$$

are satisfied, stop;

Step 7. Update new value of  $(T_1)_i^{n+1}$ ,  $(T_m)_i^{n+1}$  and  $(T_N)_i^{n+1}$  to the current time step  $n$ .

#### 4.3.2 3D Case

In Section 4.3.2, for the purpose of coding, an algorithm for the 3D first improved CN scheme and the 3D second improved CN with the temperature  $T_l$ ,  $T_m$  and  $T_N$  is developed. A Gauss-Seidel method is used to solve the linear system from the two improved schemes. In details, the algorithm works through following steps:

Step 1. Set the initial value for  $(T_1)_{ijk}^n$ ,  $(T_m)_{ijk}^n$  and  $(T_N)_{ijk}^n$  by Eq. (3.5);

Step 2. For the 3D first improved CN scheme, solve  $(T_1)_{ijk}^n$  by Eqs. (4.19a), (4.21a) and (4.22a), and for the 3D second improved CN scheme, solve  $(T_1)_{ijk}^n$  by Eqs. (4.19a), (4.22a) and (4.24a);

Step 3. For the 3D first improved CN scheme, solve  $(T_m)_{ijk}^n$  by substituting the value of  $(T_1)_{ijk}^{n+1}$  into Eqs. (4.19b), (4.21b) and (4.22b), and for in the 3D second improved CN scheme, solve  $(T_m)_{ijk}^n$  by substituting the value of  $(T_1)_{ijk}^{n+1}$  into Eqs. (4.19b), (4.22b) and (4.24b);

Step 4. For the 3D first improved CN scheme, solve  $(T_N)_{ijk}^n$  by substituting the value of  $(T_m)_{ijk}^{n+1}$  into Eqs. (4.20c), (4.21c) and (4.22c), and for the 3D second improved CN scheme, solve  $(T_N)_{ijk}^n$  by substituting the value of  $(T_m)_{ijk}^{n+1}$  into Eqs. (4.19c), (4.22c) and (4.24c);

Step 6. Check the convergence of Gauss-Seidel iteration, with a tolerance and a small number  $tol$ , if the following condition:

$$\max \left\| (T_1)_{ijk}^{n+1(new)} - (T_1)_{ijk}^{n+1(old)} \right\| \leq tol ,$$

$$\max \left\| (T_m)_{ijk}^{n+1(new)} - (T_m)_{ijk}^{n+1(old)} \right\| \leq tol ,$$

$$\max \left\| (T_N)_{ijk}^{n+1(new)} - (T_N)_{ijk}^{n+1(old)} \right\| \leq tol$$

are satisfied, stop;

Step 7. Update new value to  $(T_1)_{ijk}^{n+1}$ ,  $(T_m)_{ijk}^{n+1}$  and  $(T_N)_{ijk}^{n+1}$  to current time step  $n$ .

## CHAPTER FIVE

### NUMERICAL EXAMPLES

In Chapter Five, three numerical examples are provided to verify the availability of the parabolic models in an  $N$ -carrier system and improved CN schemes in Chapter Three and in Chapter Four.

#### 5.1 1D Case

The first example Eq. (5.1) is in 1D spherical coordinates, which is satisfied with the governing equation Eq. (3.1). It is solved by the 1D improved CN scheme Eqs. (4.2), (4.16) and (4.17) and the 1D CN scheme Eqs. (4.2) and (4.3).

##### 5.1.1 Example Description

This example is a *Three*-carrier system with three variables  $T_1$ ,  $T_2$  and  $T_3$ . The governing equation for this example is:

$$\begin{aligned} \frac{\partial T_1}{\partial t} = \frac{2}{r^2} \frac{\partial}{\partial r} \left( r^2 \frac{\partial T_1}{\partial r} \right) - \pi^2 (T_1 - T_2) - \pi^2 (T_1 - T_3) \\ + 2\pi^2 e^{-\pi t} \cos \pi r + \frac{5}{r} \pi e^{-\pi t} \sin \pi r, \end{aligned} \quad (5.1a)$$

$$\frac{\partial T_2}{\partial t} = \frac{2}{r^2} \frac{\partial}{\partial r} \left( r^2 \frac{\partial T_2}{\partial r} \right) + \pi^2 (T_1 - T_2) - \pi^2 (T_2 - T_3) + \frac{4}{r} \pi e^{-\pi t} \sin \pi r, \quad (5.1b)$$

$$\frac{\partial T_3}{\partial t} = \frac{2}{r^2} \frac{\partial}{\partial r} \left( r^2 \frac{\partial T_3}{\partial r} \right) + \pi^2 (T_2 - T_3) + \pi^2 (T_1 - T_3) + \frac{3}{r} \pi e^{-\pi t} \sin \pi r. \quad (5.1c)$$

The boundary condition for this is Eq. (3.3), and the initial condition for this example is

$T_1 = \frac{5}{4} \cos \pi r$ ,  $T_2 = \cos \pi r$  and  $T_3 = \frac{3}{4} \cos \pi r$ . The exact solution for Eq. (5.1) is:

$$T_1 = \frac{5}{4} e^{-\pi^2 t} \cos \pi r, \quad (5.2a)$$

$$T_2 = e^{-\pi^2 t} \cos \pi r, \quad (5.2b)$$

$$T_3 = \frac{3}{4} e^{-\pi^2 t} \cos \pi r. \quad (5.2c)$$

In the 1D improved CN scheme, the grid step size  $\Delta r$  and the time step size  $\Delta t$  are set as following combination:  $2 \times 10^{-3}$  and  $2 \times 10^{-3}$ ,  $10^{-3}$  and  $10^{-3}$ ,  $5 \times 10^{-4}$  and  $5 \times 10^{-4}$ . In the 1D CN scheme, the grid step size  $\Delta r$  and the time step size  $\Delta t$  are set as following combination:  $2 \times 10^{-5}$  and  $2 \times 10^{-5}$ ,  $10^{-5}$  and  $10^{-5}$ ,  $5 \times 10^{-6}$  and  $5 \times 10^{-6}$ . Also, the upper boundary for time  $t_0$  as 1.0 is set in this example. The schemes are programed by Fortran 77, and the source code can be found in APPENDIX.

### 5.1.2 Results and Analysis

In order to evaluate the difference between the numerical solution and the exact solution for each scheme,  $l_2$ -norm error is defined as

$$E(I, \Delta t) = \max_{0 \leq n \Delta t \leq t_0} \sqrt{\frac{\Delta r}{3} \sum_{m=1}^3 \sum_{i=1}^I \left\{ (T_m)_i^n - (T_m^{exact})_i^n \right\}^2}, \quad (5.3)$$

where  $(T_m)_i^n$  is the numerical solution for the carrier  $m$ , and  $(T_m^{exact})_i^n$  is the exact solution for the carrier  $m$ .

In order to analyze the order of the scheme, the convergence rates are defined as

$$\log_2 \left[ \frac{E(I_1, \Delta t)}{E(I_2, \Delta t)} \right] \quad (5.4a)$$

and

$$\log_2 \left[ \frac{E(I, \Delta t_1)}{E(I, \Delta t_2)} \right], \quad (5.4b)$$

with respect to the spatial variable  $r$  and the temporal variable  $t$ , respectively.

The maximum  $l_2$ -norm error Eq. (5.3) and comparisons of convergence rates Eq. (5.4) are in Table 5.1 and Table 5.2. The  $l_2$ -norm errors along the time  $t$  for both schemes are plotted in Figure 5.1. The numerical result for the 1D improved CN scheme are plotted in Figure 5.2, Figure 5.3 and Figure 5.4, and the numerical result for the 1D CN scheme are plotted in Figure 5.5, Figure 5.6 and Figure 5.7.

Table 1 will show the numerical result when  $\Delta t = 10^{-5}$ ,  $I = 51, 101$ , and  $201$  for the the 1D improved CN scheme, and  $I = 50, 100$ , and  $200$  for the 1D CN scheme, respectively.

Table 5.1 Comparison of  $l_2$ -norm errors and convergence rates with respect to  $r$  of the 1D improved CN scheme and the 1D CN scheme with  $0 \leq t \leq 1.0$ ,  $\Delta t = 10^{-5}$ .

grid	$l_2$ -norm error for the 1D improved CN scheme	convergence rate	$l_2$ -norm error for the 1D CN scheme	convergence rate
I=51	$4.02888 \times 10^{-4}$	-	$6.04009 \times 10^{-2}$	-
I=101	$1.00495 \times 10^{-4}$	2.003	$3.00986 \times 10^{-2}$	1.005
I=201	$2.49340 \times 10^{-5}$	2.011	$1.50240 \times 10^{-2}$	1.002

As shown in Table 1, the convergence rate of the 1D improved CN scheme is about 2 with respect to the spatial variable  $r$ , while the one for the 1D CN scheme is about 1 with respect to the spatial variable  $r$ . Furthermore, comparing the  $l_2$ -norm errors of numerical solutions between the 1D improved CN scheme and the 1D CN scheme in Table 5.1 will show that the 1D improved CN scheme is more accurate than the 1D CN scheme.

In order to calculate the convergence rate with respect to the temporal variable  $t$ ,  $I = 10^5$  for the 1D improved CN scheme,  $I = 10^5$  for the 1D CN scheme, and  $\Delta t = 2 \times 10^{-2}$ ,  $10^{-2}$ , and  $5 \times 10^{-3}$  are chosen, respectively. Table 5.2 shows that the convergence rates of both schemes with respect to the temporal variable  $t$  are about 2, and  $l_2$ -norm errors of the numerical solution of both schemes are nearly same. There are as expected because the truncation error of the 1D improved CN scheme is  $O(\Delta t^2)$  with respect to the temporal variable  $t$ .

Table 5.2 Comparison of  $l_2$ -norm errors and convergence rates with respect to  $t$  of the 1D the improved CN scheme and the 1D CN scheme.

$\Delta t$	$l_2$ -norm error for the 1D improved CN method	convergence rate	$l_2$ -norm error for the 1D CN scheme	convergence rate
0.02	$2.95456 \times 10^{-3}$	-	$2.95151 \times 10^{-3}$	-
0.01	$7.36237 \times 10^{-4}$	2.005	$7.33922 \times 10^{-4}$	2.008
0.005	$1.83243 \times 10^{-4}$	2.006	$1.81036 \times 10^{-4}$	2.019

Figure 5.1 shows  $l_2$ -norm errors of the 1D improved CN scheme and the 1D CN scheme along the time  $t$  with  $0 \leq t \leq 1.0$ . From Figure 5.1 it can be seen that, when  $\Delta r = 10^{-3}$  and  $\Delta t = 10^{-3}$ , the 1D improved CN scheme will produce a  $l_2$ -norm error about  $10^{-5}$ , so the 1D CN scheme is second-order accuracy, which can also be seen in Table 5.1. Figure 5.1 shows that, when  $\Delta r = 10^{-5}$  and  $\Delta t = 10^{-5}$ , the 1D CN scheme will produce a  $l_2$ -norm error about  $10^{-5}$ , so the 1D CN scheme is first-order, which can also be seen in Table 5.1. Also, from Figure 5.1, the 1D improved CN scheme is more accurate than the 1D CN scheme.

Figure 5.2 is the distribution of the temperature  $T_1$  along the radial distance  $r$  at different time: (a)  $t = 0.1$  (b)  $t = 0.2$  and (c)  $t = 1.0$ . Figure 5.3 is the change of temperature  $T_2$  along the radial distance  $r$  at different time (a)  $t = 0.1$  (b)  $t = 0.2$  and (c)  $t =$

1.0. Figure 5.4 is the change of the temperature  $T_3$  along the radial distance  $r$  at different time (a)  $t = 0.1$  (b)  $t = 0.2$  and (c)  $t = 1.0$ .

Figure 5.5 is the distribution of the temperature  $T_1$  along the radial distance  $r$  at different time: (a)  $t = 0.1$  (b)  $t = 0.2$  and (c)  $t = 1.0$ . Figure 5.6 is the change of temperature  $T_2$  along the radial distance  $r$  at different time (a)  $t = 0.1$  (b)  $t = 0.2$  and (c)  $t = 1.0$ . Figure 5.7 is the change of the temperature  $T_3$  along the radial distance  $r$  at different time (a)  $t = 0.1$  (b)  $t = 0.2$  and (c)  $t = 1.0$ .

Figure 5.2, Figure 5.3 and Figure 5.4 show that: there is a match between the numerical solution and the exact solution in (a), (b) and (c). Also, from Figure 5.2, Figure 5.3 and Figure 5.4, it is can be seen that the temperature is  $T_1 > T_2 > T_3$ , which is satisfied with our hypothesis in Figure 2.1.

Figure 5.5, Figure 5.6 and Figure 5.7 show that: in (a), (b) there is a match between the numerical solution and the exact solution, but in (c) the numerical solution and the exact solution do not match.

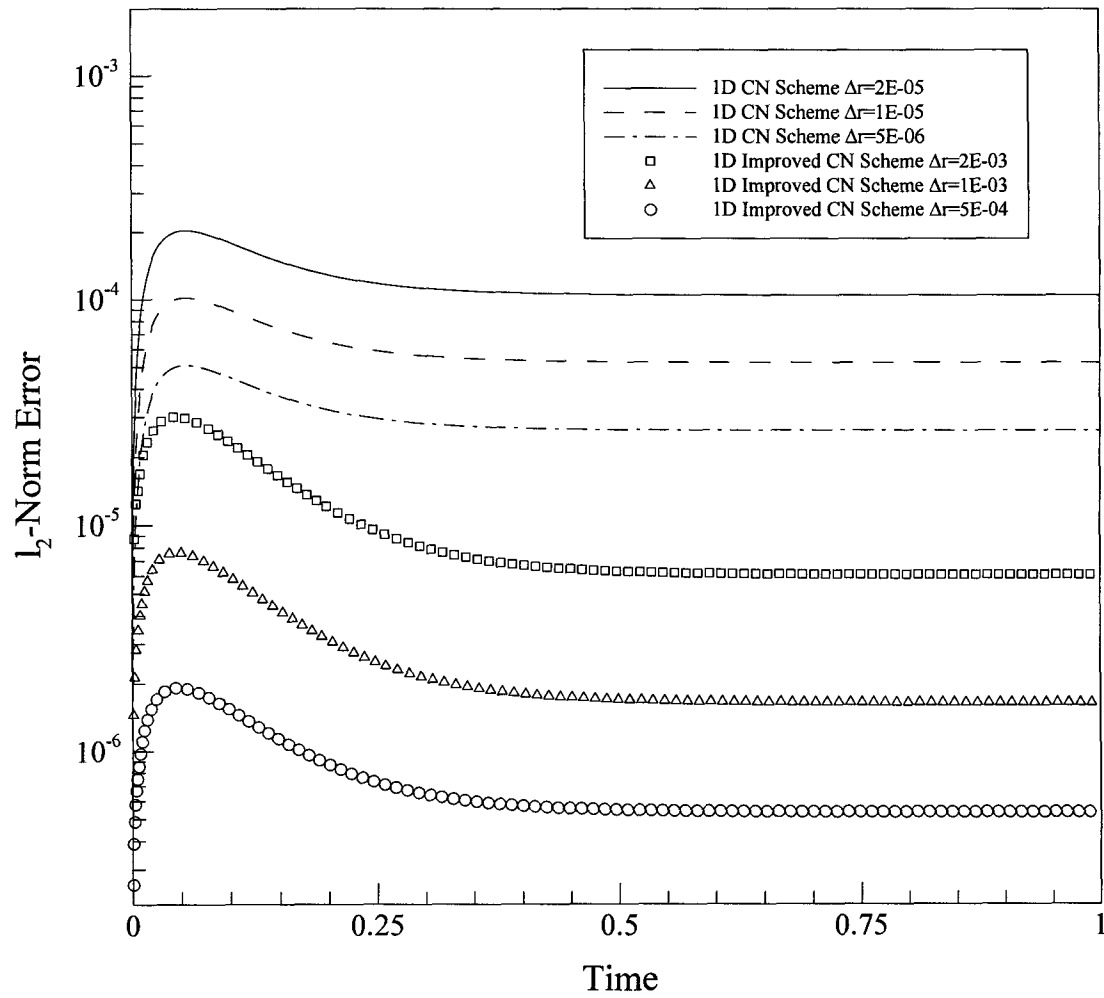


Figure 5.1 Comparison of  $l_2$ -norm errors between the 1D improved CN scheme and the 1D CN scheme along the time  $t$ .

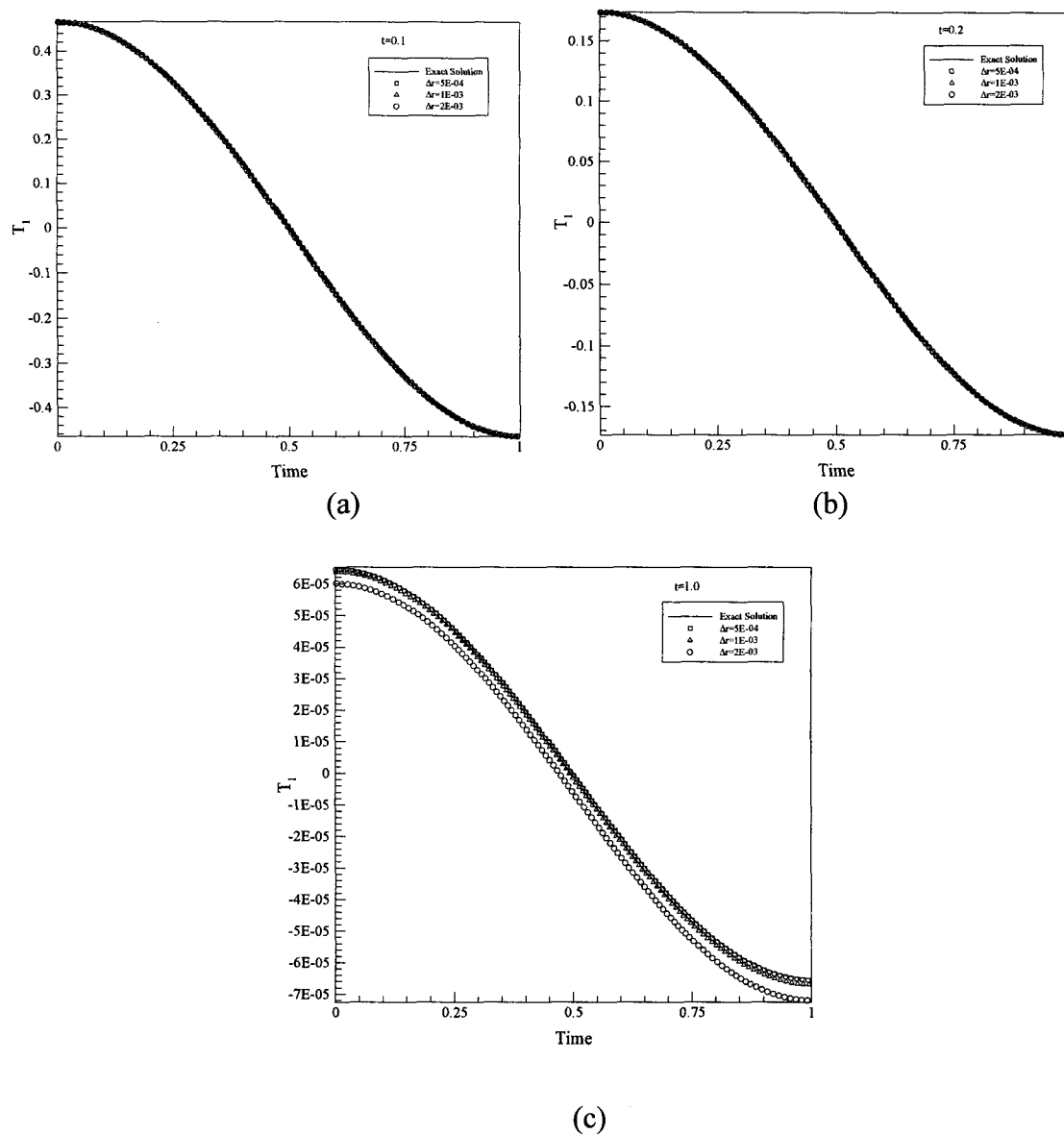


Figure 5.2 Distribution of the temperature  $T_1$  from the 1D improved CN scheme along the radial distance  $r$  at different time (a)  $t = 0.1$  (b)  $t = 0.2$  and (c)  $t = 1.0$  with  $\Delta r = 2 \times 10^{-3}$ ,  $10^{-3}$  and  $5 \times 10^{-4}$ .

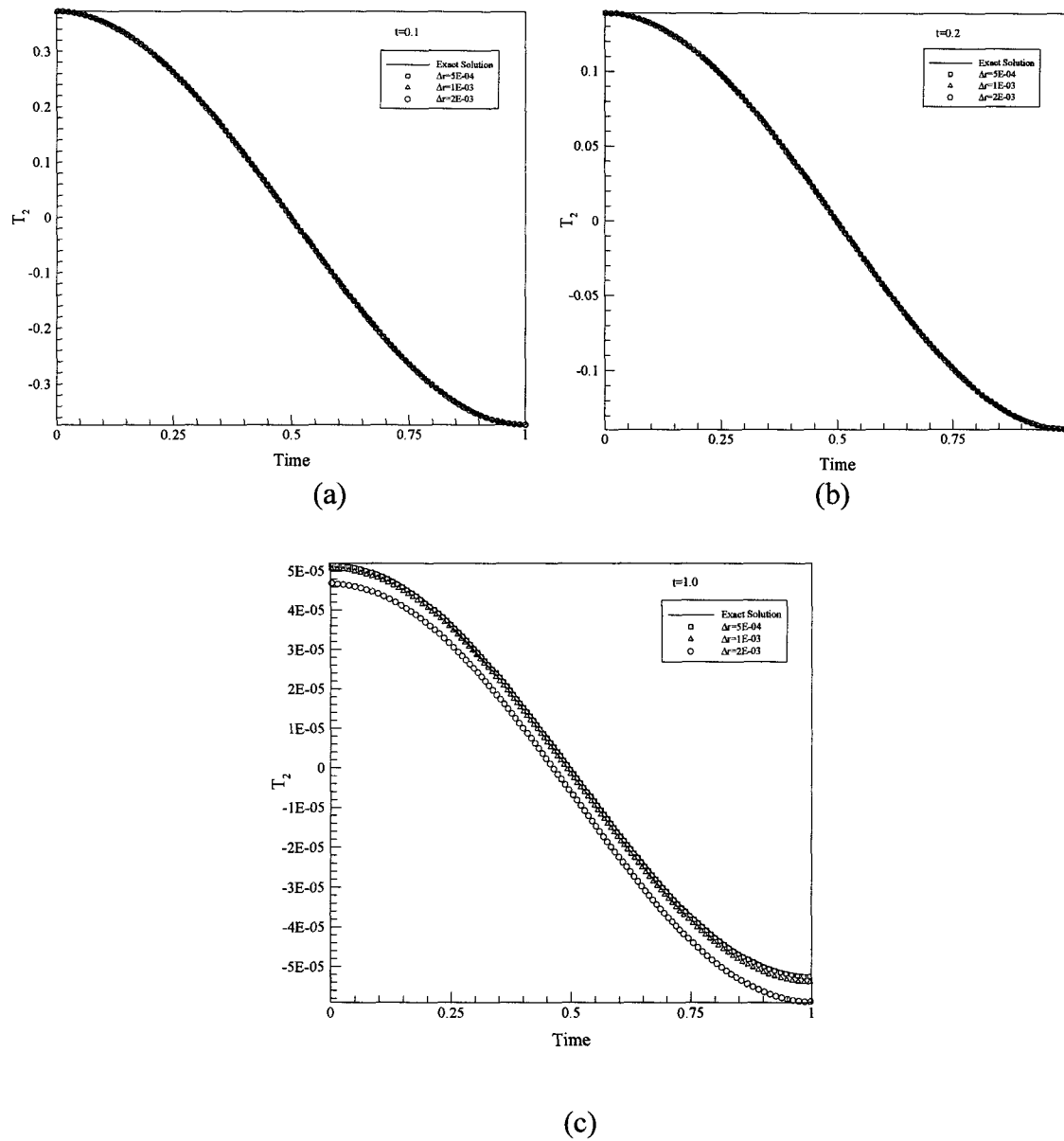


Figure 5.3 Distribution of the temperature  $T_2$  from the 1D improved CN scheme along the radial distance  $r$  at different time (a)  $t = 0.1$  (b)  $t = 0.2$  and (c)  $t = 1.0$  with  $\Delta r = 2 \times 10^{-3}$ ,  $10^{-3}$  and  $5 \times 10^{-4}$ .

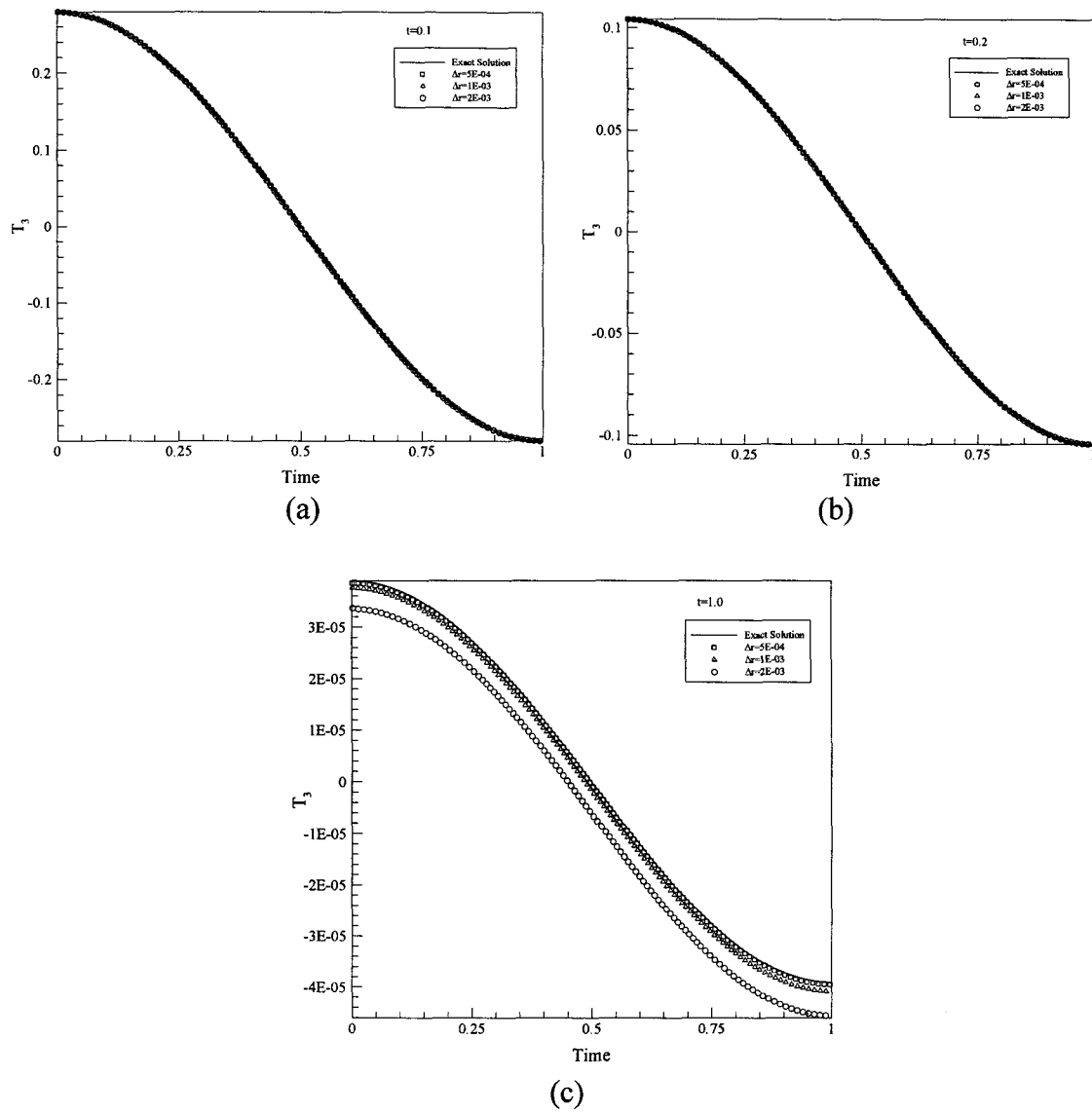


Figure 5.4 Distribution of the temperature  $T_3$  from the 1D improved CN scheme along the radial distance  $r$  at different time (a)  $t = 0.1$  (b)  $t = 0.2$  and (c)  $t = 1.0$  with  $\Delta r = 2 \times 10^{-3}$ ,  $10^{-3}$  and  $5 \times 10^{-4}$ .

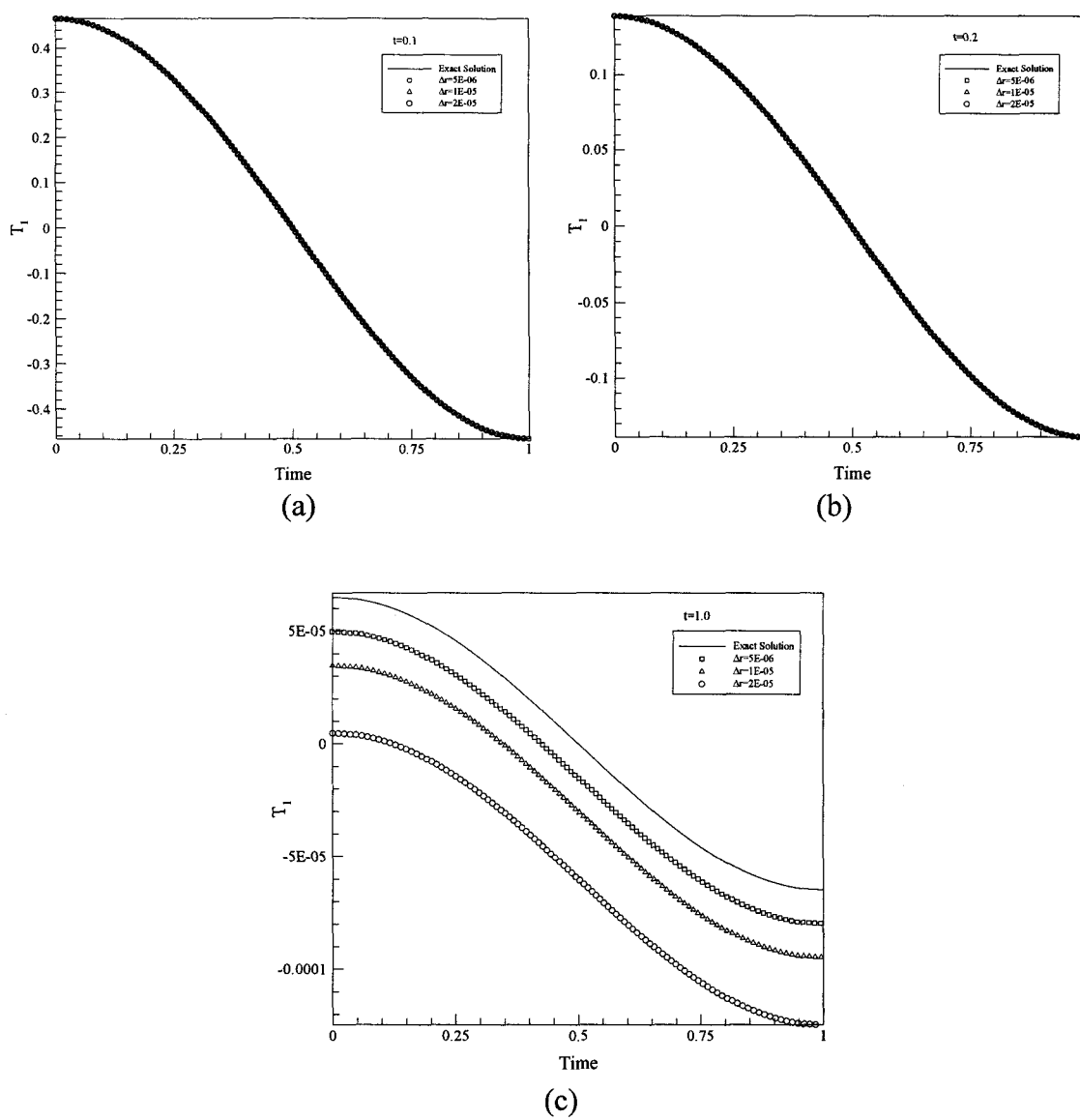


Figure 5.5 Distribution of the temperature  $T_1$  from the 1D CN scheme along the radial distance  $r$  at different time (a)  $t = 0.1$  (b)  $t = 0.2$  and (c)  $t = 1.0$  with  $\Delta r = 2 \times 10^{-5}$ ,  $10^{-5}$  and  $5 \times 10^{-6}$ .

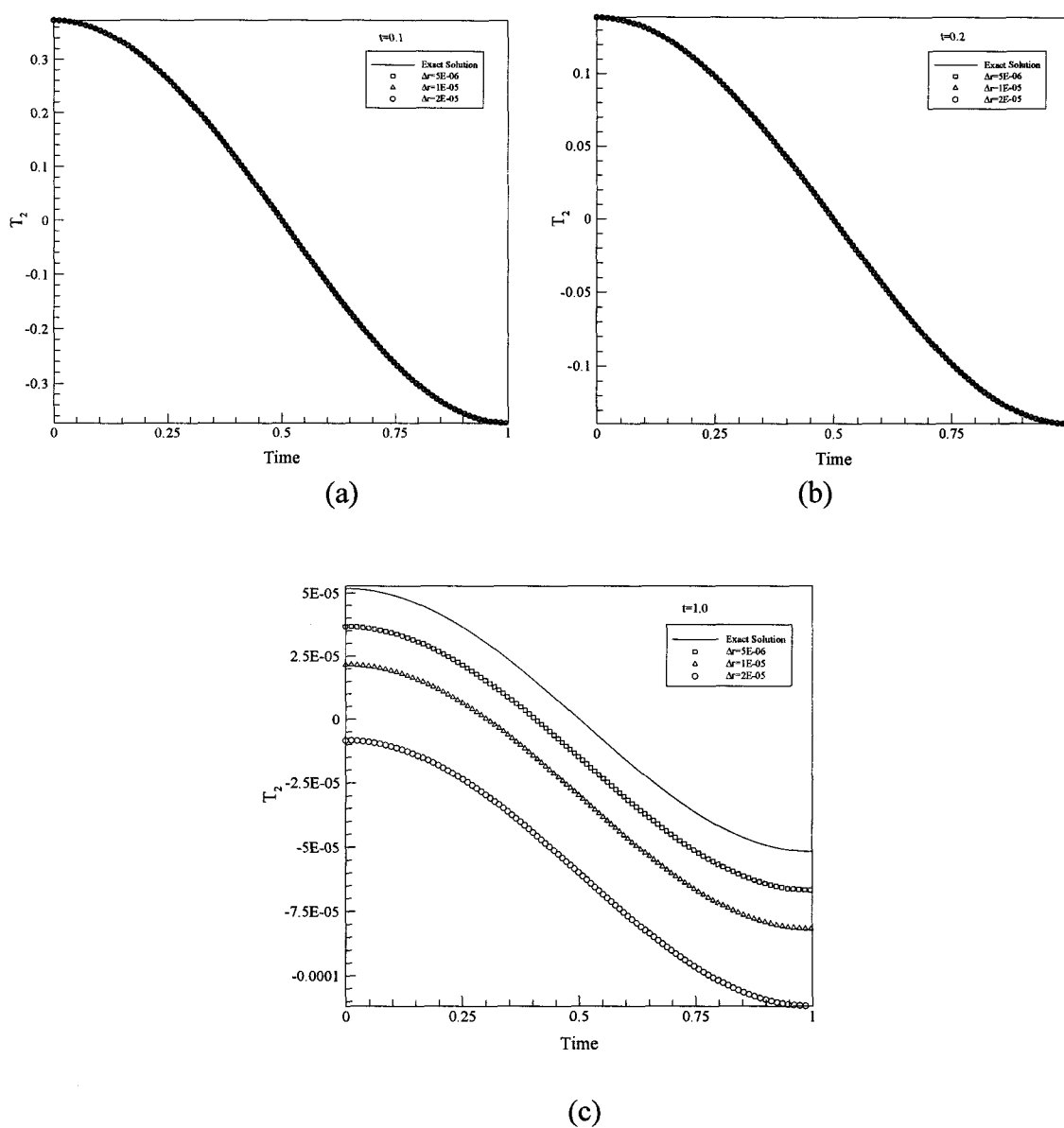


Figure 5.6 Distribution of the temperature  $T_2$  from the 1D CN along the radial distance  $r$  at different time (a)  $t = 0.1$  (b)  $t = 0.2$  and (c)  $t = 1.0$  with  $\Delta r = 2 \times 10^{-5}$ ,  $10^{-5}$  and  $5 \times 10^{-6}$ .

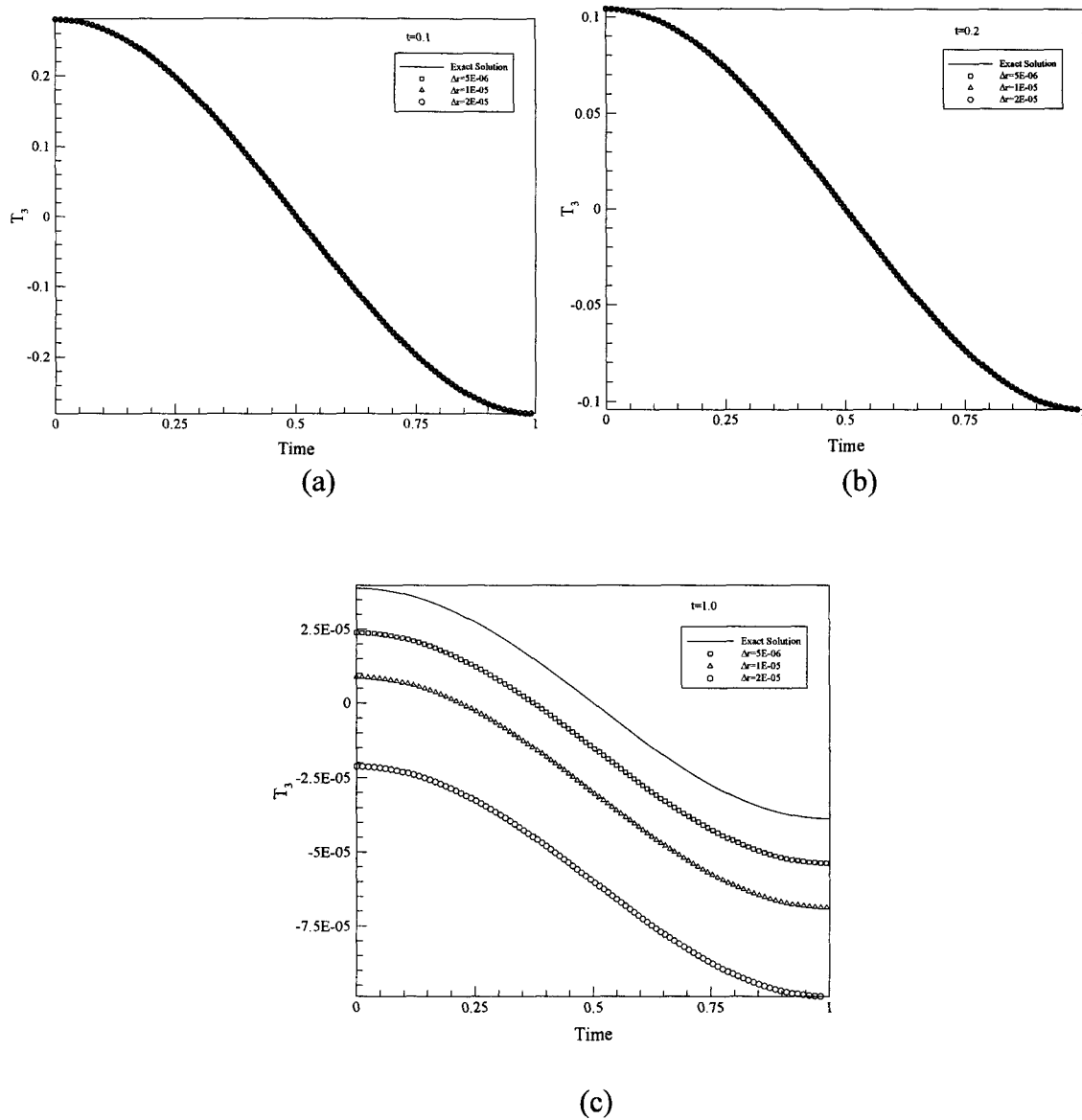


Figure 5.7 Distribution of the temperature  $T_3$  from the 1D improved CN scheme along the radial distance  $r$  at different time (a)  $t = 0.1$  (b)  $t = 0.2$  and (c)  $t = 1.0$  with  $\Delta r = 2 \times 10^{-5}$ ,  $10^{-5}$  and  $5 \times 10^{-6}$ .

## 5.2 3D First Improved CN Scheme Case

The second example Eq. (5.5) is in 3D spherical coordinates, which is satisfied with the governing equation Eq. (3.4). It is solved by the 3D first improved CN scheme Eqs. (4.19), (4.21) and (4.22) and the 3D CN scheme Eqs. (4.19) and (4.20).

### 5.2.1 Example Description

This example is a *Three-carrier* system with variable  $T_1$ ,  $T_2$  and  $T_3$ . The governing equation for this example is:

$$\begin{aligned} \frac{\partial T_1}{\partial t} = & \frac{2}{r^2} \frac{\partial}{\partial r} \left( r^2 \frac{\partial T_1}{\partial r} \right) + \frac{2}{r^2(1-\mu^2)} \frac{\partial^2 T_1}{\partial \theta^2} + \frac{2}{r^2} \frac{\partial}{\partial \mu} \left( (1-\mu^2) \frac{\partial T_1}{\partial \mu} \right) \\ & - \pi^2 (T_1 - T_3) + 2\pi^2 e^{-\pi t} \cos \pi r \sin \theta (1-\mu^2) + \frac{5}{r} \pi e^{-\pi t} \sin \pi r \sin \theta (1-\mu^2) \\ & - \frac{15}{2r^2} e^{-\pi t} \cos \pi r \sin \theta (2\mu^2 - 1), \end{aligned} \quad (5.5a)$$

$$\begin{aligned} \frac{\partial T_2}{\partial t} = & \frac{2}{r^2} \frac{\partial}{\partial r} \left( r^2 \frac{\partial T_2}{\partial r} \right) + \frac{2}{r^2(1-\mu^2)} \frac{\partial^2 T_2}{\partial \theta^2} + \frac{2}{r^2} \frac{\partial}{\partial \mu} \left( (1-\mu^2) \frac{\partial T_2}{\partial \mu} \right) \\ & - \pi^2 (T_2 - T_3) + \pi^2 e^{-\pi t} \cos \pi r \sin \theta (1-\mu^2) + \frac{4}{r} \pi e^{-\pi t} \sin \pi r \sin \theta (1-\mu^2) \\ & - \frac{6}{r^2} e^{-\pi t} \cos \pi r \sin \theta (2\mu^2 - 1), \end{aligned} \quad (5.5b)$$

$$\begin{aligned} \frac{\partial T_3}{\partial t} = & \frac{k_3}{r^2} \frac{\partial}{\partial r} \left( r^2 \frac{\partial T_3}{\partial r} \right) + \frac{k_3}{r^2(1-\mu^2)} \frac{\partial^2 T_3}{\partial \theta^2} + \frac{k_3}{r^2} \frac{\partial}{\partial \mu} \left( (1-\mu^2) \frac{\partial T_3}{\partial \mu} \right) \\ & + \pi^2 (T_1 - T_3) + \frac{3}{r} \pi e^{-\pi t} \sin \pi r \sin \theta (1-\mu^2) - \frac{9}{2r^2} e^{-\pi t} \cos \pi r \sin \theta (2\mu^2 - 1). \end{aligned} \quad (5.5c)$$

The boundary condition for this example is Eq. (4.3), and the initial condition for this example is

$$T_1 = \frac{5}{4} \cos \pi r \sin \theta (1 - \mu^2), T_2 = \cos \pi r \sin \theta (1 - \mu^2), T_3 = \frac{3}{4} \cos \pi r \sin \theta (1 - \mu^2).$$

The exact solution for Eq. (5.5) is:

$$T_1 = \frac{5}{4} e^{-\pi t} \cos \pi r \sin \theta (1 - \mu^2), \quad (5.6a)$$

$$T_2 = e^{-\pi t} \cos \pi r \sin \theta (1 - \mu^2), \quad (5.6b)$$

$$T_3 = \frac{3}{4} e^{-\pi t} \cos \pi r \sin \theta (1 - \mu^2). \quad (5.6c)$$

In the 3D first improved CN scheme and the 3D CN scheme, the time step size  $\Delta t$  is set as  $10^{-4}$ , and the grid size is set as:  $10 \times 60 \times 60$ ,  $20 \times 60 \times 60$  and  $40 \times 60 \times 60$ . Also, the upper boundary for time  $t_0$  is set as 0.2 in this example. The scheme is programmed by Fortran 77, and the source code can be found in APPENDIX.

### 5.2.2 Results and Analysis

In order to evaluate the difference between the numerical solution and the exact solution for each scheme, we define the  $l_2$ -norm error is defined as

$$E(I, \Delta t) = \max_{0 \leq n \Delta t \leq t_0} \sqrt{\frac{\Delta r}{3} \sum_{m=1}^3 \sum_{i=1}^I \left\{ (T_m)^n - (T_m^{exact})^n \right\}^2}, \quad (5.7)$$

where  $(T_m)^n$  is the numerical solution for the carrier  $m$ , and  $(T_m^{exact})^n$  is the exact solution from each scheme of the carrier  $m$ .

The convergence rate is defined as

$$\log_2 \left[ \frac{E(I_1, \Delta t)}{E(I_2, \Delta t)} \right] \quad (5.8)$$

with respect to the spatial variable  $r$ .

The maximum  $l_2$ -norm error Eq. (5.7) and comparisons of convergence rates Eq. (5.8) are in Table 5.3.  $l_2$ -norm errors along the time  $t$  for both schemes are plotted in Figure 5.8. Numerical results for the two schemes are plotted from Figure 5.9 to Figure 5.14.

Table 5.3 shows the comparison of  $l_2$ -norm errors and convergence rates between the 3D first improved CN scheme and the 3D CN scheme with  $0 \leq t \leq 0.2$ ,  $\Delta t = 10^{-4}$ .

Table 5.3 Comparison of  $l_2$ -norm errors and convergence rates between the 3D first improved CN scheme and the 3D CN scheme with  $0 \leq t \leq 0.2$ ,  $\Delta t = 10^{-4}$ .

grid	3D first improved CN scheme $l_2$ -norm error	convergence rate	3D CN scheme $l_2$ -norm error	convergence rate
11×60×60	$9.36135 \times 10^{-3}$	-	$2.56083 \times 10^{-1}$	-
21×60×60	$2.58204 \times 10^{-3}$	1.858	$1.39055 \times 10^{-1}$	0.881
41×60×60	$9.44232 \times 10^{-4}$	1.452	$7.25757 \times 10^{-2}$	0.939

As shown in Table 5.3, the convergence rate of the 3D first improved CN scheme is 1.858 and 1.452 with respect to the spatial variable  $r$ , while the one for the 3D CN scheme is 0.881 and 0.939 with respect to the spatial variable  $r$ . The result looks lower than that as expected. This is probably because the grid is not finer enough. However, due to the limitation of the computer, it will be difficult to choose a finer grid. Further study may be needed. Furthermore, comparing the  $l_2$ -norm errors of solutions between the 3D first improved CN scheme and the 3D CN scheme in Table 5.3 shows that the 3D first improved CN scheme is more accurate than the 3D CN scheme.

Figure 5.8 shows the comparison of  $l_2$ -norm errors between the 3D first improved CN scheme and the 3D CN scheme. Figure 5.8 shows that, the 3D first improved CN scheme will produce a  $l_2$ -norm error much lower than the 3D CN scheme.

Figure 5.9 is the comparison of contours of the solution  $T_1$  in the cross section of  $\theta = \frac{\pi}{2}$  at  $t = 0.1$  obtained using (a) the 3D first improved CN scheme and (b) the 3D CN scheme with (c) the exact solution. Figure 5.10 is the comparison of contours of the solution of  $T_1$  in the cross section of  $\theta = 0$  and  $\theta = \pi$  at  $t = 0.1$  obtained using (a) the 3D first improved CN scheme and (b) the 3D CN scheme with (c) the exact solution.

Figure 5.11 is the comparison of contours of the solution  $T_2$  in the cross section of  $\theta = \frac{\pi}{2}$  at  $t = 0.1$  obtained using (a) the 3D first improved CN scheme and (b) the 3D CN scheme with (c) the exact solution. Figure 5.12 is the comparison of contours of the solution of  $T_2$  in the cross section of  $\theta = 0$  and  $\theta = \pi$  at  $t = 0.1$  obtained using (a) the 3D first improved CN scheme and (b) the 3D CN scheme with (c) the exact solution.

Figure 5.13 is the comparison of contours of the solution  $T_3$  in the cross section of  $\theta = \frac{\pi}{2}$  at  $t = 0.1$  obtained using (a) the 3D first improved CN scheme and (b) the 3D CN scheme with (c) the exact solution. Figure 5.14 is the comparison of contours of the solution of  $T_3$  in the cross section of  $\theta = 0$  and  $\theta = \pi$  at  $t = 0.1$  obtained using (a) the 3D first improved CN scheme and (b) the 3D CN scheme with (c) the exact solution.

Figure 5.9 to Figure 5.14 show that: there is a match between the numerical solution from the 3D first improved CN scheme in (a) and the exact solution in (c), but the numerical solution of the 3D CN scheme in (b) and the exact solution in (c) do not match.

Figure 5.9 to Figure 5.14 also show that the temperature is  $T_1 > T_2 > T_3$ , which is satisfied with the hypothesis in Figure 2.1.

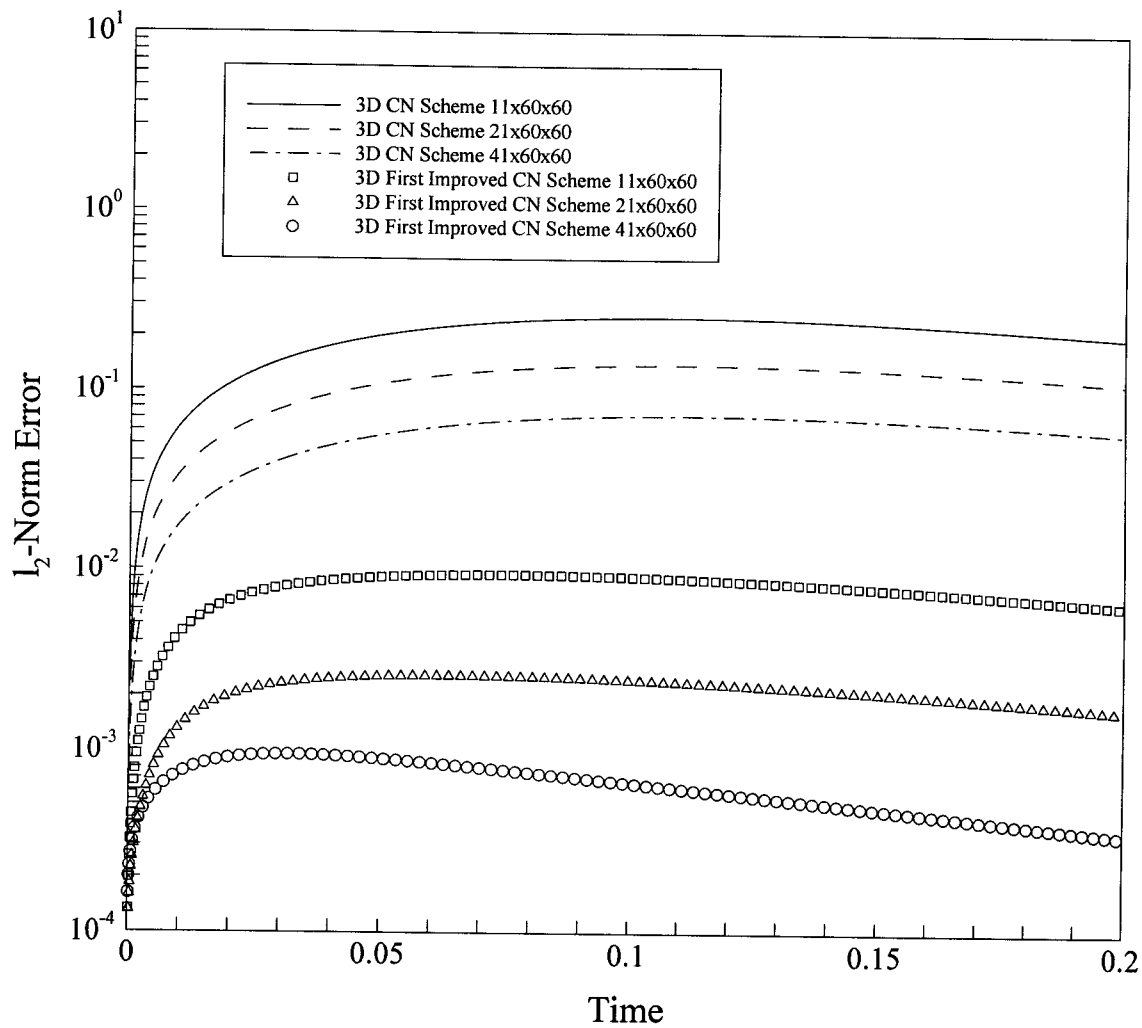


Figure 5.8 Comparison of  $l_2$ -norm errors between the 3D first improved CN scheme and the 3D CN scheme.

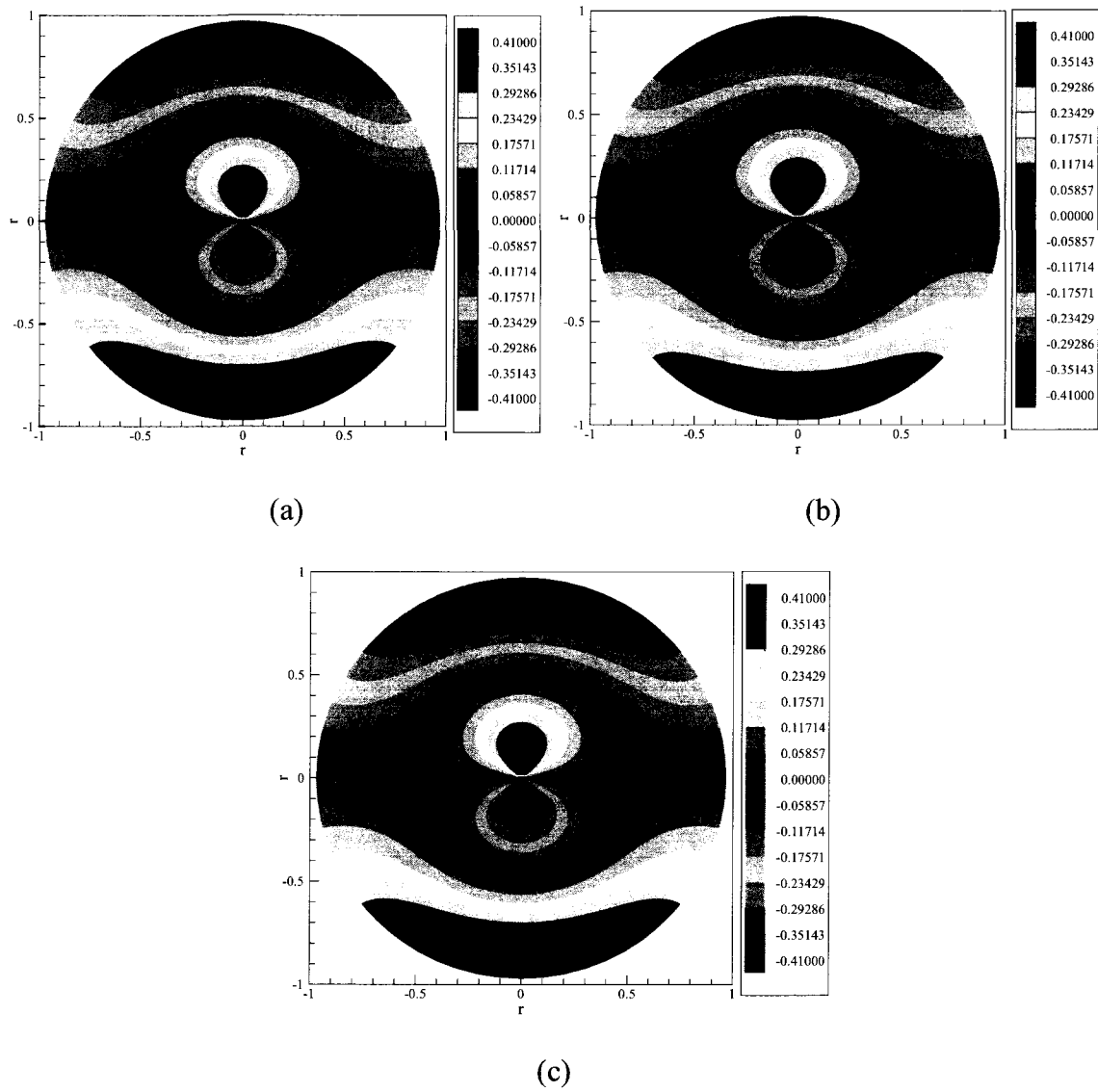


Figure 5.9 Comparison of contours of the solution  $T_l$  in the cross section of  $\theta = \frac{\pi}{2}$  at  $t = 0.1$  obtained using (a) the 3D first improved CN scheme and (b) the 3D CN scheme with (c) the exact solution.

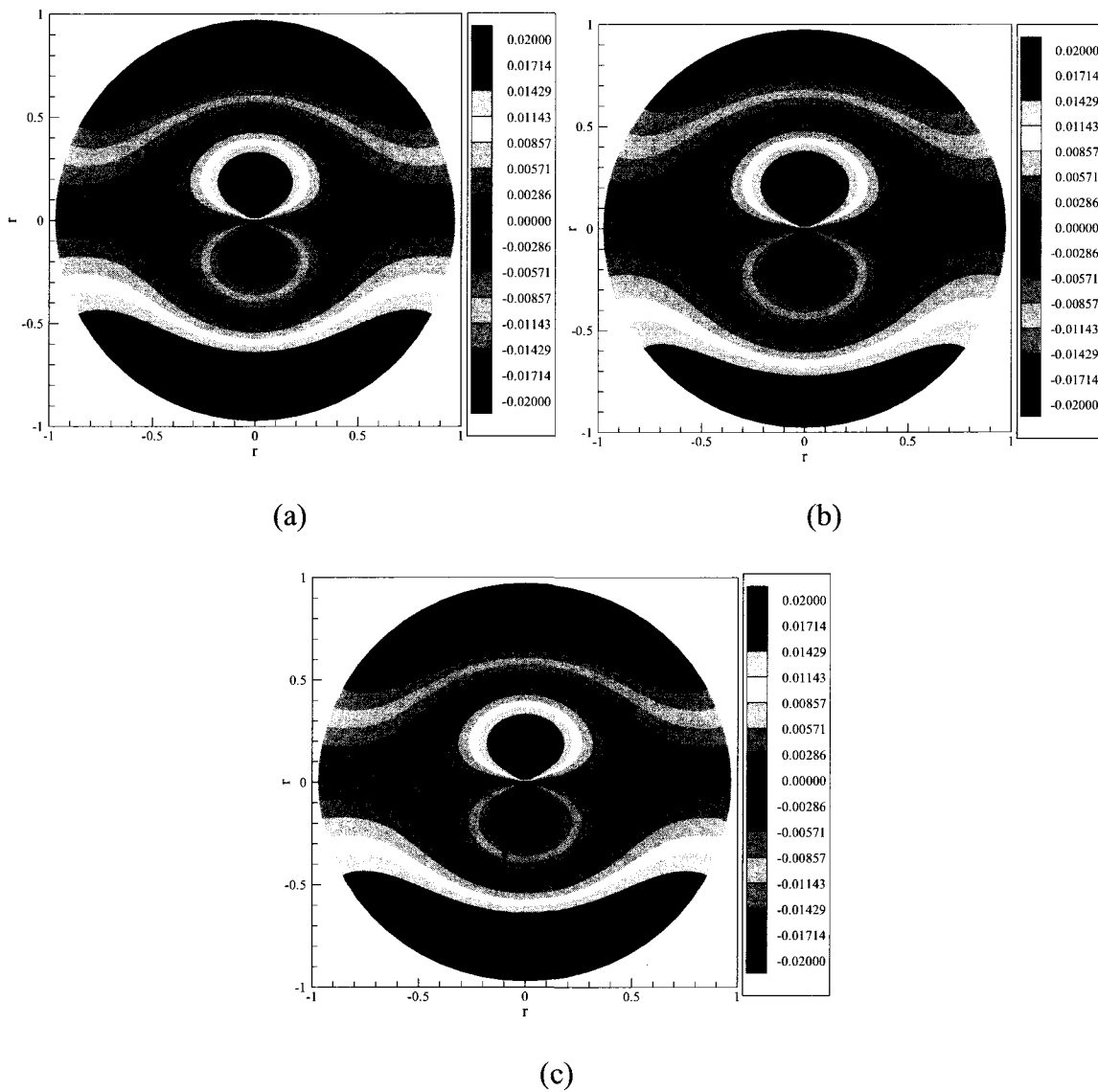


Figure 5.10 Comparison of contours of the solution of  $T_l$  in the cross section of  $\theta = 0$  and  $\theta = \pi$  at  $t = 0.1$  obtained using (a) the 3D first improved CN scheme and (b) the 3D CN scheme with (c) the exact solution.

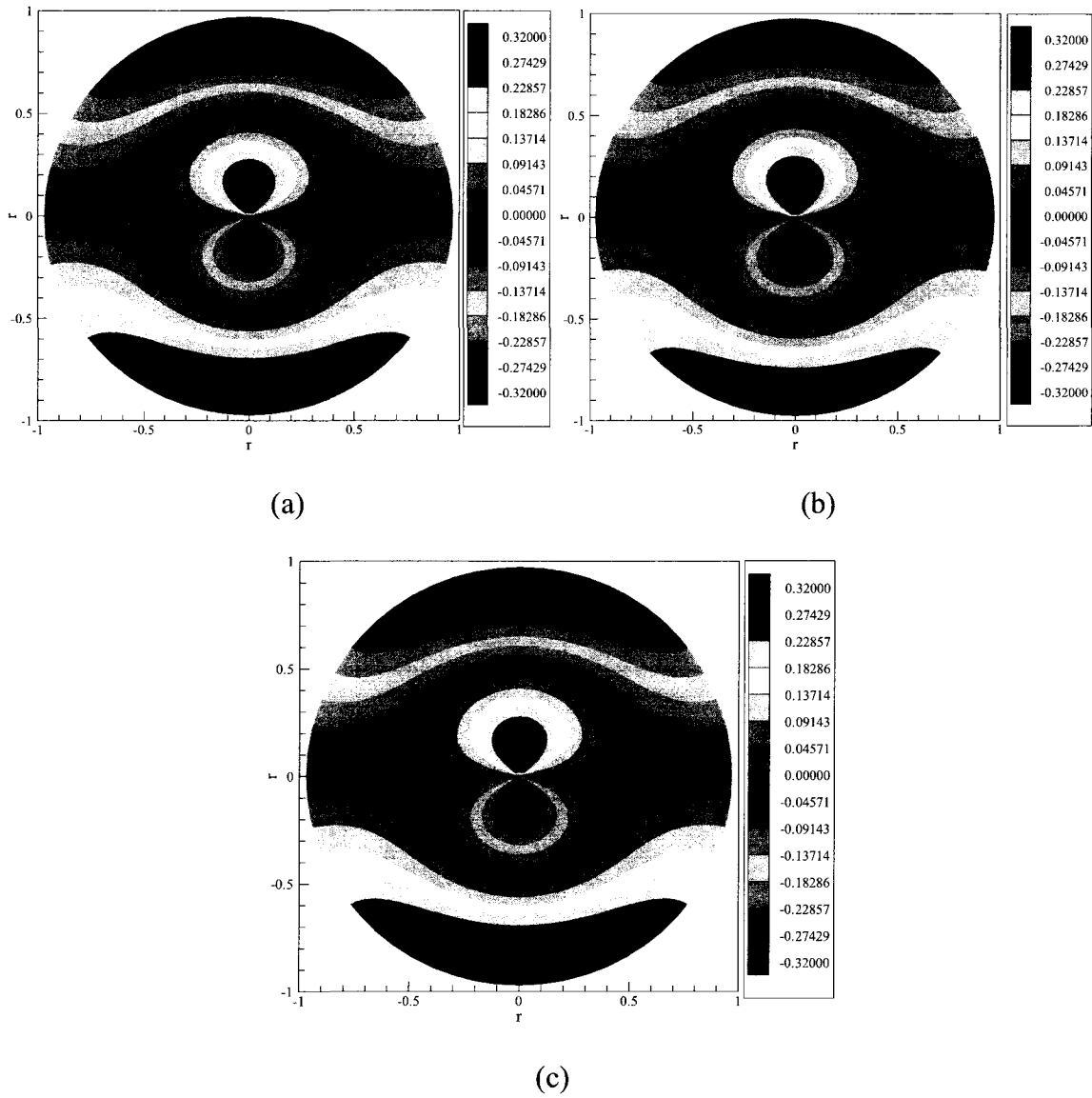


Figure 5.11 Comparison of contours of the solution  $T_2$  in the cross section of  $\theta = \frac{\pi}{2}$  at  $t = 0.1$  obtained using (a) the 3D first improved CN scheme and (b) the 3D CN scheme with (c) the exact solution.

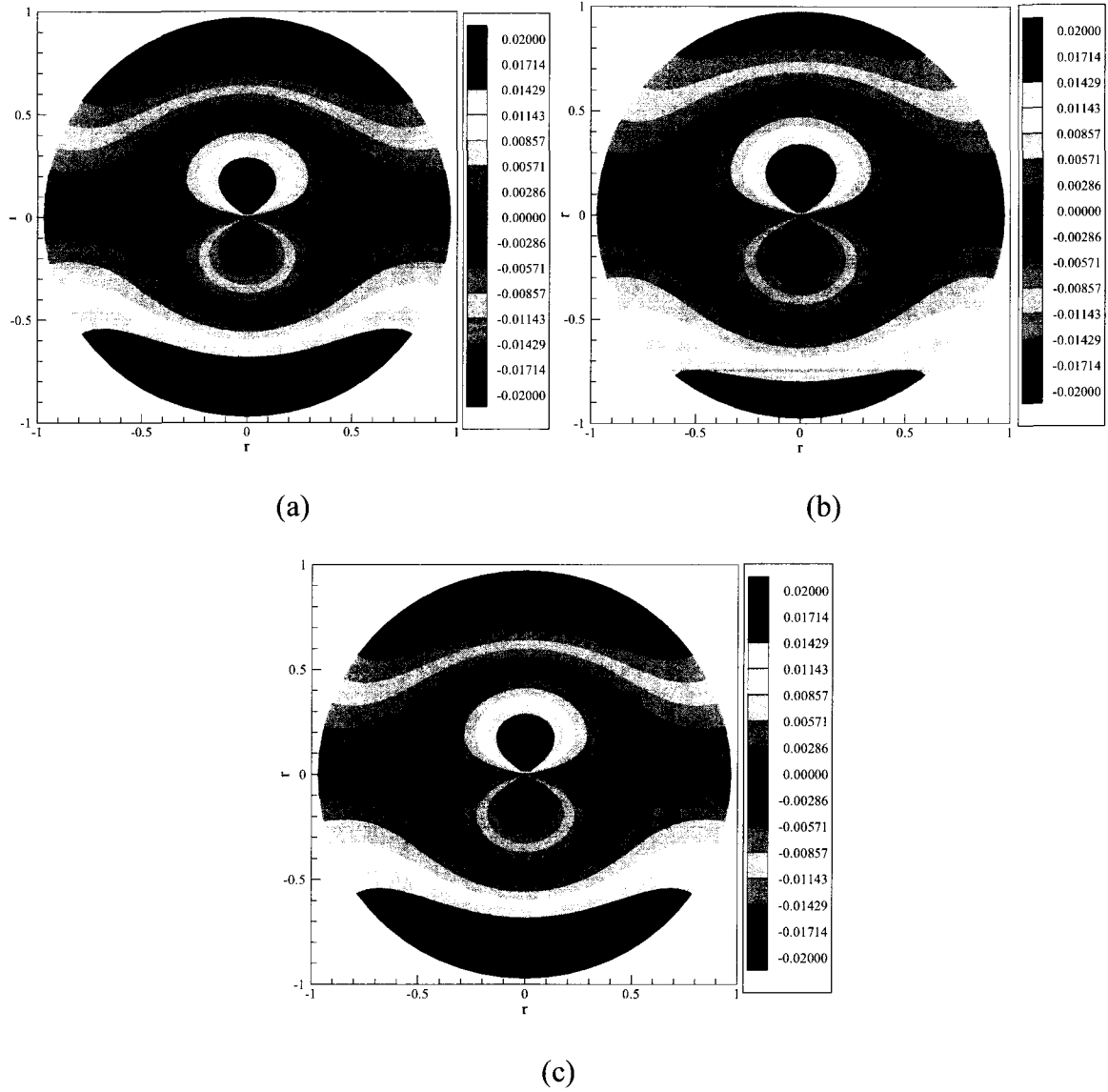


Figure 5.12 Comparison of contours of the solution of  $T_2$  in the cross section of  $\theta = 0$  and  $\theta = \pi$  at  $t = 0.1$  obtained using (a) the 3D first improved CN scheme and (b) the 3D CN scheme with (c) the exact solution.

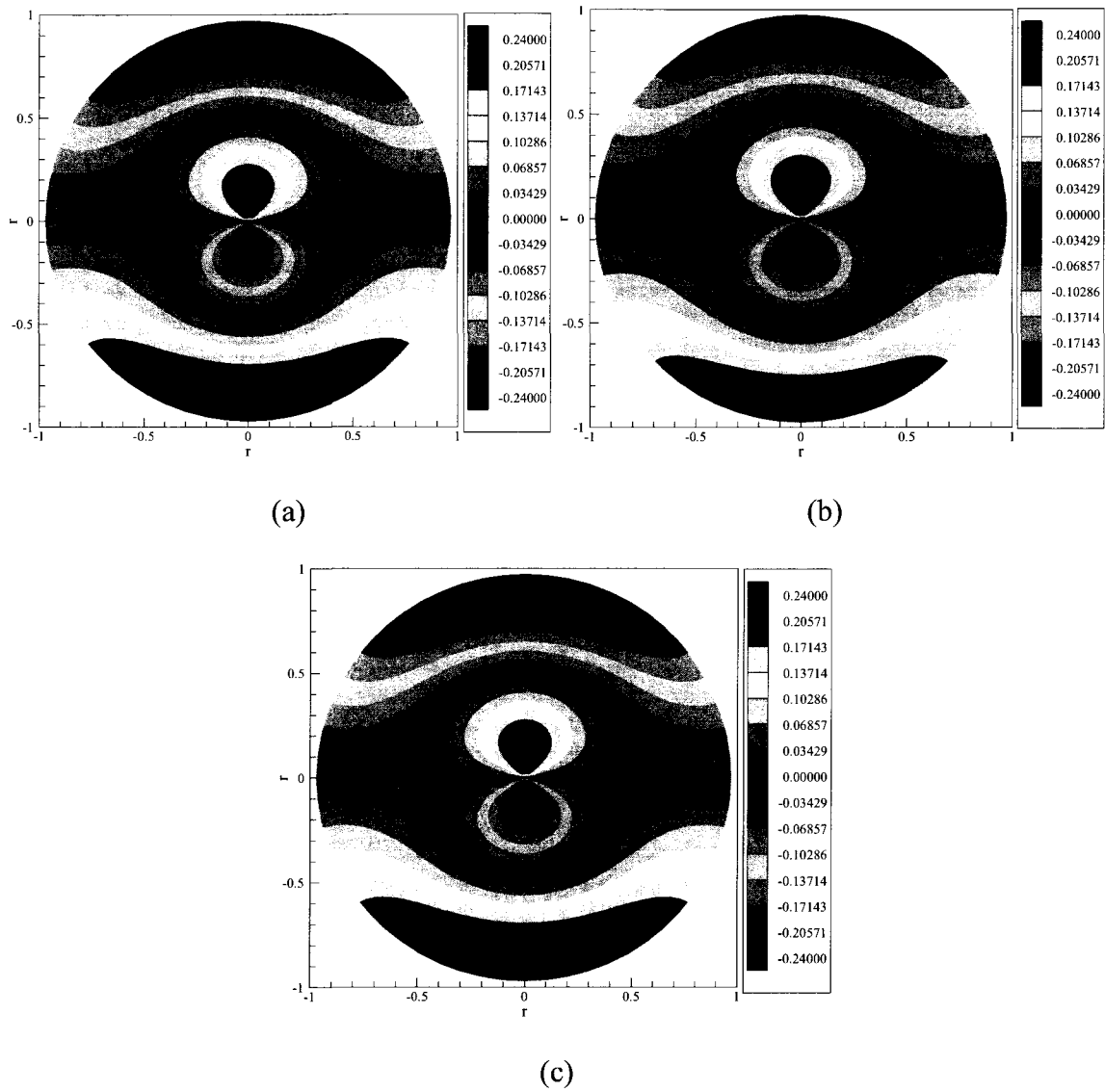


Figure 5.13 Comparison of contours of the solution  $T_3$  in the cross section of  $\theta = \frac{\pi}{2}$  at  $t = 0.1$  obtained using (a) the 3D first improved CN scheme and (b) the 3D CN scheme with (c) the exact solution.

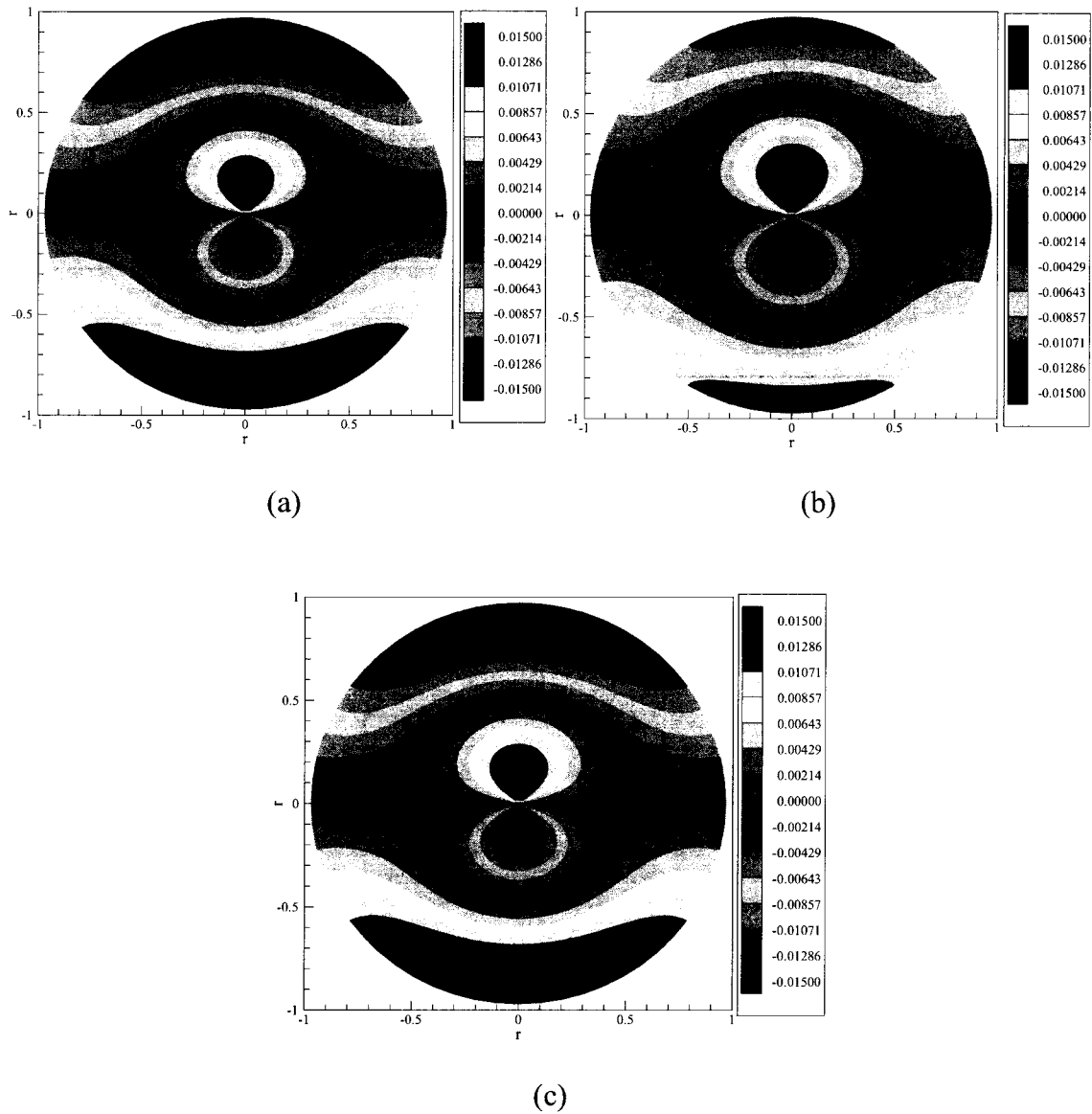


Figure 5.14 Comparison of contours of the solution of  $T_3$  in the cross section of  $\theta = 0$  and  $\theta = \pi$  at  $t = 0.1$  obtained using (a) the 3D first improved CN scheme and (b) the 3D CN scheme with (c) the exact solution.

### 5.3 3D Second Improved CN Scheme Case

The third example Eq. (5.9) is in 3D spherical coordinates, which is satisfied with the governing equation Eq. (3.4). It is solved by the 3D second improved CN scheme Eqs. (4.19), (4.22) and (4.24) and the 3D CN scheme Eqs. (4.19) and (4.20).

#### 5.3.1 Example Description

This example is a *Three*-carrier system with variable  $T_1$ ,  $T_2$  and  $T_3$ . The governing equation for this example is:

$$\begin{aligned} \frac{\partial T_1}{\partial t} = & \frac{2}{r^2} \frac{\partial}{\partial r} \left( r^2 \frac{\partial T_1}{\partial r} \right) + \frac{2}{r^2(1-\mu^2)} \frac{\partial^2 T_1}{\partial \theta^2} + \frac{2}{r^2} \frac{\partial}{\partial \mu} \left[ (1-\mu^2) \frac{\partial T_1}{\partial \mu} \right] - \pi^2 (T_1 - T_3) \\ & + 2\pi^2 e^{-\pi t} \cos \pi r \sin \theta (1-\mu^2) + \frac{5}{r} \pi e^{-\pi t} \sin \pi r \sin \theta (1-\mu^2) \\ & - \frac{15}{2r^2} e^{-\pi t} \cos \pi r \sin \theta (2\mu^2 - 1) \\ & + \pi^2 e^{-\pi t} \sin \theta (1-\mu^2) + \frac{15}{2r^2} e^{-\pi t} \sin \theta (2\mu^2 - 1), \end{aligned} \quad (5.9a)$$

$$\begin{aligned} \frac{\partial T_2}{\partial t} = & \frac{2}{r^2} \frac{\partial}{\partial r} \left( r^2 \frac{\partial T_2}{\partial r} \right) + \frac{2}{r^2(1-\mu^2)} \frac{\partial^2 T_2}{\partial \theta^2} + \frac{2}{r^2} \frac{\partial}{\partial \mu} \left[ (1-\mu^2) \frac{\partial T_2}{\partial \mu} \right] - \pi^2 (T_2 - T_3) \\ & + \pi^2 e^{-\pi t} \cos \pi r \sin \theta (1-\mu^2) + \frac{4}{r} \pi e^{-\pi t} \sin \pi r \sin \theta (1-\mu^2) \\ & - \frac{6}{r^2} e^{-\pi t} \cos \pi r \sin \theta (2\mu^2 - 1) \\ & + \pi^2 e^{-\pi t} \sin \theta (1-\mu^2) + \frac{6}{r^2} e^{-\pi t} \sin \theta (2\mu^2 - 1), \end{aligned} \quad (5.9b)$$

$$\frac{\partial T_3}{\partial t} = \frac{k_3}{r^2} \frac{\partial}{\partial r} \left( r^2 \frac{\partial T_3}{\partial r} \right) + \frac{k_3}{r^2(1-\mu^2)} \frac{\partial^2 T_3}{\partial \theta^2} + \frac{k_3}{r^2} \frac{\partial}{\partial \mu} \left[ (1-\mu^2) \frac{\partial T_3}{\partial \mu} \right]$$

$$\begin{aligned}
& + \frac{3}{r} \pi e^{-\pi t} \sin \pi r \sin \theta (1 - \mu^2) - \frac{9}{2r^2} e^{-\pi t} \cos \pi r \sin \theta (2\mu^2 - 1) \\
& + \frac{3\pi^2}{2} e^{-\pi t} \sin \theta (1 - \mu^2) + \frac{9}{2r^2} e^{-\pi t} \sin \theta (2\mu^2 - 1). \tag{5.9c}
\end{aligned}$$

The boundary condition for this is Eq. (4.3), and the initial condition for this example is:

$$T_1 = \frac{5}{4} (\cos \pi r - 1) \sin \theta (1 - \mu^2),$$

$$T_2 = (\cos \pi r - 1) \sin \theta (1 - \mu^2),$$

$$T_3 = \frac{3}{4} (\cos \pi r - 1) \sin \theta (1 - \mu^2).$$

The exact solution for Eq. (5.9) is:

$$T_1 = \frac{5}{4} e^{-\pi t} (\cos \pi r - 1) \sin \theta (1 - \mu^2), \tag{5.10a}$$

$$T_2 = e^{-\pi t} (\cos \pi r - 1) \sin \theta (1 - \mu^2), \tag{5.10b}$$

$$T_3 = \frac{3}{4} e^{-\pi t} (\cos \pi r - 1) \sin \theta (1 - \mu^2). \tag{5.10c}$$

In the 3D second improved CN scheme and the 3D CN scheme, the time step size  $\Delta t$  is set as  $10^{-4}$ , and the grid size is set as:  $10 \times 60 \times 60$ ,  $20 \times 60 \times 60$  and  $40 \times 60 \times 60$ . Also, we set the upper bound for time  $t_0$  as 0.2 in this example. The scheme is programmed by Fortran 77, and the source code can be found in APPENDIX.

### 5.3.2 Results and Analysis

The maximum  $l_2$ -norm error Eq. (5.7) and comparisons of convergence rates Eq. (5.8) are in Table 5.4. The  $l_2$ -norm error along the time  $t$  for both schemes are plotted in Figure 5.15. Numerical results for the two schemes are plotted from Figure 5.16 to Figure 5.21.

Table 5.4 shows the comparison of  $l_2$ -norm errors and convergence rates between the 3D second improved scheme and the 3D CN scheme with  $0 \leq t \leq 0.2$ ,  $\Delta t = 10^{-4}$ .

Table 5.4 Comparison of  $l_2$ -norm errors and convergence rates between the 3D second improved CN scheme and the 3D CN scheme with  $0 \leq t \leq 0.2$ ,  $\Delta t = 10^{-4}$ .

grid	3D second improved CN scheme $l_2$ -norm error	convergence rate	3D CN scheme $l_2$ -norm error	convergence rate
10×60×60	$1.08186 \times 10^{-2}$	-	$2.78749 \times 10^{-1}$	-
20×60×60	$2.10944 \times 10^{-3}$	2.359	$1.44811 \times 10^{-1}$	0.945
40×60×60	$5.49806 \times 10^{-4}$	1.940	$7.34437 \times 10^{-2}$	0.980

As shown in Table 5.4, the convergence rate of the 3D second improved scheme is about 2 with respect to the spatial variable  $r$ , while the one for the 3D CN scheme is about 1 with respect to the spatial variable  $r$ . Furthermore, comparing the  $l_2$ -norm errors of solutions between the 3D second improved scheme and the 3D CN scheme in Table 5.4 shows that the 3D second improved scheme is more accurate than the 3D CN scheme.

Figure 5.15 shows the comparison of  $l_2$ -norm errors between the 3D second improved CN scheme and the 3D CN scheme. From Figure 5.15 it can be seen that, the 3D second improved scheme will produce a  $l_2$ -norm error much lower than the 3D CN scheme.

Figure 5.16 is the comparison of contours of the solution  $T_I$  in the cross section of  $\theta = \frac{\pi}{2}$  at  $t = 0.1$  obtained using (a) the 3D second improved CN scheme and (b) the 3D CN scheme with (c) the exact solution. Figure 5.17 is the comparison of contours of the solution of  $T_I$  in the cross section of  $\theta = 0$  and  $\theta = \pi$  at  $t = 0.1$  obtained using (a) the 3D second improved CN scheme and (b) the 3D CN scheme with (c) the exact solution.

Figure 5.18 is the comparison of contours of the solution  $T_2$  in the cross section of  $\theta = \frac{\pi}{2}$  at  $t = 0.1$  obtained using (a) the 3D second improved CN scheme and (b) the 3D CN scheme with (c) the exact solution. Figure 5.19 is the comparison of contours of the solution of  $T_2$  in the cross section of  $\theta = 0$  and  $\theta = \pi$  at  $t = 0.1$  obtained using (a) the 3D second improved CN scheme and (b) the 3D CN scheme with (c) the exact solution.

Figure 5.20 is the comparison of contours of the solution  $T_3$  in the cross section of  $\theta = \frac{\pi}{2}$  at  $t = 0.1$  obtained using (a) the 3D second improved CN scheme and (b) the 3D CN scheme with (c) the exact solution. Figure 5.21 is the comparison of contours of the solution of  $T_3$  in the cross section of  $\theta = 0$  and  $\theta = \pi$  at  $t = 0.1$  obtained using (a) the 3D second improved CN scheme and (b) the 3D CN scheme with (c) the exact solution.

Figure 5.16 to Figure 5.21 show that: there is a good match between the numerical solution from the 3D second improved CN scheme in (a) and the exact solution in (c), but the numerical solution of the 3D CN scheme in (b) and the exact solution in (c) do not match.

From Figure 5.16 to Figure 5.21, it is can be seen that the temperature is  $T_1 > T_2 > T_3$ , which is satisfied with the hypothesis in Figure 2.1.

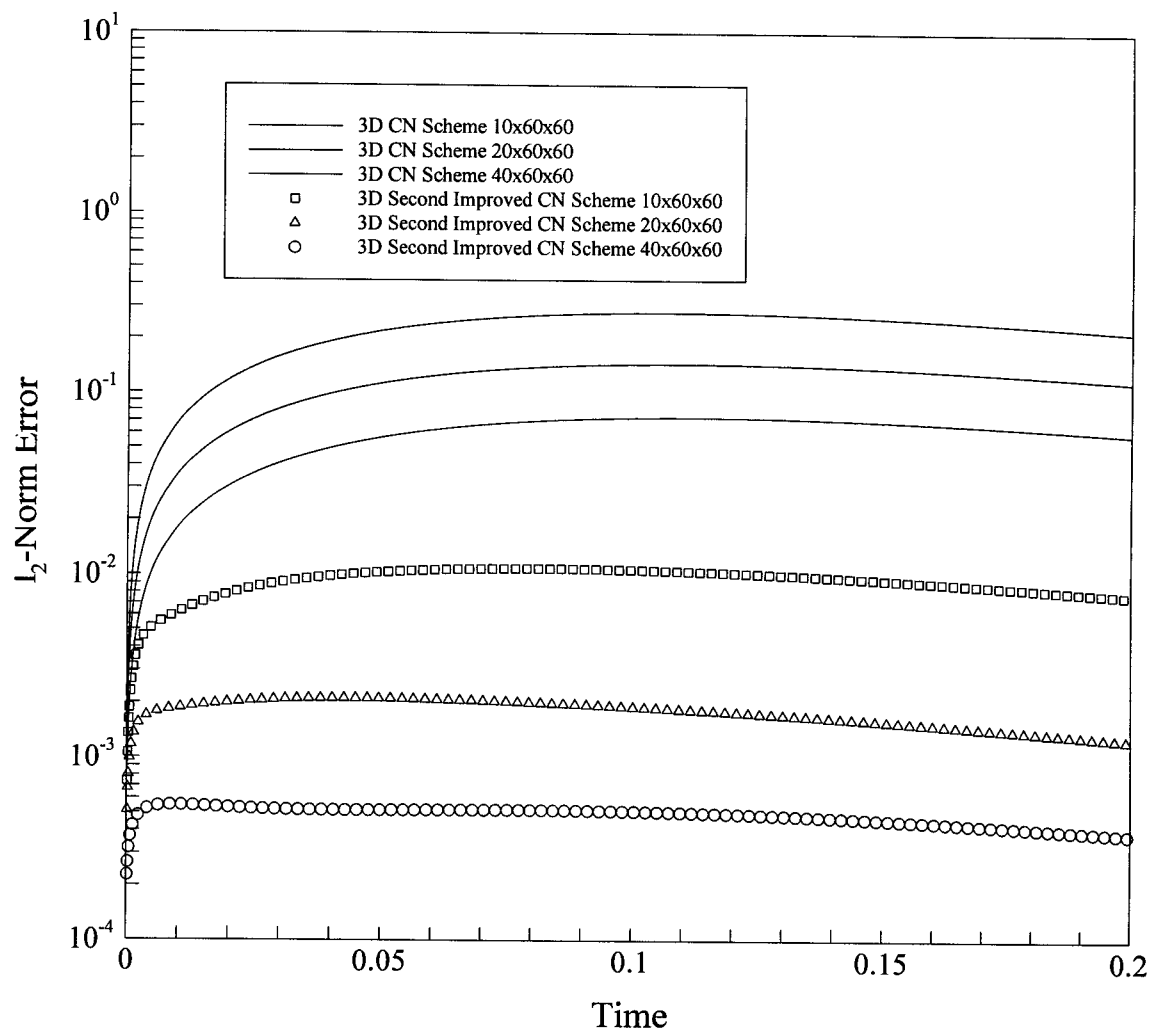


Figure 5.15 Comparison of  $l_2$ -norm errors between the 3D second improved CN scheme and the 3D CN scheme.

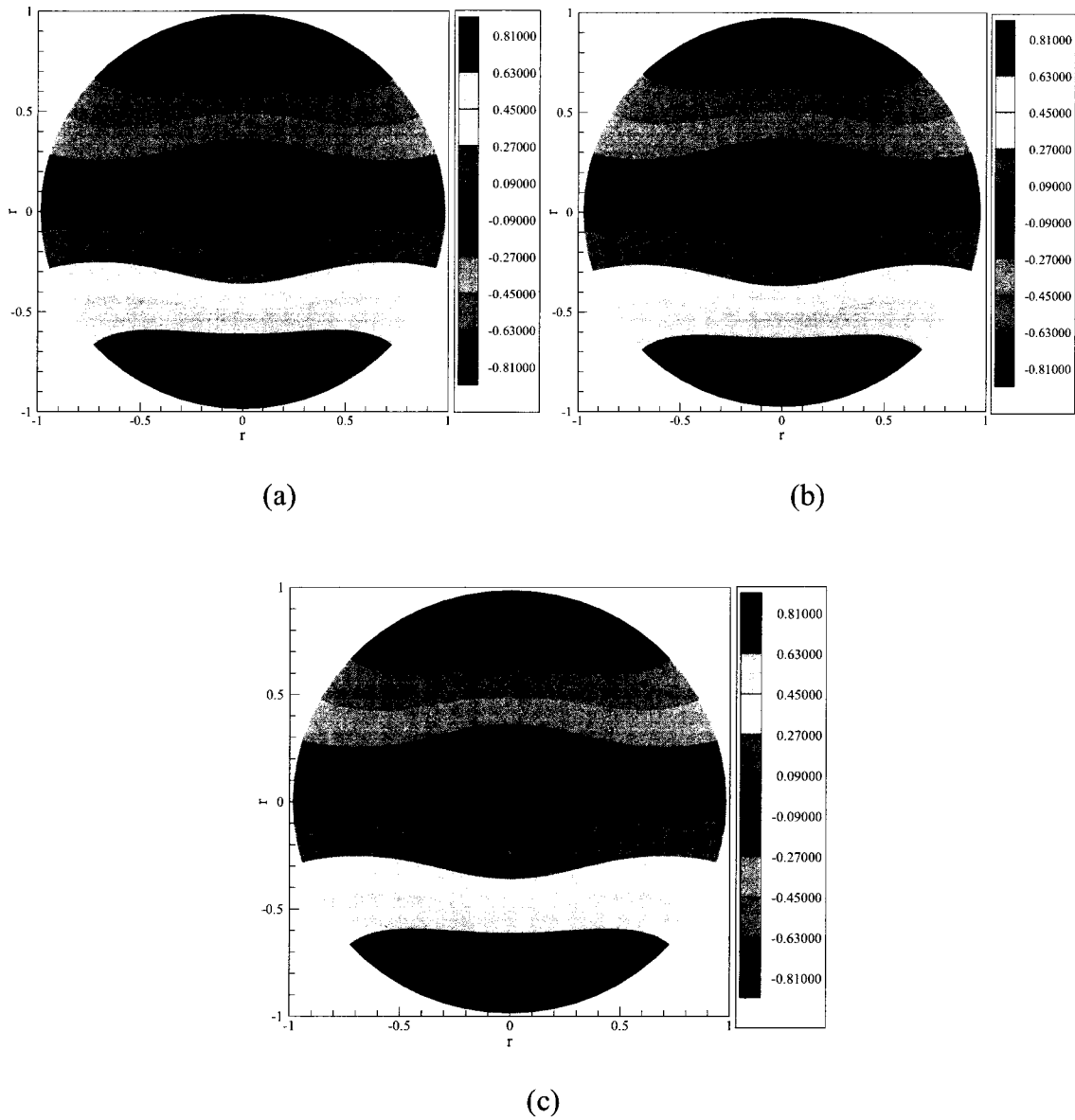


Figure 5.16 Comparison of contours of the solution  $T_I$  in the cross section of  $\theta = \frac{\pi}{2}$  at  $t = 0.1$  obtained using (a) the 3D second improved CN scheme and (b) the 3D CN scheme with (c) the exact solution.

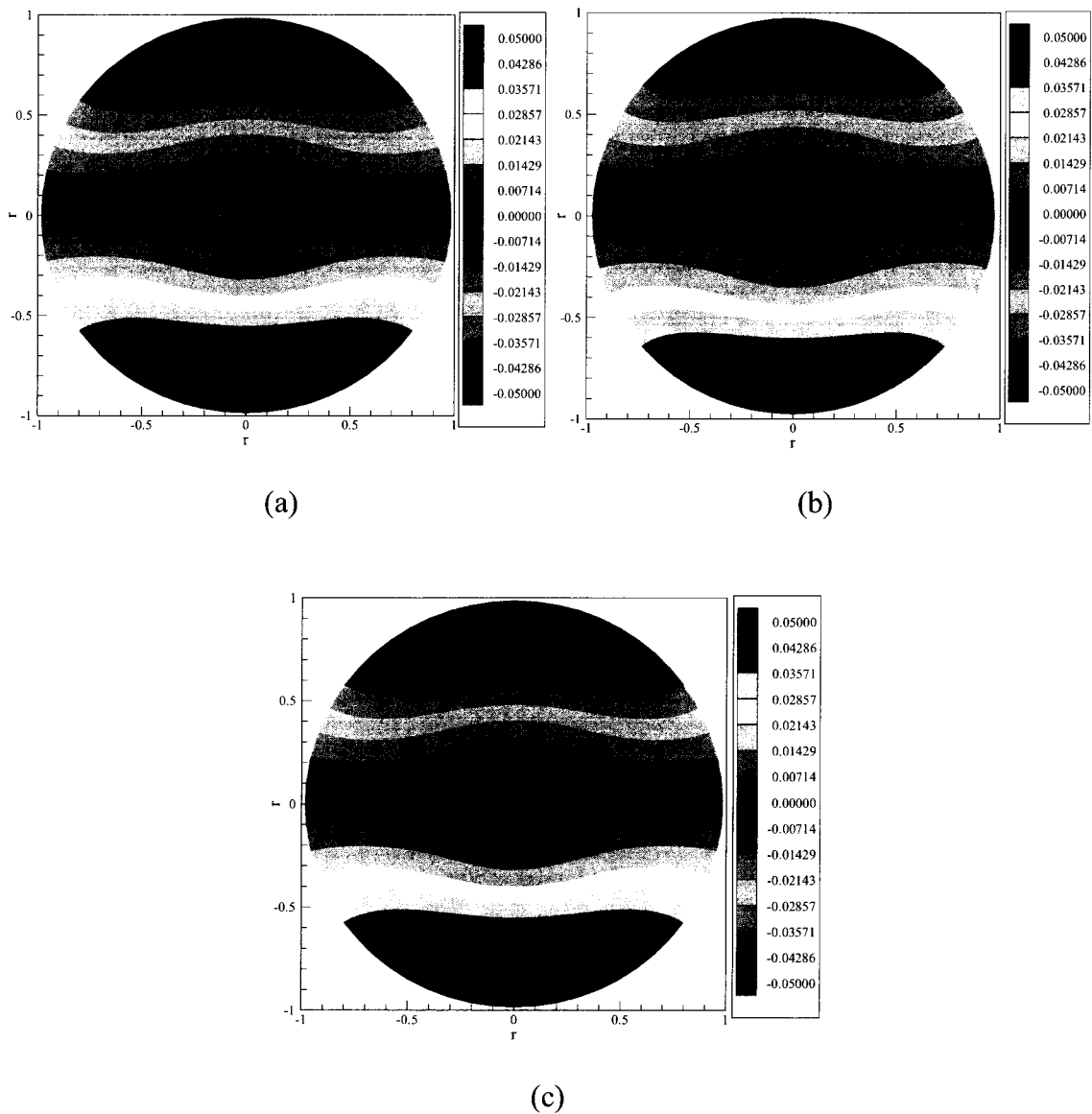


Figure 5.17 Comparison of contours of the solution of  $T_I$  in the cross section of  $\theta = 0$  and  $\theta = \pi$  at  $t = 0.1$  obtained using (a) the 3D second improved CN scheme and (b) the 3D CN scheme with (c) the exact solution.

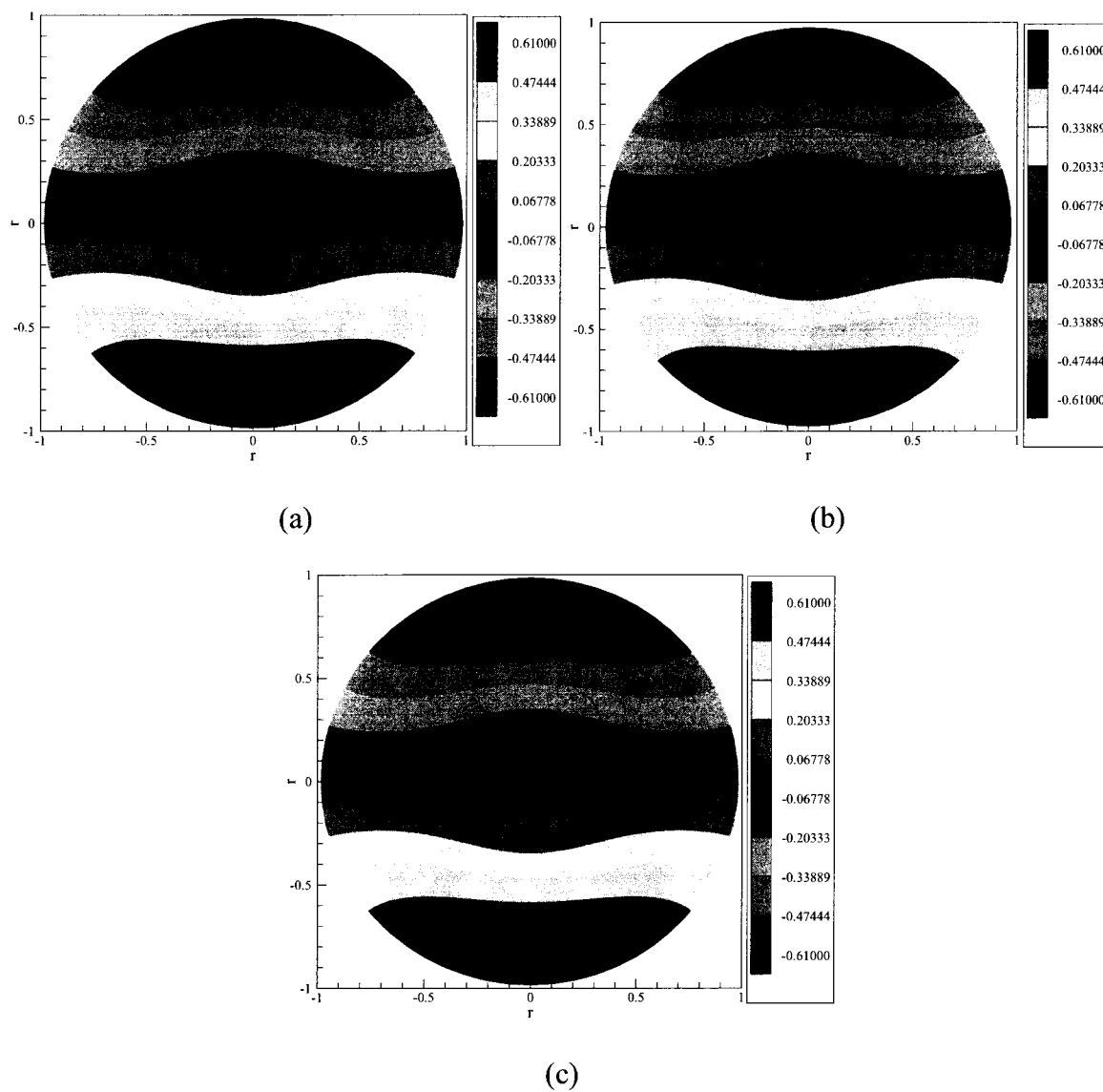


Figure 5.18 Comparison of contours of the solution  $T_2$  in the cross section of  $\theta = \frac{\pi}{2}$  at  $t = 0.1$  obtained using (a) the 3D second improved CN scheme and (b) the 3D CN scheme with (c) the exact solution.

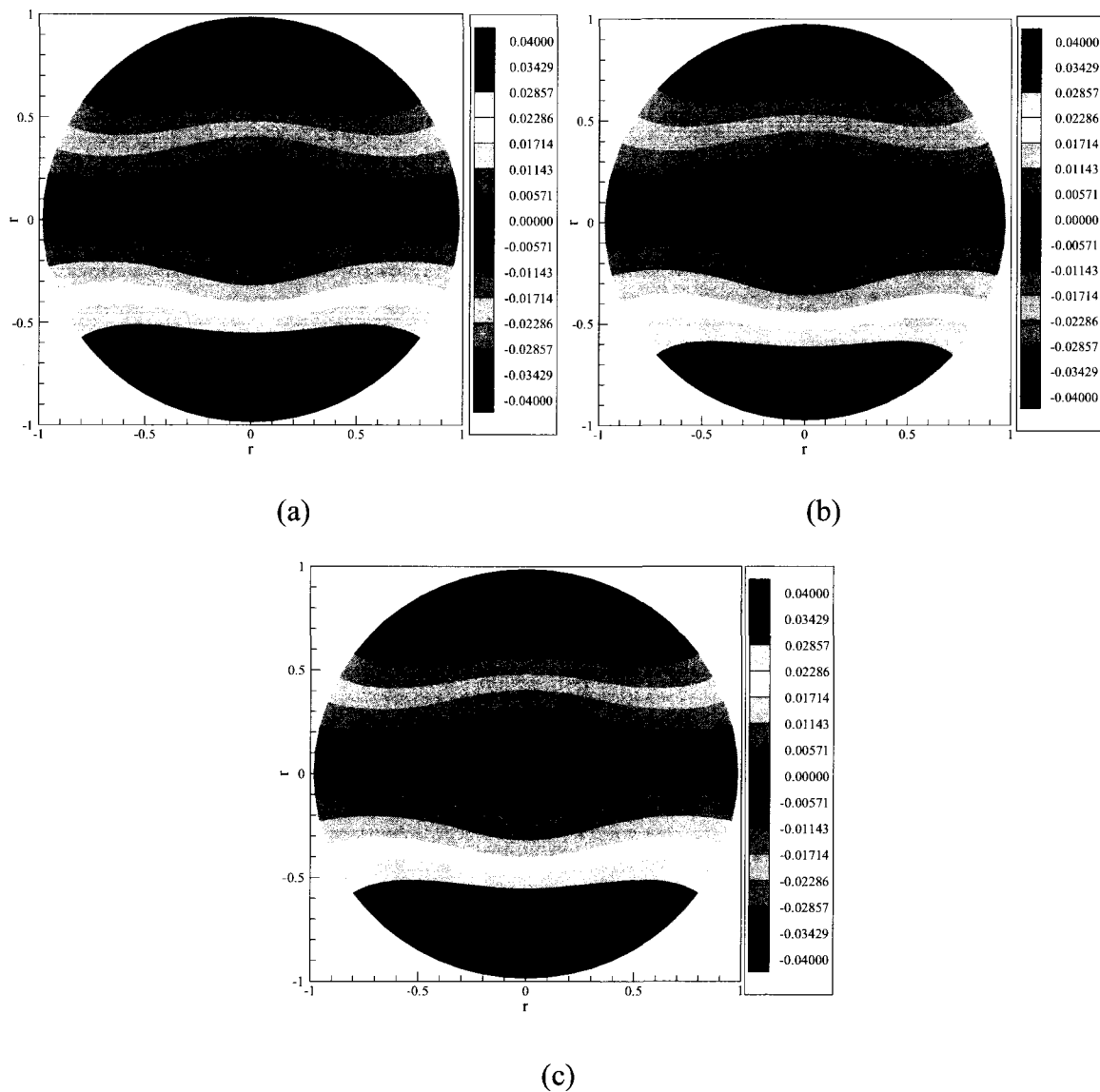


Figure 5.19 Comparison of contours of the solution of  $T_2$  in the cross section of  $\theta = 0$  and  $\theta = \pi$  at  $t = 0.1$  obtained using (a) the 3D second improved CN scheme and (b) the 3D CN scheme with (c) the exact solution.

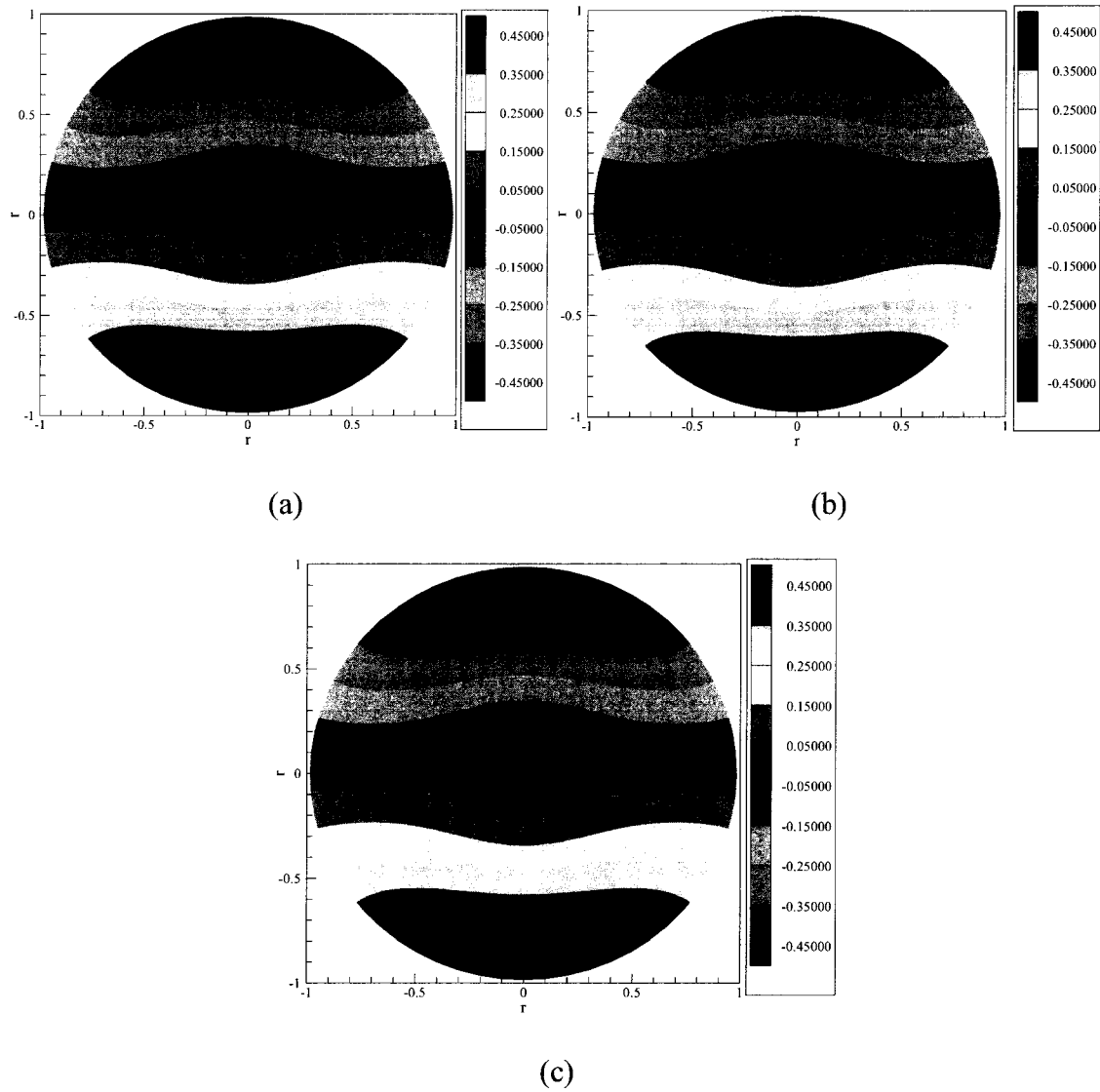


Figure 5.20 Comparison of contours of the solution  $T_3$  in the cross section of  $\theta = \frac{\pi}{2}$  at  $t = 0.1$  obtained using (a) the 3D second improved CN scheme and (b) the 3D CN scheme with (c) the exact solution.

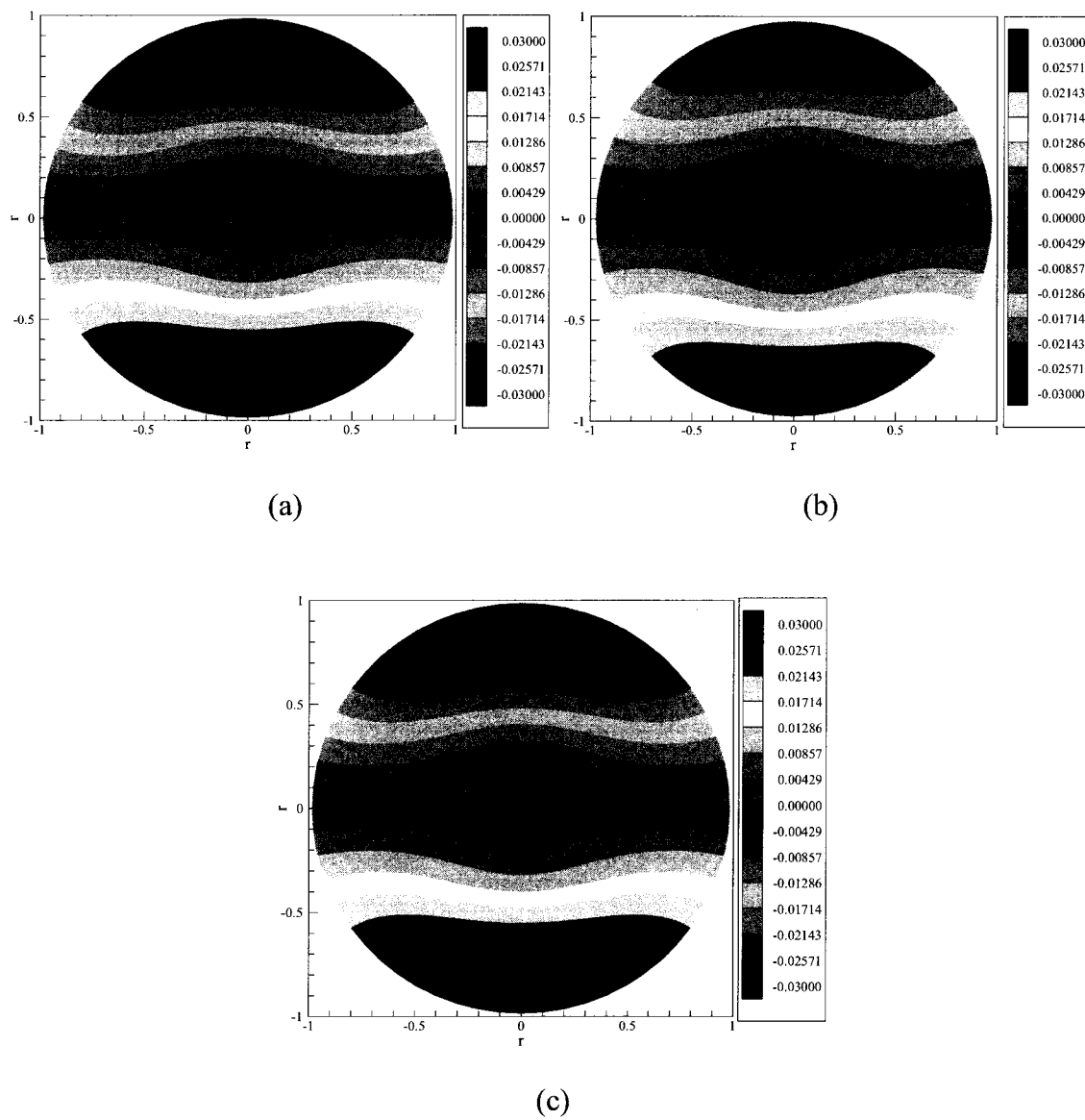


Figure 5.21 Comparison of contours of the solution of  $T_3$  in the cross section of  $\theta = 0$  and  $\theta = \pi$  at  $t = 0.1$  obtained using (a) the 3D second improved CN scheme and (b) the 3D CN scheme with (c) the exact solution.

## CHAPTER SIX

### CONCLUSION

This dissertation developed the parabolic models for the non-equilibrium heating in an  $N$ -carrier system in 1D and 3D spherical coordinates, respectively.

For 1D case, the well-posedness of the parabolic model in an  $N$ -carrier system in 1D spherical coordinates is proved. To solve the model, 1D improved CN scheme is developed. Also, the stability of the 1D improved CN scheme is proved.

A numerical example for 1D improved CN scheme is provided. Results shows that, to achieve a match between the numerical solution and the exact solution, while the 1D CN scheme needs a grid of  $I = 10^5$ , the 1D improved CN scheme only needs a grid of  $I = 10^3$ .

The convergence rates for the 1D improved CN scheme and the 1D CN scheme are calculated, and the results show that the convergence rate of the 1D improved CN scheme is about 2 with respect to both spatial and temporal variables, and the convergence rate of the 1D CN scheme is about 1 and about 2 with respect to both spatial and temporal variables, respectively.

For 3D case, the well-posedness of the parabolic model in an  $N$ -carrier system in 3D spherical coordinates is proved. To solve the model, two improved CN scheme are developed: the 3D first improved CN scheme and the 3D second improved CN scheme. Also, the stability of the two improved CN schemes is proved.

A numerical example for each 3D improved CN scheme is provided respectively. Results shows that, with the grid of  $41 \times 60 \times 60$ , both the 3D first improved CN scheme and the 3D second improved CN scheme provide a match between the numerical solution and the exact solution, but the 3D CN scheme does not.

The convergence rates for the 3D CN scheme, the 3D first improved CN scheme and the 3D second improved CN scheme are calculated, and results show that the convergence rate of both the 3D first improved CN scheme and the 3D second improved CN scheme are about 2 with respect to spatial variable, and the convergence rate of 3D CN scheme is about 1 with respect to the spatial variable.

Since the parabolic two-step model may lose accuracy when the laser pulse duration is much shorter than the electron-lattice thermal relaxation time [2], [48], the future research is needed to develop the hyperbolic model in an  $N$ -carrier system in spherical coordinates.

## **APPENDIX**

### **SOURCE CODE FOR NUMERICAL EXAMPLES**

# 1. SOURCE CODE FOR 1D IMPROVED CN SCHEME

C 2-time level 1D improved CN

C Mar. 2009

C Main Program

```

DIMENSION t1(0:1005),t2(0:1005),t3(0:1005)
DIMENSION r(0:1005),rh(0:1005),t1_exact(0:1005)
DIMENSION t2_exact(0:1005),t3_exact(0:1005)
DIMENSION t1old(0:1005),t1new(0:1005),t2old(0:1005)
DIMENSION
t2new(0:1005),t3old(0:1005),t3new(0:1005)
DIMENSION d1(0:1005),d2(0:1005),d3(0:1005)
DIMENSION f1(0:1005),f2(0:1005),f3(0:1005)
DIMENSION a(0:1005),b(0:1005),c(0:1005),e(0:1005)
DIMENSION errorT1(0:1005),errorT2(0:1005)
DIMENSION
errorT3(0:1005),error_max(0:1005),ff(0:1005)
DOUBLE PRECISION t1,t2,t3,t1old,t1new,t2old,t2new
DOUBLE PRECISION t3old,t3new,d1,d2,d3,f1,f2,f3
DOUBLE PRECISION
a,b,c,e,t1_exact,t2_exact,t3_exact
DOUBLE PRECISION c1,c2,c3,errorT1,errorT2,errorT3
DOUBLE PRECISION error_max,err_max_err,rrt,r,rh
DOUBLE PRECISION dt,dr,pi,tol
DOUBLE PRECISION temp1, temp2, temp3, temp4
DOUBLE PRECISION theta1,theta2,aa,bb,th

```

C II: number of grid

C NN: number of time step

C value assignment

```

theta1=(sqrt(5.0)+1.0)/2.0
dt=0.001
II=1001
NN=1000
pi=3.14159265358979323846
th=theta1+II
theta2=(sqrt(4.0+3.0*th*(th-1.0))-1.0)/(3.0*th)
dr=1.0/(II-1.0+theta1+theta2)
rrt=dt/(dr*dr)
DO i=1,II
r(i)=theta1*dr+(i-1)*dr
ENDDO
DO i=1,II-1
rh(i)=r(i)+0.5*dr
ENDDO

tol=1.0e-14
c1=1.25
c2=1.00
c3=0.75
aa=r(1)*r(1)*theta1
$ /((r(1)+0.5*dr)*(r(1)+0.5*dr)*(theta1/2.0+1.0/3.0))
bb=r(II)*r(II)*theta2
$ /((r(II)-0.5*dr)*(r(II)-0.5*dr)*(theta2/2.0+1.0/3.0))

```

C PRINT \*, aa, bb

C initial condition

DO i=1,II

C time level (n-1)

```

t1(i)=c1*cos(pi*r(i))
t2(i)=c2*cos(pi*r(i))
t3(i)=c3*cos(pi*r(i))
ENDDO

```

C Begin time iteration

n=0

C Begin Gauss-Seidel Iteration

```

1 DO i=1,II
t1old(i)=t1(i)
t2old(i)=t2(i)
t3old(i)=t3(i)
ENDDO

```

C Begin Thomas Algorithm

```

DO i=2,II-1
b(i)=rrt*rh(i-1)*rh(i-1)/(r(i)*r(i))
a(i)=1.0+rrt*rh(i-1)*rh(i-1)*rh(i-1)+rh(i)*rh(i)/(r(i)*r(i))+dt*pi*pi
c(i)=rrt*rh(i)*rh(i)/(r(i)*r(i))
ENDDO
a(1)=1.0+rrt*rh(1)*rh(1)*aa/(r(1)*r(1))+dt*pi*pi
c(1)=rrt*rh(1)*rh(1)*aa/(r(1)*r(1))
b(1)=0.0
a(II)=1.0+rrt*rh(II-1)*rh(II-1)*bb/(r(II)*r(II))+dt*pi*pi
b(II)=rrt*rh(II-1)*rh(II-1)*bb/(r(II)*r(II))
c(II)=0.0
e(0)=0.0
DO i=1,II
e(i)=c(i)/(a(i)-b(i)*e(i-1))
ENDDO

```

C Thomas Algorithm for t1

```

2 d1(1)=(1.0-rrt*rh(1)*rh(1)*aa/(r(1)*r(1))-dt*pi*pi)*t1(1)
& +rrt*rh(1)*rh(1)*aa*t1(2)/(r(1)*r(1))
& +dt*pi*pi*(t2old(1)+t2(1))/2.0
& +dt*pi*pi*(t3old(1)+t3(1))/2.0
& +2.0*dt*exp(-pi*pi*dt*(n+0.5))*pi*pi*cos(pi*r(1))
& +5.0*dt*exp(-pi*pi*dt*(n+0.5))*pi*sin(pi*r(1))/r(1)

```

```

d1(II)=(1.0-rrt*rh(II-1)*rh(II-1)*bb/(r(II)*r(II))
& -dt*pi*pi)*t1(II)
& +rrt*rh(II-1)*rh(II-1)*bb*t1(II-1)/(r(II)*r(II))
& +dt*pi*pi*(t2old(II)+t2(II))/2.0
& +dt*pi*pi*(t3old(II)+t3(II))/2.0
& +2.0*dt*exp(-pi*pi*dt*(n+0.5))*pi*pi*cos(pi*r(II))
& +5.0*dt*exp(-pi*pi*dt*(n+0.5))*pi*sin(pi*r(II))/r(II)

```

DO i=2,II-1

```

d1(i)=rrt*rh(i-1)*rh(i-1)*t1(i-1)/(r(i)*r(i))
& +(1.0-rrt*(rh(i-1)*rh(i-1)+rh(i)*rh(i))/(r(i)*r(i))
& -dt*pi*pi)*t1(i)
& +rrt*rh(i)*rh(i)*t1(i+1)/(r(i)*r(i))
& +dt*pi*pi*(t2old(i)+t2(i))/2.0
& +dt*pi*pi*(t3old(i)+t3(i))/2.0
& +2.0*dt*exp(-pi*pi*dt*(n+0.5))*pi*pi*cos(pi*r(i))
& +5.0*dt*exp(-pi*pi*dt*(n+0.5))*pi*sin(pi*r(i))/r(i)
ENDDO

```

f1(0)=0.0

DO i=1,II

f1(i)=(d1(i)+b(i)\*f1(i-1))/(a(i)-b(i)\*e(i-1))

ENDDO

t1new(II+1)=0.0

DO i=1,II

m=II+1-i

t1new(m)=e(m)\*t1new(m+1)+f1(m)

ENDDO

C Thomas Algorithm for t2

```

d2(1)=(1.0-rrt*rh(1)*rh(1)*aa/(r(1)*r(1))-dt*pi*pi)*t2(1)
& +rrt*rh(1)*rh(1)*aa*t2(2)/(r(1)*r(1))

```

```

& +dt*pi*pi*(t1new(1)+t1(1))/2.0
& +dt*pi*pi*(t3old(1)+t3(1))/2.0
& +dt*exp(-pi*pi*dt*(n+0.5))*pi*pi*cos(pi*r(1))
& +4.0*dt*exp(-pi*pi*dt*(n+0.5))*pi*sin(pi*r(1))/r(1)

d2(II)=(1.0-rrt*rh(II-1)*rh(II-1)*bb/(r(II)*r(II))
& -dt*pi*pi)*t2(II)
& +rrt*rh(II-1)*rh(II-1)*bb*t2(II-1)/(r(II)*r(II))
& +dt*pi*pi*(t1new(II)+t1(II))/2.0
& +dt*pi*pi*(t3old(II)+t3(II))/2.0
& +dt*exp(-pi*pi*dt*(n+0.5))*pi*pi*cos(pi*r(II))
& +4.0*dt*exp(-pi*pi*dt*(n+0.5))*pi*sin(pi*r(II))/r(II)

DO i=2,II-1
d2(i)=rrt*rh(i-1)*rh(i-1)*t2(i-1)/(r(i)*r(i))
& +(1.0-rrt*(rh(i-1)*rh(i-1)+rh(i)*rh(i)))/(r(i)*r(i))
& -dt*pi*pi)*t2(i)
& +rrt*rh(i)*rh(i)*t2(i+1)/(r(i)*r(i))
& +dt*pi*pi*(t1new(i)+t1(i))/2.0
& +dt*pi*pi*(t3old(i)+t3(i))/2.0
& +dt*exp(-pi*pi*dt*(n+0.5))*pi*pi*cos(pi*r(i))
& +4.0*dt*exp(-pi*pi*dt*(n+0.5))*pi*sin(pi*r(i))/r(i)
ENDDO

f2(0)=0.0
DO i=1,II
f2(i)=(d2(i)+b(i)*f2(i-1))/(a(i)-b(i)*e(i-1))
ENDDO
t2new(II+1)=0.0
DO i=1,II
m=II+1-i
t2new(m)=e(m)*t2new(m+1)+f2(m)
ENDDO
C Thomas Algorithm for B
d3(1)=(1.0-rrt*rh(1)*rh(1)*aa/(r(1)*r(1))-dt*pi*pi)*t3(1)
& +rrt*rh(1)*rh(1)*aa*t3(2)/(r(1)*r(1))
& +dt*pi*pi*(t1new(1)+t1(1))/2.0
& +dt*pi*pi*(t2new(1)+t2(1))/2.0
& +3.0*dt*exp(-pi*pi*dt*(n+0.5))*pi*sin(pi*r(1))/r(1)

d3(II)=(1.0-rrt*rh(II-1)*rh(II-1)*bb/(r(II)*r(II))
& -dt*pi*pi)*t3(II)
& +rrt*rh(II-1)*rh(II-1)*bb*t3(II-1)/(r(II)*r(II))
& +dt*pi*pi*(t1new(II)+t1(II))/2.0
& +dt*pi*pi*(t2new(II)+t2(II))/2.0
& +3.0*dt*exp(-pi*pi*dt*(n+0.5))*pi*sin(pi*r(II))/r(II)

DO i=2,II-1
d3(i)=rrt*rh(i-1)*rh(i-1)*t3(i-1)/(r(i)*r(i))
& +(1.0-rrt*(rh(i-1)*rh(i-1)+rh(i)*rh(i)))/(r(i)*r(i))
& -dt*pi*pi)*t3(i)
& +rrt*rh(i)*rh(i)*t3(i+1)/(r(i)*r(i))
& +dt*pi*pi*(t1new(i)+t1(i))/2.0
& +dt*pi*pi*(t2new(i)+t2(i))/2.0
& +3.0*dt*exp(-pi*pi*dt*(n+0.5))*pi*sin(pi*r(i))/r(i)
ENDDO

f3(0)=0.0
DO i=1,II
f3(i)=(d3(i)+b(i)*f3(i-1))/(a(i)-b(i)*e(i-1))
ENDDO
t3new(II+1)=0.0
DO i=1,II
m=II+1-i
t3new(m)=e(m)*t3new(m+1)+f3(m)
ENDDO
C calculate err

max_err=0.0
DO i=1,II
err=abs(t1new(i)-t1old(i))
IF(err.GT.max_err)THEN
max_err=err
ENDIF
err=abs(t2new(i)-t2old(i))
IF(err.GT.max_err)THEN
max_err=err
ENDIF
err=abs(t3new(i)-t3old(i))
IF(err.GT.max_err)THEN
max_err=err
ENDIF
ENDDO
IF(max_err.le.tol)GOTO 3
C print *, max_err
DO i=1,II
t1old(i)=t1new(i)
t2old(i)=t2new(i)
t3old(i)=t3new(i)
ENDDO
GOTO 2
C end Gauss-Seidel Iteration
C Calculate exact solutions
3 DO i=1,II
t1_exact(i)=c1*exp(-pi*pi*dt*(n+1.0))*cos(pi*r(i))
t2_exact(i)=c2*exp(-pi*pi*dt*(n+1.0))*cos(pi*r(i))
t3_exact(i)=c3*exp(-pi*pi*dt*(n+1.0))*cos(pi*r(i))
ENDDO
C Calculate err
DO i=1,II
errorT1(i)=abs(t1new(i)-t1_exact(i))
errorT2(i)=abs(t2new(i)-t2_exact(i))
errorT3(i)=abs(t3new(i)-t3_exact(i))
ENDDO

temp1=0.0
temp2=0.0
temp3=0.0
temp4=0.0

error_max(n)=0.0
DO i=1,II

temp1=temp1+errorT1(i)*errorT1(i)
temp2=temp2+errorT2(i)*errorT2(i)
temp3=temp3+errorT3(i)*errorT3(i)

ENDDO

temp4=temp1+temp2+temp3
error_max(n)=sqrt(dr*temp4/3.0)
C Next time iteration
n=n+1
PRINT *,n
IF(n.EQ.NN)GOTO 4

DO i=1,II
t1(i)=t1new(i)
t2(i)=t2new(i)
t3(i)=t3new(i)
ENDDO

GOTO 1
C Output
4 OPEN(unit=77,file='N=50ar3.dat')
DO n=1,NN

```

```

WRITE(77,1000) n*dt,error_max(n)
ENDDO
1000 FORMAT(f18.6, e18.10)
END

```

## 2. SOURCE CODE FOR 3D FIRST IMPROVED CN SCHEME

```

C 2-time level 3D first improved CN
C nsystem36.f
C Oct. 2009

```

```

DIMENSION t1(0:50,-1:110,0:110),t2(0:50,-1:110,0:110)
DIMENSION t3(0:50,-
1:110,0:110),gamma(0:50),gammah(0:50)
DIMENSION phi(-1:110),u(0:110),uh(0:110)
DIMENSION t1_exact(0:50,-
1:110,0:110),t2_exact(0:50,-1:110,0:110)
DIMENSION t3_exact(0:50,-1:110,0:110),t1oldgs(0:50,-
1:110,0:110)
DIMENSION t1newgs(0:50,-1:110,0:110),t2oldgs(0:50,-
1:110,0:110)
DIMENSION t2newgs(0:50,-1:110,0:110),t3oldgs(0:50,-
1:110,0:110)
DIMENSION t3newgs(0:50,-1:110,0:110),t1oldj(0:50,-
1:110,0:110)
DIMENSION t1newj(0:50,-1:110,0:110),t2oldj(0:50,-
1:110,0:110)
DIMENSION t2newj(0:50,-1:110,0:110),t3oldj(0:50,-
1:110,0:110)
DIMENSION t3newj(0:50,-1:110,0:110),errorT1(0:50,-
1:110,0:110)
DIMENSION errorT2(0:50,-1:110,0:110),errorT3(0:50,-
1:110,0:110)
DIMENSION error_max(0:5010)
DOUBLE PRECISION
t1,t2,t3,Q1dt,Q2dt,Q3dt,d1,d2,d3,abc,c1,c2,c3
DOUBLE PRECISION
t1oldgs,t1newgs,t2oldgs,t2newgs,t3oldgs,t3newgs
DOUBLE PRECISION
t1oldj,t1newj,t2oldj,t2newj,t3oldj,t3newj
DOUBLE PRECISION
t1_exact,t2_exact,t3_exact,abl,abr
DOUBLE PRECISION
errorT1,errorT2,errorT3,error_max
DOUBLE PRECISION
error_maxj,error_maxgs,errj,errgs,er
DOUBLE PRECISION err_max,tr,tp,ts,gamma,gammah
DOUBLE PRECISION phi,u,uh,theta1,theta2,th
DOUBLE PRECISION dt,dgamma,dphi,du,pi,tolj,tolgs
DOUBLE PRECISION
cr1,cr2,cs,cp1,cp2,temp1,temp2,temp3,temp4
DOUBLE PRECISION
c11dt,c12dt,c13dt,c21dt,c22dt,c23dt,c31dt,c32dt
C value assignment

```

```

dt=0.0001
II=11
JJ=60
KK=60
NN=1000
pi=3.14159265358979323846
theta1=(sqrt(5.0)+1.0)/2.0
th=theta1+II
theta2=(sqrt(4.0+3.0*th*(th-1.0))-1.0)/(3.0*th)

```

```

C the first order scheme

```

```

C theta1=1.0
C theta2=1.0
dgamma=1.0/(II-1.0+theta1+theta2)
dphi=2.0*pi/JJ
du=2.0/KK
tr=dt/(dgamma*dgamma)
ts=dt/(dphi*dphi)
tp=dt/(du*du)
tolgs=1.0D-6
tolj=1.0D-8
c1=1.25
c2=1.00
c3=0.75

DO i=1,II
gamma(i)=(theta1+(i-1))*dgamma
ENDDO
DO i=1,II-1
gammah(i)=gamma(i)+0.5*dgamma
ENDDO
DO j=0,JJ-1
phi(j)=j*dphi
ENDDO
DO k=0,KK
u(k)=k*du-1.0
ENDDO
DO k=0,KK-1
uh(k)=u(k)+0.5*du
ENDDO

abl=gamma(1)*gamma(1)*theta1
& /(gammah(1)*gammah(1)*(theta1/2.0+1.0/3.0))
abr=gamma(II)*gamma(II)*theta2
& /(gammah(II-1)*gammah(II-1)*(theta2/2.0+1.0/3.0))
C the first order scheme
C abl=1.0
C abr=1.0
C initial condition
DO i=1,II
DO j=0,JJ-1
DO k=0,KK
t1(i,j,k)=c1*cos(pi*gamma(i))*sin(phi(j))*(1.0-u(k)*u(k))
t2(i,j,k)=c2*cos(pi*gamma(i))*sin(phi(j))*(1.0-u(k)*u(k))
t3(i,j,k)=c3*cos(pi*gamma(i))*sin(phi(j))*(1.0-u(k)*u(k))
ENDDO
ENDDO
ENDDO

C boundary condition
DO i=1,II
DO j=0,JJ-1
t1(i,j,0)=0.0
t2(i,j,0)=0.0
t3(i,j,0)=0.0
t1(i,j,KK)=0.0
t2(i,j,KK)=0.0
t3(i,j,KK)=0.0
ENDDO
ENDDO

DO i=1,II
DO k=0,KK
t1(i,-1,k)=t1(i,JJ-1,k)
t2(i,-1,k)=t2(i,JJ-1,k)
t3(i,-1,k)=t3(i,JJ-1,k)
t1(i,JJ,k)=t1(i,0,k)
t2(i,JJ,k)=t2(i,0,k)
t3(i,JJ,k)=t3(i,0,k)
ENDDO
ENDDO

```

```

C Begin time iteration
n=0
C Begin Gauss-Seidel Iteration
1 DO i=1,II
  DO j=-1,JJ
  DO k=0,KK
  t1oldgs(i,j,k)=t1(i,j,k)
  t2oldgs(i,j,k)=t2(i,j,k)
  t3oldgs(i,j,k)=t3(i,j,k)
  ENDDO
  ENDDO
  ENDDO

C Jacobi for T1
C initial condition for Jacobi
2 DO i=1,II
  DO j=-1,JJ
  DO k=0,KK
  t1oldj(i,j,k)=t1oldgs(i,j,k)
  ENDDO
  ENDDO
  ENDDO

C RHS
3 DO j=0,JJ-1
  DO k=1,KK-1
  c11dt=dt*2.0*pi*pi*exp(-
pi*pi*dt*(n+0.5))*cos(pi*gamma(1))
& *sin(phi(j))*(1.0-
u(k)*u(k))*gamma(1)*gamma(1)*(1.0-u(k)*u(k))

  c12dt=dt*5.0*pi*exp(-
pi*pi*dt*(n+0.5))*sin(pi*gamma(1))
& *sin(phi(j))*(1.0-u(k)*u(k))*gamma(1)*(1.0-u(k)*u(k))

  c13dt=dt*6.0*c1*exp(-
pi*pi*dt*(n+0.5))*cos(pi*gamma(1))
& *sin(phi(j))*(2.0*u(k)*u(k)-1.0)*(1.0-u(k)*u(k))

  Q1dt=c11dt+c12dt-c13dt

  cr1=gammah(1)*gammah(1)*tr*(1.0-u(k)*u(k))
  cs=ts
  cp1=(1.0-uh(k)*uh(k))*tp*(1.0-u(k)*u(k))
  cp2=(1.0-uh(k-1)*uh(k-1))*tp*(1.0-u(k)*u(k))

  abc=gamma(1)*gamma(1)*(1.0-
u(k)*u(k))+abl*cr1+2.0*cs+cp1+cp2
& +dt*pi*pi*gamma(1)*gamma(1)*(1.0-u(k)*u(k))
  d1=abl*cr1*t1oldj(2,j,k)+abl*cr1*t1(2,j,k)
& +(gamma(1)*gamma(1)*(1.0-u(k)*u(k))
& -abl*cr1-2.0*cs-cp1-cp2
& -dt*pi*pi*gamma(1)*gamma(1)*(1.0-
u(k)*u(k)))*t1(1,j,k)
& +cs*t1oldj(1,j+1,k)+cs*t1(1,j+1,k)
& +cs*t1oldj(1,j-1,k)+cs*t1(1,j-1,k)
& +cp1*t1oldj(1,j,k+1)+cp1*t1(1,j,k+1)
& +cp2*t1oldj(1,j,k-1)+cp2*t1(1,j,k-1)
& +dt*pi*pi*(t2oldgs(1,j,k)+t2(1,j,k))
& *gamma(1)*gamma(1)*(1.0-u(k)*u(k))/2.0
& +dt*pi*pi*(t3oldgs(1,j,k)+t3(1,j,k))
& *gamma(1)*gamma(1)*(1.0-u(k)*u(k))/2.0+Q1dt

  t1newj(1,j,k)=d1/abc
  ENDDO
  ENDDO
  ENDDO

  DO i=2,II-1
  DO j=0,JJ-1
  DO k=1,KK-1
    c11dt=dt*2.0*pi*pi*exp(-
pi*pi*dt*(n+0.5))*cos(pi*gamma(i))
& *sin(phi(j))*(1.0-
u(k)*u(k))*gamma(i)*gamma(i)*(1.0-u(k)*u(k))

    c12dt=dt*5.0*pi*exp(-
pi*pi*dt*(n+0.5))*sin(pi*gamma(i))
& *sin(phi(j))*(1.0-u(k)*u(k))*gamma(i)*(1.0-u(k)*u(k))

    c13dt=dt*6.0*c1*exp(-
pi*pi*dt*(n+0.5))*cos(pi*gamma(i))
& *sin(phi(j))*(2.0*u(k)*u(k)-1.0)*(1.0-u(k)*u(k))

    Q1dt=c11dt+c12dt-c13dt

    cr1=gammah(i)*gammah(i)*tr*(1.0-u(k)*u(k))
    cr2=gammah(i-1)*gammah(i-1)*tr*(1.0-u(k)*u(k))
    cs=ts
    cp1=(1.0-uh(k)*uh(k))*tp*(1.0-u(k)*u(k))
    cp2=(1.0-uh(k-1)*uh(k-1))*tp*(1.0-u(k)*u(k))

    abc=gamma(i)*gamma(i)*(1.0-
u(k)*u(k))+cr1+cr2+2.0*cs
& +cp1+cp2+dt*pi*pi*gamma(i)*gamma(i)*(1.0-
u(k)*u(k))
    d1=cr1*t1oldj(i+1,j,k)+cr1*t1(i+1,j,k)
& +(gamma(i)*gamma(i)*(1.0-u(k)*u(k))-cr1-cr2-2.0*cs-
cp1-cp2
& -dt*pi*pi*gamma(i)*gamma(i)*(1.0-
u(k)*u(k)))*t1(i,j,k)
& +cr2*t1oldj(i-1,j,k)+cr2*t1(i-1,j,k)
& +cs*t1oldj(i,j+1,k)+cs*t1(i,j+1,k)
& +cs*t1oldj(i,j-1,k)+cs*t1(i,j-1,k)
& +cp1*t1oldj(i,j,k+1)+cp1*t1(i,j,k+1)
& +cp2*t1oldj(i,j,k-1)+cp2*t1(i,j,k-1)
& +dt*pi*pi*(t2oldgs(i,j,k)+t2(i,j,k))
& *gamma(i)*gamma(i)*(1.0-u(k)*u(k))/2.0
& +dt*pi*pi*(t3oldgs(i,j,k)+t3(i,j,k))
& *gamma(i)*gamma(i)*(1.0-u(k)*u(k))/2.0+Q1dt

    t1newj(i,j,k)=d1/abc
    ENDDO
    ENDDO
    ENDDO

    DO j=0,JJ-1
    DO k=1,KK-1
    c11dt=dt*2.0*pi*pi*exp(-
pi*pi*dt*(n+0.5))*cos(pi*gamma(II))
& *sin(phi(j))*(1.0-
u(k)*u(k))*gamma(II)*gamma(II)*(1.0-u(k)*u(k))

    c12dt=dt*5.0*pi*exp(-
pi*pi*dt*(n+0.5))*sin(pi*gamma(II))
& *sin(phi(j))*(1.0-u(k)*u(k))*gamma(II)*(1.0-u(k)*u(k))

    c13dt=dt*6.0*c1*exp(-
pi*pi*dt*(n+0.5))*cos(pi*gamma(II))
& *sin(phi(j))*(2.0*u(k)*u(k)-1.0)*(1.0-u(k)*u(k))

    Q1dt=c11dt+c12dt-c13dt

    cr2=gammah(II-1)*gammah(II-1)*tr*(1.0-u(k)*u(k))
    cs=ts
    cp1=(1.0-uh(k)*uh(k))*tp*(1.0-u(k)*u(k))
    cp2=(1.0-uh(k-1)*uh(k-1))*tp*(1.0-u(k)*u(k))

    abc=gamma(II)*gamma(II)*(1.0-
u(k)*u(k))+abr*cr2+2.0*cs+cp1+cp2
& +dt*pi*pi*gamma(II)*gamma(II)*(1.0-u(k)*u(k))

```

```

      d1=abr*cr2*t1oldj(II-1,j,k)+abr*cr2*t1(II-1,j,k)
      & +(gamma(II)*gamma(II)*(1.0-u(k)*u(k))-abr*cr2-
2.0*cs-cp1-cp2
      & -pi*pi*dt*gamma(II)*gamma(II)*(1.0-
u(k)*u(k))*t1(II,j,k)
      & +cs*t1oldj(II,j+1,k)+cs*t1(II,j+1,k)
      & +cs*t1oldj(II,j-1,k)+cs*t1(II,j-1,k)
      & +cp1*t1oldj(II,j,k+1)+cp1*t1(II,j,k+1)
      & +cp2*t1oldj(II,j,k-1)+cp2*t1(II,j,k-1)
      & +dt*pi*pi*(t2oldgs(II,j,k)+t2(II,j,k))
      & *gamma(II)*gamma(II)*(1.0-u(k)*u(k))/2.0
      & +dt*pi*pi*(t3oldgs(II,j,k)+t3(II,j,k))
      & *gamma(II)*gamma(II)*(1.0-u(k)*u(k))/2.0+Q1dt

      t1newj(II,j,k)=d1/abc
      ENDDO
      ENDDO

C boundary condition
DO i=1,II
DO j=0,JJ-1
t1newj(i,j,0)=0
t1newj(i,j,KK)=0
ENDDO
ENDDO

DO i=1,II
DO k=0,KK
t1newj(i,-1,k)=t1newj(i,JJ-1,k)
t1newj(i,JJ,k)=t1newj(i,0,k)
ENDDO
ENDDO

C error for Jacobi
error_maxj=0.0
DO i=1,II
DO j=0,JJ-1
DO k=1,KK-1
errj=abs(t1newj(i,j,k)-t1oldj(i,j,k))
IF(errj.GT.error_maxj)THEN
error_maxj=errj
ENDIF
ENDDO
ENDDO
ENDDO

C update for Jacobi
DO i=1,II
DO j=-1,JJ
DO k=0,KK
t1oldj(i,j,k)=t1newj(i,j,k)
ENDDO
ENDDO
ENDDO

C print *, "1",error_maxj
IF(error_maxj.GT.tolj)GOTO 3

C update from Jacobi to Gauss-Seidel
DO i=1,II
DO j=-1,JJ
DO k=0,KK
t1newgs(i,j,k)=t1newj(i,j,k)
ENDDO
ENDDO
ENDDO

C Jacobi for T2
C initial condition for Jacobi
DO i=1,II
DO j=-1,JJ
DO k=0,KK
t2oldj(i,j,k)=t2oldgs(i,j,k)
ENDDO
ENDDO
ENDDO

4 DO j=0,JJ-1
DO k=1,KK-1
c21dt=dt*pi*pi*exp(-
pi*pi*dt*(n+0.5))*cos(pi*gamma(1))
& *sin(phi(j))*(1.0-
u(k)*u(k))*gamma(1)*gamma(1)*(1.0-u(k)*u(k))

c22dt=dt*4.0*pi*exp(-
pi*pi*dt*(n+0.5))*sin(pi*gamma(1))
& *sin(phi(j))*(1.0-u(k)*u(k))*gamma(1)*(1.0-u(k)*u(k))

c23dt=dt*6.0*c2*exp(-
pi*pi*dt*(n+0.5))*cos(pi*gamma(1))
& *sin(phi(j))*(2.0*u(k)*u(k)-1.0)*(1.0-u(k)*u(k))

Q2dt=c21dt+c22dt-c23dt

cr1=gammah(1)*gammah(1)*tr*(1.0-u(k)*u(k))
cs=ts
cp1=(1.0-uh(k)*uh(k))*tp*(1.0-u(k)*u(k))
cp2=(1.0-uh(k-1)*uh(k-1))*tp*(1.0-u(k)*u(k))

abc=gamma(1)*gamma(1)*(1.0-
u(k)*u(k))+abl*cr1+2.0*cs+cp1+cp2
& +dt*pi*pi*gamma(1)*gamma(1)*(1.0-u(k)*u(k))
d2=abl*cr1*t2oldj(2,j,k)+abl*cr1*t2(2,j,k)
& +(gamma(1)*gamma(1)*(1.0-u(k)*u(k))-abl*cr1-
2.0*cs-cp1-cp2
& -dt*pi*pi*gamma(1)*gamma(1)*(1.0-
u(k)*u(k))*t2(1,j,k)
& +cs*t2oldj(1,j+1,k)+cs*t2(1,j+1,k)
& +cs*t2oldj(1,j-1,k)+cs*t2(1,j-1,k)
& +cp1*t2oldj(1,j,k+1)+cp1*t2(1,j,k+1)
& +cp2*t2oldj(1,j,k-1)+cp2*t2(1,j,k-1)
& +dt*pi*pi*(t1newgs(1,j,k)+t1(1,j,k))
& *gamma(1)*gamma(1)*(1.0-u(k)*u(k))/2.0
& +dt*pi*pi*(t3oldgs(1,j,k)+t3(1,j,k))
& *gamma(1)*gamma(1)*(1.0-u(k)*u(k))/2.0+Q2dt

t2newj(1,j,k)=d2/abc
ENDDO
ENDDO

DO i=2,II-1
DO j=0,JJ-1
DO k=1,KK-1
c21dt=dt*pi*pi*exp(-
pi*pi*dt*(n+0.5))*cos(pi*gamma(i))
& *sin(phi(j))*(1.0-
u(k)*u(k))*gamma(i)*gamma(i)*(1.0-u(k)*u(k))

c22dt=dt*4.0*pi*exp(-
pi*pi*dt*(n+0.5))*sin(pi*gamma(i))
& *sin(phi(j))*(1.0-u(k)*u(k))*gamma(i)*(1.0-u(k)*u(k))

c23dt=dt*6.0*c2*exp(-
pi*pi*dt*(n+0.5))*cos(pi*gamma(i))
& *sin(phi(j))*(2.0*u(k)*u(k)-1.0)*(1.0-u(k)*u(k))

Q2dt=c21dt+c22dt-c23dt

cr1=gammah(i)*gammah(i)*tr*(1.0-u(k)*u(k))
cr2=gammah(i-1)*gammah(i-1)*tr*(1.0-u(k)*u(k))
cs=ts

```

```

cp1=(1.0-uh(k)*uh(k))*tp*(1.0-u(k)*u(k))
cp2=(1.0-uh(k-1)*uh(k-1))*tp*(1.0-u(k)*u(k))

abc=gamma(i)*gamma(i)*(1.0-
u(k)*u(k))+cr1+cr2+2.0*cs+cp1+cp2
& +dt*pi*pi*gamma(i)*gamma(i)*(1.0-u(k)*u(k))
d2=cr1*t2oldj(i+1,j,k)+cr1*t2(i+1,j,k)
& +(gamma(i)*gamma(i)*(1.0-u(k)*u(k))-cr1-cr2-2.0*cs-
cp1-cp2
& -dt*pi*pi*gamma(i)*gamma(i)*(1.0-
u(k)*u(k))*t2(i,j,k)
& +cr2*t2oldj(i-1,j,k)+cr2*t2(i-1,j,k)
& +cs*t2oldj(i,j+1,k)+cs*t2(i,j+1,k)
& +cs*t2oldj(i,j-1,k)+cs*t2(i,j-1,k)
& +cp1*t2oldj(i,j,k+1)+cp1*t2(i,j,k+1)
& +cp2*t2oldj(i,j,k-1)+cp2*t2(i,j,k-1)
& +dt*pi*pi*(t1newgs(i,j,k)+t1(i,j,k))
& *gamma(i)*gamma(i)*(1.0-u(k)*u(k))/2.0
& +dt*pi*pi*(t3oldgs(i,j,k)+t3(i,j,k))
& *gamma(i)*gamma(i)*(1.0-u(k)*u(k))/2.0+Q2dt

t2newj(i,j,k)=d2/abc
ENDDO
ENDDO
ENDDO

DO j=0, JJ-1
DO k=1, KK-1
c21dt=dt*pi*pi*exp(-
pi*pi*dt*(n+0.5))*cos(pi*gamma(II))
& *sin(phi(j))*(1.0-
u(k)*u(k))*gamma(II)*gamma(II)*(1.0-u(k)*u(k))

c22dt=dt*4.0*pi*exp(-
pi*pi*dt*(n+0.5))*sin(pi*gamma(II))
& *sin(phi(j))*(1.0-u(k)*u(k))*gamma(II)*(1.0-u(k)*u(k))

c23dt=dt*6.0*c2*exp(-
pi*pi*dt*(n+0.5))*cos(pi*gamma(II))
& *sin(phi(j))*(2.0*u(k)*u(k)-1.0)*(1.0-u(k)*u(k))

Q2dt=c21dt+c22dt-c23dt

cr2=gammah(II-1)*gammah(II-1)*tr*(1.0-u(k)*u(k))
cs=ts
cp1=(1.0-uh(k)*uh(k))*tp*(1.0-u(k)*u(k))
cp2=(1.0-uh(k-1)*uh(k-1))*tp*(1.0-u(k)*u(k))

abc=gamma(II)*gamma(II)*(1.0-
u(k)*u(k))+abr*cr2+2.0*cs+cp1+cp2
& +dt*pi*pi*gamma(II)*gamma(II)*(1.0-u(k)*u(k))
d2=abr*cr2*t2oldj(II-1,j,k)+abr*cr2*t2(II-1,j,k)
& +(gamma(II)*gamma(II)*(1.0-u(k)*u(k))-abr*cr2-
2.0*cs-cp1-cp2
& -dt*pi*pi*gamma(II)*gamma(II)*(1.0-
u(k)*u(k))*t2(II,j,k)
& +cs*t2oldj(II,j+1,k)+cs*t2(II,j+1,k)
& +cs*t2oldj(II,j-1,k)+cs*t2(II,j-1,k)
& +cp1*t2oldj(II,j,k+1)+cp1*t2(II,j,k+1)
& +cp2*t2oldj(II,j,k-1)+cp2*t2(II,j,k-1)
& +dt*pi*pi*(t1newgs(II,j,k)+t1(II,j,k))
& *gamma(II)*gamma(II)*(1.0-u(k)*u(k))/2.0
& +dt*pi*pi*(t3oldgs(II,j,k)+t3(II,j,k))
& *gamma(II)*gamma(II)*(1.0-u(k)*u(k))/2.0+Q2dt

t2newj(II,j,k)=d2/abc
ENDDO
ENDDO

C boundary condition

DO i=1,II
DO j=0, JJ-1
t2newj(i,j,0)=0.0
t2newj(i,j, KK)=0.0
ENDDO
ENDDO

DO i=1,II
DO k=0, KK
t2newj(i,-1,k)=t2newj(i, JJ-1,k)
t2newj(i, JJ,k)=t2newj(i,0,k)
ENDDO
ENDDO

C error for Jacobi
error_maxj=0.0
DO i=1,II
DO j=0, JJ-1
DO k=1, KK-1
errj=abs(t2newj(i,j,k)-t2oldj(i,j,k))
IF(errj.GT.error_maxj)THEN
error_maxj=errj
ENDIF
ENDDO
ENDDO
ENDDO

C update for Jacobi
DO i=1,II
DO j=-1, JJ
DO k=0, KK
t2oldj(i,j,k)=t2newj(i,j,k)
ENDDO
ENDDO
ENDDO

C print *, "2",error_maxj
IF(error_maxj.GT.tolj)GOTO 4

C update from Jacobi to Gauss-Seidel
DO i=1,II
DO j=-1, JJ
DO k=0, KK
t2newgs(i,j,k)=t2newj(i,j,k)
ENDDO
ENDDO
ENDDO

C Jacobi for T3
C initial condition for Jacobi
DO i=1,II
DO j=-1, JJ
DO k=0, KK
t3oldj(i,j,k)=t3oldgs(i,j,k)
ENDDO
ENDDO
ENDDO

5 DO j=0, JJ-1
DO k=1, KK-1
c31dt=dt*3.0*pi*exp(-
pi*pi*dt*(n+0.5))*sin(pi*gamma(1))
& *sin(phi(j))*(1.0-u(k)*u(k))*gamma(1)*(1.0-
u(k)*u(k))

c32dt=dt*6.0*c3*exp(-
pi*pi*dt*(n+0.5))*cos(pi*gamma(1))
& *sin(phi(j))*(2.0*u(k)*u(k)-1.0)*(1.0-u(k)*u(k))

Q3dt=c31dt-c32dt

```

```

cr1=gammah(1)*gammah(1)*tr*(1.0-u(k)*u(k))
cs=ts
cp1=(1.0-uh(k)*uh(k))*tp*(1.0-u(k)*u(k))
cp2=(1.0-uh(k-1)*uh(k-1))*tp*(1.0-u(k)*u(k))

abc=gamma(1)*gamma(1)*(1.0-
u(k)*u(k))+abl*cr1+2.0*cs+cp1+cp2
& +dt*pi*pi*gamma(1)*gamma(1)*(1.0-u(k)*u(k))
d3=abl*cr1*t3oldj(2,j,k)+abl*cr1*t3(2,j,k)
& +(gamma(1)*gamma(1)*(1.0-u(k)*u(k))-abl*cr1-
2.0*cs-cp1-cp2
& -dt*pi*pi*gamma(1)*gamma(1)*(1.0-
u(k)*u(k))*t3(1,j,k)
& +cs*t3oldj(1,j+1,k)+cs*t3(1,j+1,k)
& +cs*t3oldj(1,j-1,k)+cs*t3(1,j-1,k)
& +cp1*t3oldj(1,j,k+1)+cp1*t3(1,j,k+1)
& +cp2*t3oldj(1,j,k-1)+cp2*t3(1,j,k-1)
& +dt*pi*pi*(t1newgs(1,j,k)+t1(1,j,k))
& *gamma(1)*gamma(1)*(1.0-u(k)*u(k))/2.0
& +dt*pi*pi*(t2newgs(1,j,k)+t2(1,j,k))
& *gamma(1)*gamma(1)*(1.0-u(k)*u(k))/2.0+Q3dt

t3newj(1,j,k)=d3/abc
ENDDO
ENDDO

DO i=2,II-1
DO j=0,JJ-1
DO k=1,KK-1
c31dt=dt*3.0*pi*exp(-
pi*pi*dt*(n+0.5))*sin(pi*gamma(i))
& *sin(phi(j))*(1.0-u(k)*u(k))*gamma(i)*(1.0-u(k)*u(k))

c32dt=dt*6.0*c3*exp(-
pi*pi*dt*(n+0.5))*cos(pi*gamma(ii))
& *sin(phi(j))*(2.0*u(k)*u(k)-1.0)*(1.0-u(k)*u(k))

Q3dt=c31dt-c32dt

cr2=gammah(II-1)*gammah(II-1)*tr*(1.0-u(k)*u(k))
cs=ts
cp1=(1.0-uh(k)*uh(k))*tp*(1.0-u(k)*u(k))
cp2=(1.0-uh(k-1)*uh(k-1))*tp*(1.0-u(k)*u(k))

abc=gamma(II)*gamma(II)*(1.0-
u(k)*u(k))+abr*cr2+2.0*cs+cp1+cp2
& +dt*pi*pi*gamma(II)*gamma(II)*(1.0-u(k)*u(k))
d3=abr*cr2*t3oldj(II-1,j,k)+abr*cr2*t3(II-1,j,k)
& +(gamma(II)*gamma(II)*(1.0-u(k)*u(k))-abr*cr2-
2.0*cs-cp1-cp2
& -dt*pi*pi*gamma(II)*gamma(II)*(1.0-
u(k)*u(k))*t3(II,j,k)
& +cs*t3oldj(II,j+1,k)+cs*t3(II,j+1,k)
& +cs*t3oldj(II,j-1,k)+cs*t3(II,j-1,k)
& +cp1*t3oldj(II,j,k+1)+cp1*t3(II,j,k+1)
& +cp2*t3oldj(II,j,k-1)+cp2*t3(II,j,k-1)
& +dt*pi*pi*(t1newgs(II,j,k)+t1(II,j,k))
& *gamma(II)*gamma(II)*(1.0-u(k)*u(k))/2.0
& +dt*pi*pi*(t2newgs(II,j,k)+t2(II,j,k))
& *gamma(II)*gamma(II)*(1.0-u(k)*u(k))/2.0+Q3dt

t3newj(II,j,k)=d3/abc
ENDDO
ENDDO

C boundary condition
DO i=1,II
DO j=0,JJ-1
t3newj(i,j,0)=0
t3newj(i,j,KK)=0
ENDDO
ENDDO

DO i=1,II
DO k=0,KK
t3newj(i,-1,k)=t3newj(i,II-1,k)
t3newj(i,II,k)=t3newj(i,0,k)
ENDDO
ENDDO

C error for Jacobi
error_maxj=0.0
DO i=1,II
DO j=0,JJ-1
DO k=1,KK-1
errj=abs(t3newj(i,j,k)-t3oldj(i,j,k))
IF(errj.GT.error_maxj)THEN
error_maxj=errj
ENDIF
ENDDO
ENDDO
ENDDO

C update for Jacobi
DO i=1,II
DO j=-1,JJ
DO k=0,KK
t3oldj(i,j,k)=t3newj(i,j,k)
ENDDO

```

```

        ENDDO
        ENDDO
C   print *, "3",error_maxj
    IF(error_maxj.GT.tolj)GOTO 5

C update from Jacobi to Gauss-Seidel
    DO i=1,II
    DO j=-1,JJ
    DO k=0,KK
    t3newgs(i,j,k)=t3newj(i,j,k)
    ENDDO
    ENDDO
    ENDDO

C calculate err for Gauss-Seidel
    error_maxgs=0.0
    DO i=1,II
    DO j=0,JJ-1
    DO k=1,KK-1
    errgs=abs(t1newgs(i,j,k)-t1oldgs(i,j,k))
    IF(errgs.GT.error_maxgs)THEN
    error_maxgs=errgs
    ENDIF
    errgs=abs(t2newgs(i,j,k)-t2oldgs(i,j,k))
    IF(errgs.GT.error_maxgs)THEN
    error_maxgs=errgs
    ENDIF
    errgs=abs(t3newgs(i,j,k)-t3oldgs(i,j,k))
    IF(errgs.GT.error_maxgs)THEN
    error_maxgs=errgs
    ENDIF
    ENDDO
    ENDDO
    ENDDO
    IF(error_maxgs.LE.tolgs)GOTO 6
C   print *, max_err
    DO i=1,II
    DO j=-1,JJ
    DO k=0,KK
    t1oldgs(i,j,k)=t1newgs(i,j,k)
    t2oldgs(i,j,k)=t2newgs(i,j,k)
    t3oldgs(i,j,k)=t3newgs(i,j,k)
    ENDDO
    ENDDO
    ENDDO
    GOTO 2

C End Gauss-Seidel Iteration

C Calculate exact solutions
6   DO i=1,II
    DO j=0,JJ-1
    DO k=1,KK-1
    t1_exact(i,j,k)=c1*cos(pi*gamma(i))*sin(phi(j))
    & *(1.0-u(k)*u(k))*exp(-pi*pi*dt*(n+1.0))
    t2_exact(i,j,k)=c2*cos(pi*gamma(i))*sin(phi(j))
    & *(1.0-u(k)*u(k))*exp(-pi*pi*dt*(n+1.0))
    t3_exact(i,j,k)=c3*cos(pi*gamma(i))*sin(phi(j))
    & *(1.0-u(k)*u(k))*exp(-pi*pi*dt*(n+1.0))
    ENDDO
    ENDDO
    ENDDO
C Calculate max err
    err_max=0.0
    DO i=1,II
    DO j=0,JJ-1
    DO k=1,KK-1
    err=abs(t1newgs(i,j,k)-t1_exact(i,j,k))
    IF(err.GT.err_max)THEN
    err_max=err
    ENDIF
    err=abs(t2newgs(i,j,k)-t2_exact(i,j,k))
    IF(err.GT.err_max)THEN
    err_max=err
    ENDIF
    err=abs(t3newgs(i,j,k)-t3_exact(i,j,k))
    IF(err.GT.err_max)THEN
    err_max=err
    ENDIF
    ENDDO
    ENDDO
    ENDDO
C   PRINT *, max_err

C Calculate L2-err
    DO i=1,II
    DO j=0,JJ-1
    DO k=1,KK-1
    errorT1(i,j,k)=abs(t1newgs(i,j,k)-t1_exact(i,j,k))
    errorT2(i,j,k)=abs(t2newgs(i,j,k)-t2_exact(i,j,k))
    errorT3(i,j,k)=abs(t3newgs(i,j,k)-t3_exact(i,j,k))
    ENDDO
    ENDDO
    ENDDO

    temp1=0.0
    temp2=0.0
    temp3=0.0
    temp4=0.0
    error_max(n)=0.0
    DO i=1,II
    DO j=0,JJ-1
    DO k=1,KK-1
    temp1=temp1+errorT1(i,j,k)*errorT1(i,j,k)
    temp2=temp2+errorT2(i,j,k)*errorT2(i,j,k)
    temp3=temp3+errorT3(i,j,k)*errorT3(i,j,k)
    ENDDO
    ENDDO
    ENDDO
    temp4=temp1+temp2+temp3
    error_max(n)=sqrt(dgamma*dphi*du*temp4)
    PRINT *,n, error_max(n)

C Next time iteration
    n=n+1
    IF(n.EQ.NN)GOTO 7

    DO i=1,II
    DO j=-1,JJ
    DO k=0,KK
    t1(i,j,k)=t1newgs(i,j,k)
    t2(i,j,k)=t2newgs(i,j,k)
    t3(i,j,k)=t3newgs(i,j,k)
    ENDDO
    ENDDO
    ENDDO

    GOTO 1

C Output
7   OPEN(unit=77,file='N=50ar3_I=11_o2.dat')
    DO n=1,NN-1
    WRITE(77,1000) n*dt,error_max(n)
    ENDDO
1000 FORMAT(f18.6, e18.10)
    END

```

### 3. SOURCE CODE FOR 3D SECOND IMPROVED CN SCHEME

C 2-time level 3D second improved CN  
 C nsystem44.f  
 C Jan. 2010

```

    DIMENSION t1(0:50,-1:110,0:110),t2(0:50,-1:110,0:110)
    DIMENSION t3(0:50,-
1:110,0:110),gamma(0:50),gammah(0:50)
    DIMENSION phi(-1:110),u(0:110),uh(0:110)
    DIMENSION t1_exact(0:50,-
1:110,0:110),t2_exact(0:50,-1:110,0:110)
    DIMENSION t3_exact(0:50,-1:110,0:110),t1oldgs(0:50,-
1:110,0:110)
    DIMENSION t1newgs(0:50,-1:110,0:110),t2oldgs(0:50,-
1:110,0:110)
    DIMENSION t2newgs(0:50,-1:110,0:110),t3oldgs(0:50,-
1:110,0:110)
    DIMENSION t3newgs(0:50,-1:110,0:110),t1oldj(0:50,-
1:110,0:110)
    DIMENSION t1newj(0:50,-1:110,0:110),t2oldj(0:50,-
1:110,0:110)
    DIMENSION t2newj(0:50,-1:110,0:110),t3oldj(0:50,-
1:110,0:110)
    DIMENSION t3newj(0:50,-1:110,0:110),errorT1(0:50,-
1:110,0:110)
    DIMENSION errorT2(0:50,-1:110,0:110),errorT3(0:50,-
1:110,0:110)
    DIMENSION error_max(0:5010)
    DOUBLE PRECISION
    t1,t2,t3,Q1dt,Q2dt,Q3dt,d1,d2,d3,abc,c1,c2,c3
    DOUBLE PRECISION
    t1oldgs,t1newgs,t2oldgs,t2newgs,t3oldgs,t3newgs
    DOUBLE PRECISION
    t1oldj,t1newj,t2oldj,t2newj,t3oldj,t3newj
    DOUBLE PRECISION
    t1_exact,t2_exact,t3_exact,abl,abr
    DOUBLE PRECISION
    errorT1,errorT2,errorT3,error_max
    DOUBLE PRECISION
    error_maxj,error_maxgs,errj,errgs,err
    DOUBLE PRECISION err_max,tr,tp,ts,gamma,gammah
    DOUBLE PRECISION phi,u,uh,theta1,theta2,th,fl,f2,
    f3
    DOUBLE PRECISION dt,dgamma,dphi,du,pi,tolj,tolgs
    DOUBLE PRECISION
    cr1,cr2,cs,cp1,cp2,temp1,temp2,temp3,temp4
    DOUBLE PRECISION c11dt,c12dt,c13dt,c14dt,c15dt
    DOUBLE PRECISION c21dt,c22dt,c23dt,c24dt,c25dt
    DOUBLE PRECISION c31dt,c32dt,c33dt,c34dt

C value assignment
    dt=0.0001
    II=10
    JJ=60
    KK=60
    NN=1000
    pi=3.14159265358979323846
    theta1=1.0
    th=theta1+II
    theta2=(sqrt(4.0+3.0*th*(th-1.0))-1.0)/(3.0*th)
C the first order scheme
C   theta1=1.0
C   theta2=1.0
    dgamma=1.0/(II-1.0+theta1+theta2)
    dphi=2.0*pi/JJ
    du=2.0/KK

```

```

    tr=dt/(dgamma*dgamma)
    ts=dt/(dphi*dphi)
    tp=dt/(du*du)
    tolgs=1.0D-6
    tolj=1.0D-8
    c1=1.25
    c2=1.00
    c3=0.75

    DO i=0,II
    gamma(i)=(theta1+(i-1))*dgamma
    ENDDO
    DO i=0,II-1
    gammah(i)=gamma(i)+0.5*dgamma
    ENDDO
    DO j=0,II-1
    phi(j)=j*dphi
    ENDDO
    DO k=0,II-1
    u(k)=k*du-1.0
    ENDDO
    DO k=0,II-1
    uh(k)=u(k)+0.5*du
    ENDDO

    abl=1.0
    abr=gamma(II)*gamma(II)*theta2
    & /(gammah(II-1)*gammah(II-1)*(theta2/2.0+1.0/3.0))
C the first order scheme
C   abl=1.0
C   abr=1.0
C initial condition
    DO i=1,II
    DO j=0,II-1
    DO k=1,II-1
    t1(i,j,k)=c1*(cos(pi*gamma(i))-1.0)*sin(phi(j))*(1.0-
u(k)*u(k))
    t2(i,j,k)=c2*(cos(pi*gamma(i))-1.0)*sin(phi(j))*(1.0-
u(k)*u(k))
    t3(i,j,k)=c3*(cos(pi*gamma(i))-1.0)*sin(phi(j))*(1.0-
u(k)*u(k))
    ENDDO
    ENDDO
    ENDDO

C boundary condition
    DO i=1,II
    DO j=0,II-1
    t1(i,j,0)=0.0
    t2(i,j,0)=0.0
    t3(i,j,0)=0.0
    t1(i,j,KK)=0.0
    t2(i,j,KK)=0.0
    t3(i,j,KK)=0.0
    ENDDO
    ENDDO

    DO i=1,II
    DO k=0,II-1
    t1(i,-1,k)=t1(i,II-1,k)
    t2(i,-1,k)=t2(i,II-1,k)
    t3(i,-1,k)=t3(i,II-1,k)
    t1(i,II,k)=t1(i,0,k)
    t2(i,II,k)=t2(i,0,k)
    t3(i,II,k)=t3(i,0,k)
    ENDDO
    ENDDO

    fl=0.0
    DO j=0,II-1

```

```

DO k=0, KK-1
f1=f1+t1(1,j,k)
ENDDO
ENDDO
DO j=0, JJ-1
DO k=0, KK-1
t1(0,j,k)=f1/(JJ*KK)
ENDDO
ENDDO

f2=0.0
DO j=0, JJ-1
DO k=0, KK-1
f2=f2+t2(1,j,k)
ENDDO
ENDDO
DO j=0, JJ-1
DO k=0, KK-1
t2(0,j,k)=f2/(JJ*KK)
ENDDO
ENDDO

f3=0.0
DO j=0, JJ-1
DO k=0, KK-1
f3=f3+t3(1,j,k)
ENDDO
ENDDO
DO j=0, JJ-1
DO k=0, KK-1
t3(0,j,k)=f3/(JJ*KK)
ENDDO
ENDDO

C Begin time iteration
n=0
C Begin Gauss-Seidel Iteration
1 DO i=0, II
DO j=-1, JJ
DO k=0, KK
t1oldgs(i,j,k)=t1(i,j,k)
t2oldgs(i,j,k)=t2(i,j,k)
t3oldgs(i,j,k)=t3(i,j,k)
ENDDO
ENDDO
ENDDO

C Jacobi for T1
C initial condition for Jacobi
2 DO i=0, II
DO j=-1, JJ
DO k=0, KK
t1oldj(i,j,k)=t1oldgs(i,j,k)
ENDDO
ENDDO
ENDDO

C RHS
3 DO i=1, II-1
DO j=0, JJ-1
DO k=1, KK-1
c11dt=dt*2.0*pi*pi*exp(-
pi*pi*dt*(n+0.5))*cos(pi*gamma(i))
& *sin(phi(j))*(1.0-
u(k)*u(k))*gamma(i)*gamma(i)*(1.0-u(k)*u(k))

c12dt=dt*5.0*pi*exp(-
pi*pi*dt*(n+0.5))*sin(pi*gamma(ii))
& *sin(phi(j))*(1.0-u(k)*u(k))*gamma(ii)*(1.0-u(k)*u(k))

c13dt=-dt*6.0*c1*exp(-
pi*pi*dt*(n+0.5))*cos(pi*gamma(ii))
& *sin(phi(j))*(2.0*u(k)*u(k)-1.0)*(1.0-u(k)*u(k))

c14dt=dt*6.0*c1*exp(-pi*pi*dt*(n+0.5))
& *sin(phi(j))*(2.0*u(k)*u(k)-1.0)*(1.0-u(k)*u(k))

c15dt=dt*0.5*pi*pi*exp(-pi*pi*dt*(n+0.5))
& *sin(phi(j))*(1.0-
u(k)*u(k))*gamma(ii)*gamma(ii)*(1.0-u(k)*u(k))

Q1dt=c11dt+c12dt+c13dt+c14dt+c15dt

cr2=gammah(ii-1)*gammah(ii-1)*tr*(1.0-u(k)*u(k))
cs=ts

c11dt=dt*2.0*pi*pi*exp(-
pi*pi*dt*(n+0.5))*cos(pi*gamma(ii))
& *sin(phi(j))*(1.0-
u(k)*u(k))*gamma(ii)*gamma(ii)*(1.0-u(k)*u(k))

c12dt=dt*5.0*pi*exp(-
pi*pi*dt*(n+0.5))*sin(pi*gamma(ii))
& *sin(phi(j))*(1.0-u(k)*u(k))*gamma(ii)*(1.0-u(k)*u(k))

c13dt=-dt*6.0*c1*exp(-
pi*pi*dt*(n+0.5))*cos(pi*gamma(ii))
& *sin(phi(j))*(2.0*u(k)*u(k)-1.0)*(1.0-u(k)*u(k))

c14dt=dt*6.0*c1*exp(-pi*pi*dt*(n+0.5))
& *sin(phi(j))*(2.0*u(k)*u(k)-1.0)*(1.0-u(k)*u(k))

c15dt=dt*0.5*pi*pi*exp(-pi*pi*dt*(n+0.5))
& *sin(phi(j))*(1.0-
u(k)*u(k))*gamma(ii)*gamma(ii)*(1.0-u(k)*u(k))

Q1dt=c11dt+c12dt+c13dt+c14dt+c15dt

cr1=gammah(i)*gammah(i)*tr*(1.0-u(k)*u(k))
cr2=gammah(i-1)*gammah(i-1)*tr*(1.0-u(k)*u(k))
cs=ts
cp1=(1.0-uh(k)*uh(k))*tp*(1.0-u(k)*u(k))
cp2=(1.0-uh(k-1)*uh(k-1))*tp*(1.0-u(k)*u(k))

abc=gamma(i)*gamma(i)*(1.0-
u(k)*u(k))+cr1+cr2+2.0*cs
& +cp1+cp2+dt*pi*pi*gamma(i)*gamma(i)*(1.0-
u(k)*u(k))
d1=cr1*t1oldj(i+1,j,k)+cr1*t1(i+1,j,k)
& +(gamma(i)*gamma(i)*(1.0-u(k)*u(k))-cr1-cr2-2.0*cs-
cp1-cp2
& -dt*pi*pi*gamma(i)*gamma(i)*(1.0-
u(k)*u(k)))*t1(i,j,k)
& +cr2*t1oldj(i-1,j,k)+cr2*t1(i-1,j,k)
& +cs*t1oldj(i,j+1,k)+cs*t1(i,j+1,k)
& +cs*t1oldj(i,j-1,k)+cs*t1(i,j-1,k)
& +cp1*t1oldj(i,j,k+1)+cp1*t1(i,j,k+1)
& +cp2*t1oldj(i,j,k-1)+cp2*t1(i,j,k-1)
& +dt*pi*pi*(t2oldgs(i,j,k)+t2(i,j,k))
& *gamma(i)*gamma(i)*(1.0-u(k)*u(k))/2.0
& +dt*pi*pi*(t3oldgs(i,j,k)+t3(i,j,k))
& *gamma(i)*gamma(i)*(1.0-u(k)*u(k))/2.0+Q1dt

t1newj(i,j,k)=d1/abc
ENDDO
ENDDO
ENDDO

DO j=0, JJ-1
DO k=1, KK-1
c11dt=dt*2.0*pi*pi*exp(-
pi*pi*dt*(n+0.5))*cos(pi*gamma(ii))
& *sin(phi(j))*(1.0-
u(k)*u(k))*gamma(ii)*gamma(ii)*(1.0-u(k)*u(k))

c12dt=dt*5.0*pi*exp(-
pi*pi*dt*(n+0.5))*sin(pi*gamma(ii))
& *sin(phi(j))*(1.0-u(k)*u(k))*gamma(ii)*(1.0-u(k)*u(k))

c13dt=-dt*6.0*c1*exp(-
pi*pi*dt*(n+0.5))*cos(pi*gamma(ii))
& *sin(phi(j))*(2.0*u(k)*u(k)-1.0)*(1.0-u(k)*u(k))

c14dt=dt*6.0*c1*exp(-pi*pi*dt*(n+0.5))
& *sin(phi(j))*(2.0*u(k)*u(k)-1.0)*(1.0-u(k)*u(k))

c15dt=dt*0.5*pi*pi*exp(-pi*pi*dt*(n+0.5))
& *sin(phi(j))*(1.0-
u(k)*u(k))*gamma(ii)*gamma(ii)*(1.0-u(k)*u(k))

Q1dt=c11dt+c12dt+c13dt+c14dt+c15dt

cr2=gammah(ii-1)*gammah(ii-1)*tr*(1.0-u(k)*u(k))
cs=ts

```

```

cp1=(1.0-uh(k)*uh(k))*tp*(1.0-u(k)*u(k))
cp2=(1.0-uh(k-1)*uh(k-1))*tp*(1.0-u(k)*u(k))

abc=gamma(II)*gamma(II)*(1.0-
u(k)*u(k))+abr*cr2+2.0*cs+cp1+cp2
& +dt*pi*pi*gamma(II)*gamma(II)*(1.0-u(k)*u(k))
d1=abr*cr2*t1oldj(II-1,j,k)+abr*cr2*t1(II-1,j,k)
& +(gamma(II)*gamma(II)*(1.0-u(k)*u(k))-abr*cr2-
2.0*cs-cp1-cp2
& -pi*pi*dt*gamma(II)*gamma(II)*(1.0-
u(k)*u(k))*t1(II,j,k)
& +cs*t1oldj(II,j+1,k)+cs*t1(II,j+1,k)
& +cs*t1oldj(II,j-1,k)+cs*t1(II,j-1,k)
& +cp1*t1oldj(II,j,k+1)+cp1*t1(II,j,k+1)
& +cp2*t1oldj(II,j,k-1)+cp2*t1(II,j,k-1)
& +dt*pi*pi*(t2oldgs(II,j,k)+t2(II,j,k))
& *gamma(II)*gamma(II)*(1.0-u(k)*u(k))/2.0
& +dt*pi*pi*(t3oldgs(II,j,k)+t3(II,j,k))
& *gamma(II)*gamma(II)*(1.0-u(k)*u(k))/2.0+Q1dt

t1newj(II,j,k)=d1/abc
ENDDO
ENDDO

C boundary condition
DO i=1,II
DO j=0,JJ-1
t1newj(i,j,0)=0.0
t1newj(i,j,KK)=0.0
ENDDO
ENDDO

DO i=1,II
DO k=0,KK
t1newj(i,-1,k)=t1newj(i,JJ-1,k)
t1newj(i,JJ,k)=t1newj(i,0,k)
ENDDO
ENDDO

C update
f1=0.0
DO j=0,JJ-1
DO k=0,KK-1
f1=f1+t1newj(1,j,k)+t1(1,j,k)
ENDDO
ENDDO

DO j=0,JJ-1
DO k=1,KK-1
abc=1.0+6.0*dt/(dgamma*dgamma)+dt*pi*pi

d1=(1.0-6.0*dt/(dgamma*dgamma)-dt*pi*pi)*t1(0,j,k)
& +dt*3.0*du*f1/(JJ*dgamma*dgamma)
& +dt*pi*pi*(t2oldgs(0,j,k)+t2(0,j,k))/2.0
& +dt*pi*pi*(t3oldgs(0,j,k)+t3(0,j,k))/2.0

t1newj(0,j,k)=d1/abc
ENDDO
ENDDO

C error for Jacobi
error_maxj=0.0
DO i=1,II
DO j=0,JJ-1
DO k=1,KK-1
errj=abs(t1newj(i,j,k)-t1oldj(i,j,k))
IF(errj.GT.error_maxj)THEN
error_maxj=errj

```

```

ENDIF
ENDDO
ENDDO
ENDDO

```

```

C update for Jacobi

```

```

DO i=0,II
DO j=-1,JJ
DO k=0,KK
t1oldj(i,j,k)=t1newj(i,j,k)
ENDDO
ENDDO
ENDDO

```

```

C print *, "I",error_maxj
IF(error_maxj.GT.tolj)GOTO 3

```

```

C update from Jacobi to Gauss-Seidel

```

```

DO i=0,II
DO j=-1,JJ
DO k=0,KK
t1newgs(i,j,k)=t1newj(i,j,k)
ENDDO
ENDDO
ENDDO

```

```

C Jacobi for T2

```

```

C initial condition for Jacobi

```

```

DO i=0,II
DO j=-1,JJ
DO k=0,KK
t2oldj(i,j,k)=t2oldgs(i,j,k)
ENDDO
ENDDO
ENDDO

```

```

4 DO i=1,II-1

```

```

DO j=0,JJ-1
DO k=1,KK-1

```

```

c21dt=dt*pi*pi*exp(-
pi*pi*dt*(n+0.5))*cos(pi*gamma(i))
& *sin(phi(j))*(1.0-
u(k)*u(k))*gamma(i)*gamma(i)*(1.0-u(k)*u(k))

```

```

c22dt=dt*4.0*pi*exp(-
pi*pi*dt*(n+0.5))*sin(pi*gamma(i))
& *sin(phi(j))*(1.0-u(k)*u(k))*gamma(i)*(1.0-u(k)*u(k))

```

```

c23dt=-dt*6.0*c2*exp(-
pi*pi*dt*(n+0.5))*cos(pi*gamma(i))
& *sin(phi(j))*(2.0*u(k)*u(k)-1.0)*(1.0-u(k)*u(k))

```

```

c24dt=dt*6.0*c2*exp(-pi*pi*dt*(n+0.5))
& *sin(phi(j))*(2.0*u(k)*u(k)-1.0)*(1.0-u(k)*u(k))

```

```

c25dt=dt*pi*pi*exp(-pi*pi*dt*(n+0.5))
& *sin(phi(j))*(1.0-
u(k)*u(k))*gamma(i)*gamma(i)*(1.0-u(k)*u(k))

```

```

Q2dt=c21dt+c22dt+c23dt+c24dt+c25dt

```

```

cr1=gammah(i)*gammah(i)*tr*(1.0-u(k)*u(k))
cr2=gammah(i-1)*gammah(i-1)*tr*(1.0-u(k)*u(k))
cs=ts
cp1=(1.0-uh(k)*uh(k))*tp*(1.0-u(k)*u(k))
cp2=(1.0-uh(k-1)*uh(k-1))*tp*(1.0-u(k)*u(k))

```

```

abc=gamma(i)*gamma(i)*(1.0-
u(k)*u(k))+cr1+cr2+2.0*cs+cp1+cp2
& +dt*pi*pi*gamma(i)*gamma(i)*(1.0-u(k)*u(k))
d2=cr1*t2oldj(i+1,j,k)+cr1*t2(i+1,j,k)

```

```

& +(gamma(i)*gamma(i)*(1.0-u(k)*u(k))-cr1-cr2-2.0*cs-
cp1-cp2
& -dt*pi*pi*gamma(i)*gamma(i)*(1.0-
u(k)*u(k))*t2(i,j,k)
& +cr2*t2oldj(i-1,j,k)+cr2*t2(i-1,j,k)
& +cs*t2oldj(i,j+1,k)+cs*t2(i,j+1,k)
& +cs*t2oldj(i,j-1,k)+cs*t2(i,j-1,k)
& +cp1*t2oldj(i,j,k+1)+cp1*t2(i,j,k+1)
& +cp2*t2oldj(i,j,k-1)+cp2*t2(i,j,k-1)
& +dt*pi*pi*(t1newgs(i,j,k)+t1(i,j,k))
& *gamma(i)*gamma(i)*(1.0-u(k)*u(k))/2.0
& +dt*pi*pi*(t3oldgs(i,j,k)+t3(i,j,k))
& *gamma(i)*gamma(i)*(1.0-u(k)*u(k))/2.0+Q2dt

t2newj(i,j,k)=d2/abc
ENDDO
ENDDO
ENDDO

DO j=0, JJ-1
DO k=1, KK-1
c21dt=dt*pi*pi*exp(-
pi*pi*dt*(n+0.5))*cos(pi*gamma(II))
& *sin(phi(j))*(1.0-
u(k)*u(k))*gamma(II)*gamma(II)*(1.0-u(k)*u(k))

c22dt=dt*4.0*pi*exp(-
pi*pi*dt*(n+0.5))*sin(pi*gamma(II))
& *sin(phi(j))*(1.0-u(k)*u(k))*gamma(II)*(1.0-u(k)*u(k))

c23dt=-dt*6.0*c2*exp(-
pi*pi*dt*(n+0.5))*cos(pi*gamma(II))
& *sin(phi(j))*(2.0*u(k)*u(k)-1.0)*(1.0-u(k)*u(k))

c24dt=dt*6.0*c2*exp(-pi*pi*dt*(n+0.5))
& *sin(phi(j))*(2.0*u(k)*u(k)-1.0)*(1.0-u(k)*u(k))

c25dt=dt*pi*pi*exp(-pi*pi*dt*(n+0.5))
& *sin(phi(j))*(1.0-
u(k)*u(k))*gamma(II)*gamma(II)*(1.0-u(k)*u(k))

Q2dt=c21dt+c22dt+c23dt+c24dt+c25dt

cr2=gammah(II-1)*gammah(II-1)*tr*(1.0-u(k)*u(k))
cs=ts
cp1=(1.0-uh(k)*uh(k))*tp*(1.0-u(k)*u(k))
cp2=(1.0-uh(k-1)*uh(k-1))*tp*(1.0-u(k)*u(k))

abc=gamma(II)*gamma(II)*(1.0-
u(k)*u(k))+abr*cr2+2.0*cs+cp1+cp2
& +dt*pi*pi*gamma(II)*gamma(II)*(1.0-u(k)*u(k))
d2=abr*cr2*t2oldj(II-1,j,k)+abr*cr2*t2(II-1,j,k)
& +(gamma(II)*gamma(II)*(1.0-u(k)*u(k))-abr*cr2-
2.0*cs-cp1-cp2
& -dt*pi*pi*gamma(II)*gamma(II)*(1.0-
u(k)*u(k))*t2(II,j,k)
& +cs*t2oldj(II,j+1,k)+cs*t2(II,j+1,k)
& +cs*t2oldj(II,j-1,k)+cs*t2(II,j-1,k)
& +cp1*t2oldj(II,j,k+1)+cp1*t2(II,j,k+1)
& +cp2*t2oldj(II,j,k-1)+cp2*t2(II,j,k-1)
& +dt*pi*pi*(t1newgs(II,j,k)+t1(II,j,k))
& *gamma(II)*gamma(II)*(1.0-u(k)*u(k))/2.0
& +dt*pi*pi*(t3oldgs(II,j,k)+t3(II,j,k))
& *gamma(II)*gamma(II)*(1.0-u(k)*u(k))/2.0+Q2dt

t2newj(II,j,k)=d2/abc
ENDDO
ENDDO

C boundary condition
DO i=1,II
DO j=0, JJ-1
t2newj(i,j,0)=0.0
t2newj(i,j, KK)=0.0
ENDDO
ENDDO

DO i=1,II
DO k=0, KK
t2newj(i,-1,k)=t2newj(i, JJ-1,k)
t2newj(i, JJ,k)=t2newj(i,0,k)
ENDDO
ENDDO

C update
f2=0.0
DO j=0, JJ-1
DO k=0, KK-1
f2=f2+t2newj(1,j,k)+t2(1,j,k)
ENDDO
ENDDO

DO j=0, JJ-1
DO k=1, KK-1
abc=1.0+6.0*dt/(dgamma*dgamma)+dt*pi*pi

d2=(1.0-6.0*dt/(dgamma*dgamma)-dt*pi*pi)*t2(0,j,k)
& +dt*3.0*du*f2/(JJ*dgamma*dgamma)
& +dt*pi*pi*(t1newgs(0,j,k)+t1(0,j,k))/2.0
& +dt*pi*pi*(t3oldgs(0,j,k)+t3(0,j,k))/2.0

t2newj(0,j,k)=d2/abc
ENDDO
ENDDO

C error for Jacobi
error_maxj=0.0
DO i=1,II
DO j=0, JJ-1
DO k=1, KK-1
errj=abs(t2newj(i,j,k)-t2oldj(i,j,k))
IF(errj.GT.error_maxj)THEN
error_maxj=errj
ENDIF
ENDDO
ENDDO
ENDDO

C update for Jacobi
DO i=0,II
DO j=-1, JJ
DO k=0, KK
t2oldj(i,j,k)=t2newj(i,j,k)
ENDDO
ENDDO
ENDDO

C print *, "2", error_maxj
IF(error_maxj.GT.tolj)GOTO 4

C update from Jacobi to Gauss-Seidel
DO i=0,II
DO j=-1, JJ
DO k=0, KK
t2newgs(i,j,k)=t2newj(i,j,k)
ENDDO
ENDDO
ENDDO

C Jacobi for T3

```

```

C initial condition for Jacobi
DO i=0,II
DO j=-1,JJ
DO k=0,KK
t3oldj(i,j,k)=t3oldgs(i,j,k)
ENDDO
ENDDO
ENDDO

5 DO i=1,II-1
DO j=0,JJ-1
DO k=1,KK-1
c31dt=dt*3.0*pi*exp(-
pi*pi*dt*(n+0.5))*sin(pi*gamma(i))
& *sin(phi(j))*(1.0-u(k)*u(k))*gamma(i)*(1.0-u(k)*u(k))

c32dt=-dt*6.0*c3*exp(-
pi*pi*dt*(n+0.5))*cos(pi*gamma(i))
& *sin(phi(j))*(2.0*u(k)*u(k)-1.0)*(1.0-u(k)*u(k))

c33dt=dt*6.0*c3*exp(-pi*pi*dt*(n+0.5))
& *sin(phi(j))*(2.0*u(k)*u(k)-1.0)*(1.0-u(k)*u(k))

c34dt=dt*1.5*pi*pi*exp(-pi*pi*dt*(n+0.5))
& *sin(phi(j))*(1.0-
u(k)*u(k))*gamma(i)*gamma(i)*(1.0-u(k)*u(k))

Q3dt=c31dt+c32dt+c33dt+c34dt

cr1=gammah(i)*gammah(i)*tr*(1.0-u(k)*u(k))
cr2=gammah(i-1)*gammah(i-1)*tr*(1.0-u(k)*u(k))
cs=ts
cp1=(1.0-uh(k)*uh(k))*tp*(1.0-u(k)*u(k))
cp2=(1.0-uh(k-1)*uh(k-1))*tp*(1.0-u(k)*u(k))

abc=gamma(i)*gamma(i)*(1.0-
u(k)*u(k))+cr1+cr2+2.0*cs+cp1+cp2
& +dt*pi*pi*gamma(i)*gamma(i)*(1.0-u(k)*u(k))
d3=cr1*t3oldj(i+1,j,k)+cr1*t3(i+1,j,k)
& +(gamma(i)*gamma(i)*(1.0-u(k)*u(k))-cr1-cr2-2.0*cs-
cp1-cp2
& -pi*pi*dt*gamma(i)*gamma(i)*(1.0-
u(k)*u(k)))*t3(i,j,k)
& +cr2*t3oldj(i-1,j,k)+cr2*t3(i-1,j,k)
& +cs*t3oldj(i,j+1,k)+cs*t3(i,j+1,k)
& +cs*t3oldj(i,j-1,k)+cs*t3(i,j-1,k)
& +cp1*t3oldj(i,j,k+1)+cp1*t3(i,j,k+1)
& +cp2*t3oldj(i,j,k-1)+cp2*t3(i,j,k-1)
& +dt*pi*pi*(t1newgs(i,j,k)+t1(i,j,k))
& *gamma(i)*gamma(i)*(1.0-u(k)*u(k))/2.0
& +dt*pi*pi*(t2newgs(i,j,k)+t2(i,j,k))
& *gamma(i)*gamma(i)*(1.0-u(k)*u(k))/2.0+Q3dt

t3newj(i,j,k)=d3/abc
ENDDO
ENDDO
ENDDO

DO j=0,JJ-1
DO k=1,KK-1
c31dt=dt*3.0*pi*exp(-
pi*pi*dt*(n+0.5))*sin(pi*gamma(II))
& *sin(phi(j))*(1.0-u(k)*u(k))*gamma(II)*(1.0-u(k)*u(k))

c32dt=-dt*6.0*c3*exp(-
pi*pi*dt*(n+0.5))*cos(pi*gamma(II))
& *sin(phi(j))*(2.0*u(k)*u(k)-1.0)*(1.0-u(k)*u(k))

c33dt=dt*6.0*c3*exp(-pi*pi*dt*(n+0.5))
& *sin(phi(j))*(2.0*u(k)*u(k)-1.0)*(1.0-u(k)*u(k))

c34dt=dt*1.5*pi*pi*exp(-pi*pi*dt*(n+0.5))
& *sin(phi(j))*(2.0*u(k)*u(k)-1.0)*(1.0-u(k)*u(k))

Q3dt=c31dt+c32dt+c33dt+c34dt

cr2=gammah(II-1)*gammah(II-1)*tr*(1.0-u(k)*u(k))
cs=ts
cp1=(1.0-uh(k)*uh(k))*tp*(1.0-u(k)*u(k))
cp2=(1.0-uh(k-1)*uh(k-1))*tp*(1.0-u(k)*u(k))

abc=gamma(II)*gamma(II)*(1.0-
u(k)*u(k))+abr*cr2+2.0*cs+cp1+cp2
& +dt*pi*pi*gamma(II)*gamma(II)*(1.0-u(k)*u(k))
d3=abr*cr2*t3oldj(II-1,j,k)+abr*cr2*t3(II-1,j,k)
& +(gamma(II)*gamma(II)*(1.0-u(k)*u(k))-abr*cr2-
2.0*cs-cp1-cp2
& -dt*pi*pi*gamma(II)*gamma(II)*(1.0-
u(k)*u(k)))*t3(II,j,k)
& +cs*t3oldj(II,j+1,k)+cs*t3(II,j+1,k)
& +cs*t3oldj(II,j-1,k)+cs*t3(II,j-1,k)
& +cp1*t3oldj(II,j,k+1)+cp1*t3(II,j,k+1)
& +cp2*t3oldj(II,j,k-1)+cp2*t3(II,j,k-1)
& +dt*pi*pi*(t1newgs(II,j,k)+t1(II,j,k))
& *gamma(II)*gamma(II)*(1.0-u(k)*u(k))/2.0
& +dt*pi*pi*(t2newgs(II,j,k)+t2(II,j,k))
& *gamma(II)*gamma(II)*(1.0-u(k)*u(k))/2.0+Q3dt

t3newj(II,j,k)=d3/abc
ENDDO
ENDDO

C boundary condition
DO i=1,II
DO j=0,JJ-1
t3newj(i,j,0)=0.0
t3newj(i,j,KK)=0.0
ENDDO
ENDDO

DO i=1,II
DO k=0,KK
t3newj(i,-1,k)=t3newj(i,JJ-1,k)
t3newj(i,JJ,k)=t3newj(i,0,k)
ENDDO
ENDDO

C update
f3=0.0
DO j=0,JJ-1
DO k=0,KK-1
f3=f3+t3newj(1,j,k)+t3(1,j,k)
ENDDO
ENDDO

DO j=0,JJ-1
DO k=1,KK-1
abc=1.0+6.0*dt/(dgamma*dgamma)+dt*pi*pi

d3=(1.0-6.0*dt/(dgamma*dgamma)-dt*pi*pi)*t3(0,j,k)
& +dt*3.0*du*f3/(JJ*dgamma*dgamma)
& +dt*pi*pi*(t1newgs(0,j,k)+t1(0,j,k))/2.0
& +dt*pi*pi*(t2newgs(0,j,k)+t2(0,j,k))/2.0

t3newj(0,j,k)=d3/abc
ENDDO
ENDDO

```

```

C error for Jacobi
  error_maxj=0.0
  DO i=1,II
  DO j=0,JJ-1
  DO k=1,KK-1
  errj=abs(t3newj(i,j,k)-t3oldj(i,j,k))
  IF(errj.GT.error_maxj)THEN
    error_maxj=errj
 ENDIF
  ENDDO
  ENDDO
  ENDDO

C update for Jacobi
  DO i=0,II
  DO j=-1,JJ
  DO k=0,KK
  t3oldj(i,j,k)=t3newj(i,j,k)
  ENDDO
  ENDDO
  ENDDO

C   print *, "3",error_maxj
  IF(error_maxj.GT.tolj)GOTO 5

C update from Jacobi to Gauss-Seidel
  DO i=0,II
  DO j=-1,JJ
  DO k=0,KK
  t3newgs(i,j,k)=t3newj(i,j,k)
  ENDDO
  ENDDO
  ENDDO

C calculate err for Gauss-Seidel
  error_maxgs=0.0
  DO i=1,II
  DO j=0,JJ-1
  DO k=1,KK-1
  errgs=abs(t1newgs(i,j,k)-t1oldgs(i,j,k))
  IF(errgs.GT.error_maxgs)THEN
    error_maxgs=errgs
 ENDIF
  errgs=abs(t2newgs(i,j,k)-t2oldgs(i,j,k))
  IF(errgs.GT.error_maxgs)THEN
    error_maxgs=errgs
 ENDIF
  errgs=abs(t3newgs(i,j,k)-t3oldgs(i,j,k))
  IF(errgs.GT.error_maxgs)THEN
    error_maxgs=errgs
 ENDIF
  ENDDO
  ENDDO
  ENDDO
  IF(error_maxgs.LE.tolgs)GOTO 6
C   print *, max_err
  DO i=0,II
  DO j=-1,JJ
  DO k=0,KK
  t1oldgs(i,j,k)=t1newgs(i,j,k)
  t2oldgs(i,j,k)=t2newgs(i,j,k)
  t3oldgs(i,j,k)=t3newgs(i,j,k)
  ENDDO
  ENDDO
  ENDDO
  GOTO 2
C End Gauss-Seidel Iteration
C Calculate exact solutions
6  DO i=1,II
  DO j=0,JJ-1
  DO k=1,KK-1
  t1_exact(i,j,k)=c1*(cos(pi*gamma(i))-1.0)*sin(phi(j))
  &   *(1.0-u(k)*u(k))*exp(-pi*pi*dt*(n+1.0))
  t2_exact(i,j,k)=c2*(cos(pi*gamma(i))-1.0)*sin(phi(j))
  &   *(1.0-u(k)*u(k))*exp(-pi*pi*dt*(n+1.0))
  t3_exact(i,j,k)=c3*(cos(pi*gamma(i))-1.0)*sin(phi(j))
  &   *(1.0-u(k)*u(k))*exp(-pi*pi*dt*(n+1.0))
  ENDDO
  ENDDO
  ENDDO
C Calculate max err
  err_max=0.0
  DO i=1,II
  DO j=0,JJ-1
  DO k=1,KK-1
  err=abs(t1newgs(i,j,k)-t1_exact(i,j,k))
  IF(err.GT.err_max)THEN
    err_max=err
 ENDIF
  err=abs(t2newgs(i,j,k)-t2_exact(i,j,k))
  IF(err.GT.err_max)THEN
    err_max=err
 ENDIF
  err=abs(t3newgs(i,j,k)-t3_exact(i,j,k))
  IF(err.GT.err_max)THEN
    err_max=err
 ENDIF
  ENDDO
  ENDDO
  ENDDO
C   PRINT *, max_err

C Calculate L2-err
  DO i=1,II
  DO j=0,JJ-1
  DO k=1,KK-1
  errorT1(i,j,k)=abs(t1newgs(i,j,k)-t1_exact(i,j,k))
  errorT2(i,j,k)=abs(t2newgs(i,j,k)-t2_exact(i,j,k))
  errorT3(i,j,k)=abs(t3newgs(i,j,k)-t3_exact(i,j,k))
  ENDDO
  ENDDO
  ENDDO

  temp1=0.0
  temp2=0.0
  temp3=0.0
  temp4=0.0
  error_max(n)=0.0
  DO i=1,II
  DO j=0,JJ-1
  DO k=1,KK-1
  temp1=temp1+errorT1(i,j,k)*errorT1(i,j,k)
  temp2=temp2+errorT2(i,j,k)*errorT2(i,j,k)
  temp3=temp3+errorT3(i,j,k)*errorT3(i,j,k)
  ENDDO
  ENDDO
  ENDDO
  temp4=temp1+temp2+temp3
  error_max(n)=sqrt(dgamma*dphi*du*temp4)
  PRINT *,n, error_max(n)

C Next time iteration
  n=n+1
  IF(n.EQ.NN)GOTO 7

  DO i=0,II
  DO j=-1,JJ
  DO k=0,KK
  t1(i,j,k)=t1newgs(i,j,k)
  t2(i,j,k)=t2newgs(i,j,k)
  t3(i,j,k)=t3newgs(i,j,k)

```

```
ENDDO
ENDDO
ENDDO

GOTO 1

C Output
```

```
7 OPEN(unit=77,file='N=50ar3_I=40_o2.dat')
DO n=1,NN-1
WRITE(77,1000) n*dt,error_max(n)
ENDDO
CLOSE(77)
1000 FORMAT(f18.6, e18.10)
END
```

## REFERENCES

- [1] T. Q. Qiu and C. L. Tien, "Short-pulse laser heating on metals," *International Journal of Heat and Mass Transfer*, vol. 35, pp. 719-726, 1992.
- [2] T. Q. Qiu and C. L. Tien, "Heat transfer mechanisms during short-pulse laser heating of metals," *ASME Journal of Heat and Mass Transfer*, vol. 115, pp. 835-841, 1993.
- [3] D. Y. Tzou and W. Dai, "Thermal lagging in multi-carrier systems," *International Journal of Heat and Mass Transfer*, vol. 52, pp. 1206-1213, 2009.
- [4] W. Dai and D. Y. Tzou, "A fourth-order compact finite difference scheme for solving an  $N$ -carrier system with first-order method discretized Neumann boundary conditions," *Numerical Methods for Partial Differential Equations*, vol. 25, pp. 274-289, 2010.
- [5] W. Dai, F. Zhu and D. Y. Tzou, "A stable finite difference scheme for thermal analysis in an  $N$ -carrier system," *International Journal of Thermal Sciences*, vol. 48, pp. 1530-1541, 2009.
- [6] W. Dai, "A hyperbolic microscopic model and its numerical scheme for thermal analysis in an  $N$ -carrier system," *International Journal of Heat and Mass Transfer*, vol. 52, pp. 2379-2389, 2009.
- [7] W. Dai, "A compact LOD scheme for solving a 3D  $N$ -carrier system with first-order method discretized neumann boundary conditions," *Numerical Methods for Partial Differential Equations*, accepted.
- [8] K. Mitra, S. Kumar, A. Vedavarz and M. K. Moallemi, "Experimental evidence of hyperbolic heat conduction in processed meat," *Journal of Heat Transfer*, vol. 117, pp. 568-573, 1995.
- [9] M. G. Davies, *Building Heat Transfer*, Hoboken, NJ: John Wiley & Sons, 2004.
- [10] J. H. Lienhard IV and J. H. Lienhard V, *A Heat Transfer Textbook, 3d ed.* Cambridge MA: Phlogiston Press, 2003.

- [11] X. Du, "A Finite Difference Method for Solving Thermal Deformation in a 3D Micro-sphere Exposed to Ultrashort-pulsed Lasers," Ph.D. diss, Louisiana Tech University, 2007.
- [12] I. Kaba, "A Numerical Method to Solve the Two-step Parabolic Heat Transport Equations in a Microsphere Subjected to an Ultrafast Laser Pulse," Ph.D. diss, Louisiana Tech University, 2004.
- [13] T. Niu, "A Hyperbolic Two-step Model Based Finite Difference Method for Studying Thermal Deformation in a Micro Thin Film Heated by Ultrashort-pulsed Lasers," Ph.D. diss, Louisiana Tech University, 2007.
- [14] H. Wang, "A Finite Difference Method for Studying Thermal Deformation in Two-dimensional Micro Metal Thin Films Exposed to Ultrashort Pulsed Laser," Ph.D. diss, Louisiana Tech University, 2007.
- [15] P. Wang, "A Hyperbolic Two-step Model Based Finite Difference Method for Studying Thermal Deformation in 3D Micro Spheres Exposed to Ultrashort-pulsed Lasers," PhD diss, Louisiana Tech University, 2008.
- [16] S. Zhang, "A Finite Difference Method for Studying Thermal Deformation in 3D Thin Films Exposed to Ultrashort-pulsed Lasers," Ph.D. diss, Louisiana Tech University, 2008.
- [17] C. L. Tien, A. Majumdar and F. Gerner, *Microscale Energy Transfer*, Wastington, DC: Taylor & Francis, 1998.
- [18] M. A. Al-Nimr and S. Masoud, "Non-equilibrium laser heating of metal films," *ASME Journal of Heat Transfer*, vol. 119, pp. 188-190, 1997.
- [19] M. A. Al-Nimr, "Heat transfer mechanisms during laser heating of thin metal films," *International Journal of Thermophysics*, vol. 18, pp. 1257-1268, 1997.
- [20] M. A. Al-Nimr and V. S. Arpaci, "Picosecond thermal pulses in thin metal films," *Journal of Applied Physics*, vol. 85, pp. 2517-2521, 1999.
- [21] M. A. Al-Nimr and V. S. Arpaci, "The thermal behavior of thin metal films in the hyperbolic two-step model," *International Journal of Heat and Mass Transfer*, vol. 43, pp. 2021-2028, 2000.
- [22] M. A. Al-Nimr and M. Naji, "On the phase-lag effect on the non-equilibrium entropy production," *Micro Thermophysics Engineering*, vol. 4, pp. 231-243, 2000.
- [23] M. A. Al-Nimr, M. Naji and V. S. Arpaci, "Non-equilibrium entropy production in the effect of the dual-phase-lag heat conduction model," *ASME Journal of Heat Transfer*, vol. 122, pp. 217-222, 2000.

- [24] M. A. Al-Nimr and S. Kiwan, "Effect of thermal losses on the microscopic two-step heat conduction model," *International Journal of Heat and Mass Transfer*, vol. 44, pp. 1013-1018, 2001.
- [25] M. A. Al-Nimr, M. Header and M. Naji, "Use of the microscopic parabolic heat conduction model in place of macroscopic model validation criterion in harmonic boundary heating," *International Journal of Heat and Mass Transfer*, vol. 46, pp. 333-339, 2003.
- [26] S. I. Anisimov, B. L. Kapeliovich and T. L. Perel'man, "Electron emission from metal surface heat flux," *International Journal of Heat and Mass Transfer*, vol. 41, pp. 4063-4067, 1998.
- [27] J. K. Chen, J. E. Beraun and D. Y. Tzou, "A dual-phase-lag diffusion model for interfacial layer growth in metal matrix composites," *Journal of Material Science*, vol. 34, pp. 6183-6187, 1999.
- [28] J. K. Chen, J. E. Beraun and T. C. Carney, "A corrective smoothed particle method for boundary value problems in heat conduction," *International Journal of Numerical Methods in Engineering*, vol. 46, pp. 231-252, 1999.
- [29] J. K. Chen and J. E. Beraun, "A generalized smoothed particle hydromechanics method for nonlinear dynamic problems," *Computational Methods in Applied Mechanical Engineering*, vol. 190, pp. 225-239, 2000.
- [30] J. K. Chen, J. E. Beraun and D. Y. Tzou, "A dual-phase-lag diffusion model for predicting thin film growth," *Semiconductor Science Technology*, vol. 15, pp. 235-241, 2000.
- [31] W. Dai and R. Nassar, "A finite difference method for solving the heat transport equation at the micro-scale," *Numerical Methods for Partial Differential Equations*, vol. 15, pp. 697-708, 1999.
- [32] W. Dai and R. Nassar, "A compact finite difference scheme for solving a three dimensional heat transport equation in a thin film," *Numerical Methods for Partial Differential Equations*, vol. 16, pp. 441-458, 2000.
- [33] W. Dai and R. Nassar, "A compact finite difference scheme for solving a one-dimensional heat transport equation at the micro-scale," *Journal of Computational and Applied Mathematics*, vol. 132, pp. 431-441, 2001.
- [34] W. Dai and R. Nassar, "A finite difference method for solving 3D heat transfer equations in double layered thin film with micro-scale thickness and nonlinear interfacial conditions," *Numerical Heat Transfer, Part A*, vol. 39, pp. 21-33, 2001.

- [35] W. Dai and R. Nassar, "Compact ADI scheme for solving parabolic differential equations," *Numerical Methods for Partial Differential Equations*, vol. 18, pp. 129-142, 2002.
- [36] W. Dai and R. Nassar, "An unconditionally stable finite difference scheme for solving 3D heat transport equation in a sub-micro thin film," *Journal of Computational and Applied Mathematics*, vol. 145, pp. 247-260, 2002.
- [37] W. Dai and R. Nassar, "A three level finite difference scheme for solving micro heat transport equations with temperature-dependent thermal properties," *Numerical Heat Transfer, Part B*, vol. 45, pp. 509-523, 2003.
- [38] W. Dai, L. Shen and R. Nassar, "A convergent three-level finite difference scheme for solving a dual-phase-lagging heat transport equation in spherical coordinates," *Numerical Methods for Partial Differential Equations*, vol. 20, pp. 60-71, 2004.
- [39] W. Dai, G. Li, R. Nassar and L. Shen, "An unconditionally stable three level finite difference scheme for solving parabolic two-step micro heat transport equations in a three-dimensional double-layered thin film," *International Journal for Numerical Methods in Engineering*, vol. 59, pp. 493-509, 2004.
- [40] W. Dai, L. Shen, R. Nassar and T. Zhu, "A stable and convergent three-level finite difference scheme for solving a dual-phase-lagging heat transport equation in spherical coordinates," *International Journal of Heat and Mass Transfer*, vol. 47, pp. 1817-1825, 2004.
- [41] W. Dai, L. Shen and T. Zhu, "A stable three-level finite difference scheme for solving a three-dimensional dual-phase-lagging heat transport equation in spherical coordinates," *Numerical Heat Transfer, Part B*, vol. 46, pp. 121-139, 2004.
- [42] W. Dai and T. Niu, "A finite difference method for solving nonlinear hyperbolic two-step model in a double-layered thin film exposed to ultrashort pulsed lasers with nonlinear interfacial conditions," *Nonlinear Analysis: Hybrid Systems C Series*, vol. 2, pp. 121-143, 2008.
- [43] T. Q. Qiu and C. L. Tien, "Short-femtosecond laser heating of multi-layer metals I. analysis," *International Journal of Heat and Mass Transfer*, vol. 37, pp. 2789-2797, 1994.
- [44] T. Q. Qiu, T. Juhasz, Suarez, W. E. Bron and C. L. Tien, "Femtosecond laser heating of multi-layer metals II. experiments," *International Journal of Heat and Mass Transfer*, vol. 37, pp. 2789-2808, 1994.
- [45] D. Y. Tzou, "An engineering assessment of the relaxation time in thermal wave propagation," *International Journal of Heat and Mass Transfer*, vol. 117, pp. 1837-1840, 1993.

- [46] D. Y. Tzou, M. N. Ozisik and R. J. Chiffelle, "The lattice temperature in the microscopic two-step model," *Journal of Heat Transfer*, vol. 116, pp. 1034-1038, 1994.
- [47] D. Y. Tzou, "A unified field approach for heat conduction from macro- to micro-scales," *Journal of Heat Transfer*, vol. 117, pp. 1837-1840, 1995.
- [48] D. Y. Tzou, "The generalized lagging response in small-scale and high-rate heating," *International Journal of Heat and Mass Transfer*, vol. 38, pp. 3231-3240, 1995.
- [49] D. Y. Tzou, "Experimental support for the lagging behavior in heat propagation," *Journal of Thermophysics and Heat Transfer*, vol. 6, pp. 686-693, 1995.
- [50] D. Y. Tzou and Y. S. Zhang, "An analytic study on the fast-transient process in small scales," *International Journal of Engineering*, vol. 33, pp. 1449-1463, 1995.
- [51] D. Y. Tzou, "Ultrafast heat transport: the lagging behavior," *44th SPIE's Annual Meeting*, Denver, Colorado, 1999.
- [52] D. Y. Tzou and K. S. Chiu, "Temperature-dependent thermal lagging in ultrafast laser heating," *International Journal of Heat and Mass Transfer*, vol. 44, pp. 1725-1734, 2001.
- [53] D. Y. Tzou, "Micro heat transfer and fluid flow," *45th SPIE's Annual Meeting*, San Diego, California, 2000.
- [54] D. Y. Tzou, J. K. Chen and J. E. Beraun, "Hot-electron blast induced by ultrashort-pulsed lasers in layered media," *International Journal of Heat and Mass Transfer*, vol. 45, pp. 3369-3382, 2002.
- [55] M. Kaganov, I. Lifshitz and M. Tanatarov, "Relaxation between electrons and crystalline lattices," *Soviet Physics Journal of Experimental and Theoretical Physics*, vol. 4, pp. 173-178, 1957.
- [56] H. Wang, W. Dai and R. Melnik, "A finite difference method for studying thermal deformation in a double-layered thin film exposed to ultrashort pulsed lasers," *International Journal of Thermal Sciences*, vol. 45, pp. 1179-1196, 2006.
- [57] H. Wang, W. Dai, R. Nassar and R. Melnik, "A finite difference method for studying thermal deformation in a thin film exposed to ultrashort pulsed lasers," *International Journal of Heat and Mass Transfer*, vol. 49, pp. 2712-2723, 2006.

- [58] H. Wang, W. Dai and A. Bejan, "Optimal temperature distribution in a 3D triple layered skin structure embedded with artery and vein vasculature and induced by electromagnetic radiation," *International Journal of Heat and Mass Transfer*, vol. 50, pp. 1843-1854, 2007.
- [59] H. Wang, W. Dai and L. G. Hewavitharana, "A finite difference method for studying thermal deformation in a double-layered thin film with imperfect interfacial contact exposed to ultrashort pulsed lasers," *International Journal of Thermal Sciences*, vol. 47, pp. 7-24, 2008.
- [60] S. Zhang, W. Dai, H. Wang and R. V. N. Melnik, "A finite difference method for studying thermal deformation in a 3D thin film exposed to ultrashort pulsed lasers," *International Journal of Heat and Mass Transfer*, vol. 51, pp. 1979-1995, 2008.
- [61] S. Zhang, P. Wang and W. Dai, "A finite difference method for studying thermal deformation in 3D double-layered micro-structures exposed to ultrashort-pulsed lasers," *The Open Applied Mathematics Journal*, vol. 2, pp. 104-125, 2008.
- [62] X. Du, W. Dai and P. Wang, "A finite difference method for studying thermal deformation in a 3D micro-sphere exposed to ultrashort pulsed lasers," *Numerical Heat Transfer, Part A*, vol. 53, pp. 457-484, 2008.
- [63] I. Kaba and W. Dai, "A stable three-level finite difference scheme for solving the parabolic two-step model in a 3D micro-sphere heated by ultrashort-pulsed lasers," *Journal of Computational and Applied Mathematics*, vol. 181, pp. 125-147, 2005.
- [64] L. C. Evans, *Partial Differential Equations*, Providence, RI: American Mathematical Society, 1998.
- [65] K. W. Morton and D. F. Mayers, *Numerical Solution of Partial Differential Equations*, London, UK: Cambridge University Press, 1994.

## VITA

### BASIC INFORMATION

Contact Information      Di Zhao, Ph.D. student  
                                    Computational Analysis and Modeling Program  
                                    Louisiana Tech University  
Phone                         318-497-1825  
E-Mail                        dzh002@latech.edu  
Web                          www.latech.edu/~dzh002  
Mailing Address            P.O. Box 1721, Ruston, LA 71273

### EDUCATION

Ph.D.    Computational Analysis and Modeling, Louisiana Tech University, September 2005-May 2010  
          Dissertation: Accurate and stable numerical methods for solving micro heat transfer models in an  $N$ -carrier system in spherical coordinates  
          Advisor: Dr. Weizhong Dai  
M.E.     Environmental Engineering, China Agricultural University, September 2001-July 2004  
          Thesis: The study of Cadmium-Arsenic interaction in wheat  
          Advisor: Dr. Yongguan Zhu and Prof. Lijiang Xia  
B.A.     Agricultural Environmental Protection, Hunan Agricultural University, September 1996-June 2000

### PUBLICATIONS (September 2005-May 2010)

2010

D. Zhao and W. Dai, "Accurate finite difference schemes for solving a 3D micro heat transfer model in an  $N$ -carrier system with Neumann boundary condition in spherical coordinates," *Journal of Computational and Applied Mathematics*, submitted.

2009

D. Zhao, "Preconditioning GMRES(m) for finite volume discretization of incompressible Navier-Stokes equation by Hermitian/skew-Hermitian separation," *SIAM Conference on Applied Linear Algebra 2009*, October, 2009.

W. Dai and D. Zhao, "An improved Crank-Nicholson scheme for solving a micro heat transfer model in an  $N$ -carrier system with Neumann boundary condition in spherical coordinates," *Applied Numerical Mathematics*, submitted.

D. Zhao, "Acceleration of Hermitian/skew-Hermitian separation for incompressible Navier-Stokes equation by parallel Gram-Schmidt process of GMRES(m)," *Fifth M.I.T. Conference on Computational Fluid and Solid Mechanics - Focus: Advances in CFD*, June, 2009.

2008

D. Zhao, "Parameter tuning of Support Vector Machine by Monte Carlo and directed walking algorithm," *American Computing Conference*, March, 2008.

2007

D. Zhao, "Speed up genome-wide association studies by parallel Markov Chain Monte Carlo," *Conference on Emerging Design and Analysis Issues in Genomic Studies in Population, Harvard University*, October, 2007.

D. Zhao, "Non-negative matrix factorization to speed up interior point method of SVM training," *Stanford 50: State of the Art and Future Directions of Computational Mathematics and Numerical Computing*, March, 2007.

2006

"Combined of independent component analysis and Support Vector Machines on gene expression profile classification of lung cancer," June, 2006, Preprint.

"Solution of the problem of unbalance of expression profile data using asymmetrical soft margin SVM," June, 2006, Preprint.

"Performance enhancement of SVM-RFE with soft margin and kernel function," April, 2006, Preprint.

"Gene expression profile diagnostic prediction of lung cancer with Support Vector Machines by dimensional reduction," January, 2006, Preprint.